THE KOONYA PROSPECT, ROSEBERY, TASMANIA.

by

STEPHEN HALL

A thesis submitted in partial fulfilment of
the requirements for the degree of
Graduate Diploma of Science with Honours.

CENTRE FOR ORE DEPOSIT
AND EXPLORATION STUDIES

Geology Department,
University of Tasmania.
January 1990

Abstract

Koonya is a small lead-zinc prospect located approximately three kilometres south of Rosebery and about one kilometre east of the Rosebery fault. It lies within the basal sequence of the Cambrian Central Volcanic Complex on the western side of the Mount Read Volcanic belt. The Koonya prospect occurs in the same stratigraphic sequence that hosts the Rosebery and Hercules ore deposits.

The geology of the Koonya area is dominated by variable altered, rhyolitic feldspar-phyric volcanics. These units have flow(?) banding and shard like textures throughout the groundmass and may be either unusual lavas or pyroclastics. Grading observed in several areas suggests an upright facing for the sequence.

Three mineralized horizons were recognised at Koonya. The major horizon contains a thin massive sulphide lens and its vein style down dip continuation (zone B). In three dimensions the massive sulphide and zone B are part of a more complex horizon of mineralization. This horizon shows a distinct mineralogical zonation from a chalcopyrite-pyrite-arsenopyrite-tetrahedrite-aikinite-native bismuth assemblage in the south (similar to the copper-rich assemblage seen at Rosebery), to a galena-sphalerite-pyrite-chalcopyrite-pyrrhotite assemblage which dominates the massive sulphide to the north.

The mineralization pre-dates the Devonian regional deformation and thus pre-dates the Devonian granite intrusion in the area. Temperatures for deposition of the mineralization, based on the mineral assemblages, ranged from greater than 270°C for the copper rich zone to less than 250°C for the massive sulphide. Zinc ratio distributions indicate that the massive sulphide was formed from lead saturated fluids, but the other types of mineralization were deposited from either lead undersaturated fluids, or formed at temperatures below 200°C. Lead isotope studies indicate the lead in the mineralization is Cambrian in age and sulphur isotopes suggest the sulphur was dominantly derived from seawater.

Two major alteration events occurred at Koonya; alteration associated with mineralization and a later stage alteration, often associated with post-cleavage veining. The alteration associated with the main lead-zinc mineralized zone has a very distinctive arrangement directly related to the position of the mineralization. Above the mineralization the alteration is dominated by a quartz-sericite-pyrite assemblage but below the mineralization the alteration is dominated by a sericite assemblage.

Geochemical studies of the alteration have shown that originally the altered rocks were very similar. The alteration has produced mass and/or volume changes in excess of ±30% of the original mass/volume. Major element changes during alteration included depletion of sodium, calcium and silica and enrichment of potassium, iron, magnesium and manganese.

Oxygen isotope studies suggest that the main mineralizing fluid was dominated by heated seawater, supporting the previous conclusion reached from sulphur isotope studies, that seawater was the major component of the mineralizing fluid.

Studies of chlorites formed during alteration revealed that the chlorite has been re-equilibrated during later metamorphism. The metamorphic temperature recorded by the chlorites is approximately 310°C to 340°C. The very different composition of chlorites from the quartz-sericite-pyrite altered zone and the sericite altered zone suggest that they were formed under different conditions. An unusual feature of the chlorites at Koonya is their very high manganese values, with MnO in excess of 5% in some samples.

A three stage model is proposed to explain the genesis of the major mineralized horizon at Koonya. Initially the host rhyolitic sequence was extensively sericitized. The second stage involved deposition of the sulphide mineralization as veins, fracture fillings(?) and disseminations, and co-incident quartz-sericite-pyrite alteration of the hanging wall. In the third stage the host rock sequence is folded and deformed, causing re-orientation of the mineralization.

Contents

List of figures

List of Tables

List of Plates

Acknowledgements

I would like to thank a number of people for various contributions to this project.

Firstly, I would like to thank the Tasmanian Mines Department for providing the scholarship that allowed me to undertake this year. I also wish to thank G. Green for his assistance, time and the use of the Mines Department computing and XRD facilities. Thanks to Pasminco for providing both the project and financial assistance. Thanks also to R. Large for his supervision of the project.

I would like to acknowledge assistance from R. Berry, D. Huston, K. Harris, M. Power, W. Jablonski, and P. Robinson for their help with various analyses, and S. Stephens for thin section preparation. Finally, I wish to acknowledge the assistance of B. Gemmel, J. Stolz, R. Large, J. Hills, D. Huston and R. Berry for proof reading various parts of the thesis.

INTRODUCTION

The Koonya prospect is just over three kilometres south of the Rosebery mine. It lies approximately halfway between the Rosebery and Hercules mines and about one kilometre to the east of the Rosebery fault (see figure 1). The sequence in the immediate area of Koonya is considered to be dipping east at 45° to 60° (Lees 1987).

The Koonya prospect occurs on the side of a moderate west to south-west dipping slope. The vegetation within the prospect area is fairly light, being dominated by knee-high grasses. The Koonya prospect is covered to a large extent by thin glacial erratics (0 to 6 metres), and only bulldozed tracks contain any outcrops of the underlying rock. Two adits were driven into the Koonya prospect in the early 1900's, both intersecting a thin massive sulphide horizon. It is this mineralization which is of prime interest to this study.

Project Aims

This project has two major objectives.

The first is to describe the geology, alteration and mineralization of the Koonya prospect, Rosebery, Tasmania.

The second is to decide on the likely genesis for the Koonya mineralization.

Work History

The Koonya mineralization was discovered in the early 1900's by John Wills, the discoverer of the Hercules orebody. Initially he sank a shaft on an auriferous gossanous outcrop. He then cut an adit into the side of the Koonya prospect in order to intersect the ore horizon at a lower level. Instead of the anticipated gold rich orebody, the adit intersected a thin horizon of massive lead-zinc mineralization which Wills subsequently mined. Later, a second adit was driven into the hillside, below the first, again intersecting the lead-zinc mineralization. In both cases, the mineralization was found to be approximately 1 to 2 metres thick and about 30 to 40 metres wide.

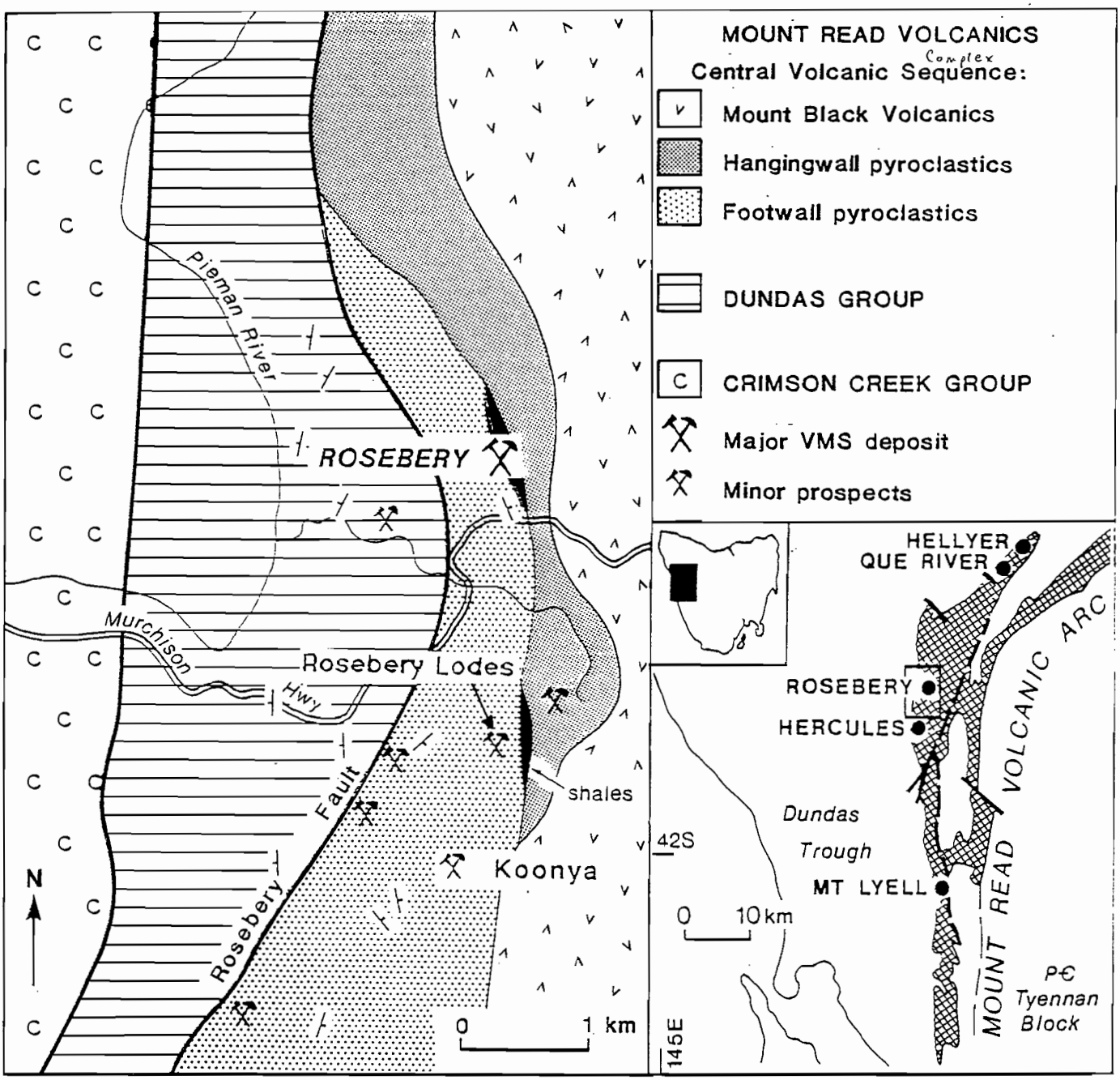

Figure 1: The geology of the Rosebery-Koonya area
(modified after Corbett and Lees 1987)

In 1973-74 two holes, Kp196 and Kp201, were drilled by Electrolytic Zinc (now Pasminco) to test the down dip extension of the mineralization. Another two holes, Kp199 and Kp200, were also drilled to test the width of the mineralization. During 1988 and early 1989 seven holes, Kp303 to Kp309 inclusive, were drilled into the Koonya area. Only four of these holes were designed to test the Koonya mineralized horizon, these being Kp305, Kp306, Kp307 and Kp308. Drillhole Kp303 was designed to intersect a gravity anomaly and drillholes Kp304 and Kp309 were designed to provide further information on the north-south section through the Koonya area.

Previous Studies

Very few studies of the Koonya prospect have been made. Loftus Hills (1915) described the mineralization intersected in the upper adit as being part of a large dome structure, with the crest of the dome intersected by the upper adit. Finucane (1932) briefly described the geology exposed in the two adits. He described the adits as going from an altered unit above the ore horizon, changing to a relatively unaltered feldspar porphyritic unit below the mineralization. He considered the altered units to originally have been porphyritic with phenocrysts of feldspar.

Rutherford (1986) very briefly described the Koonya mineralization as lead-zinc stringer style veins within a sequence of lavas and intrusives. He suggested that the mineralization may be of Cambrian age and a replacement orebody associated with the syn-genetic exhalative Rosebery Lodes mineralization. Lees (1987) completed detailed mapping of the Rosebery mine lease which includes the Koonya prospect. He briefly described the mineralization as vein style and considered it to be hosted by pyroclastics within the Rosebery footwall sequence. Both Lees (1987) and Rutherford (1986) based their descriptions on observations made from drillholes Kp196, Kp199, Kp200 and Kp201. Hunns (1988) briefly described some oxygen isotope work carried out just east of the main Koonya prospect by Green (1986) and briefly comments on the zinc ratio distribution (presumably plotted from old assays carried out by Electrolytic Zinc).

Field Work Completed

In early-mid 1989 original logs of drillholes Kp308, Kp306, Kp307 and Kp305 were undertaken for this study (note: Kp308 was re-logged by a contract geologist). Re-logging of the 1973-74 drillholes Kp196, Kp199, Kp200 and Kp201 was required and involved substantial rewriting of the logs including a significant re-interpretation of the footwall-hanging wall contact in one hole. Also re-logging of some recently logged drill holes, namely Kp303, Kp304 and Kp309 was undertaken. Both Kp304 and Kp309 were significantly modified from the original logs. Some minor surface mapping of the Koonya prospect was undertaken and an examination of the upper adit of the old workings was carried out in order to ascertain any geological relationships and to take several massive sulphide ore samples.

Chapter 1: REGIONAL GEOLOGY

Section 1.1: The Mount Read Volcanics

The Mount Read Volcanics are an arcuate belt of Cambrian volcanic rocks some 10 to 15 kilometres wide and 210 kilometres in length (figure 1.1). They occupy part of a trough sequence, collectively termed the Dundas trough, which many authors consider to have formed by rifting of a Precambrian crust (eg. Corbett and Solomon 1989). Geochemically the bulk of the Mount Read Volcanics are medium to high potassium, calc-alkaline volcanics. The majority of the volcanics are rhyolitic to andesitic in composition, with basalts constituting only a minor percentage of the volcanic belt (Corbett and Lees 1987).

On the eastern side the Mount Read Volcanics unconformably overlies the Tyennan region, a sequence of Precambrian greenschist to amphibolite grade metasediments. On the western side the Mount Read Volcanics are either faulted against, conformably overlain by or interfinger with a predominantly sedimentary sequence with lesser volcanics, termed the Dundas Group (eg. Corbett and Lees 1987). The Dundas group often contains abundant detritus from the Central Volcanic Complex of the Mount Read Volcanics.

The Mount Read Volcanics have undergone at least two major phases of deformation, the first occurred in the late Cambrian to early Ordovician and the second during the Devonian. The effect of the earlier deformation event on much of the volcanic sequence is obscured by strong overprinting resulting from the Devonian event.

At least some localized cleavage development occurred during the Cambrian although no evidence has been found in the Dundas trough to support the idea of a regionally developed cleavage (eg. Corbett and Turner 1989). It was during this late Cambrian early Ordovician deformation that the Denison Group siliciclastics were deposited, predominantly in fault-controlled grabens adjacent to the Tyennan region.

During the Devonian deformational event, two major fold phases were developed, an early regional fold phase with a NNW trend and a second phase of folding and faulting generally with WNW and NW trends. The second phase is most obvious in the area between Queenstown and Zeehan (Corbett & Lees 1987). The major effect of the Devonian deformation was to produce a strong cleavage and recrystallization in much of the volcanic belt (Corbett and Solomon 1989).

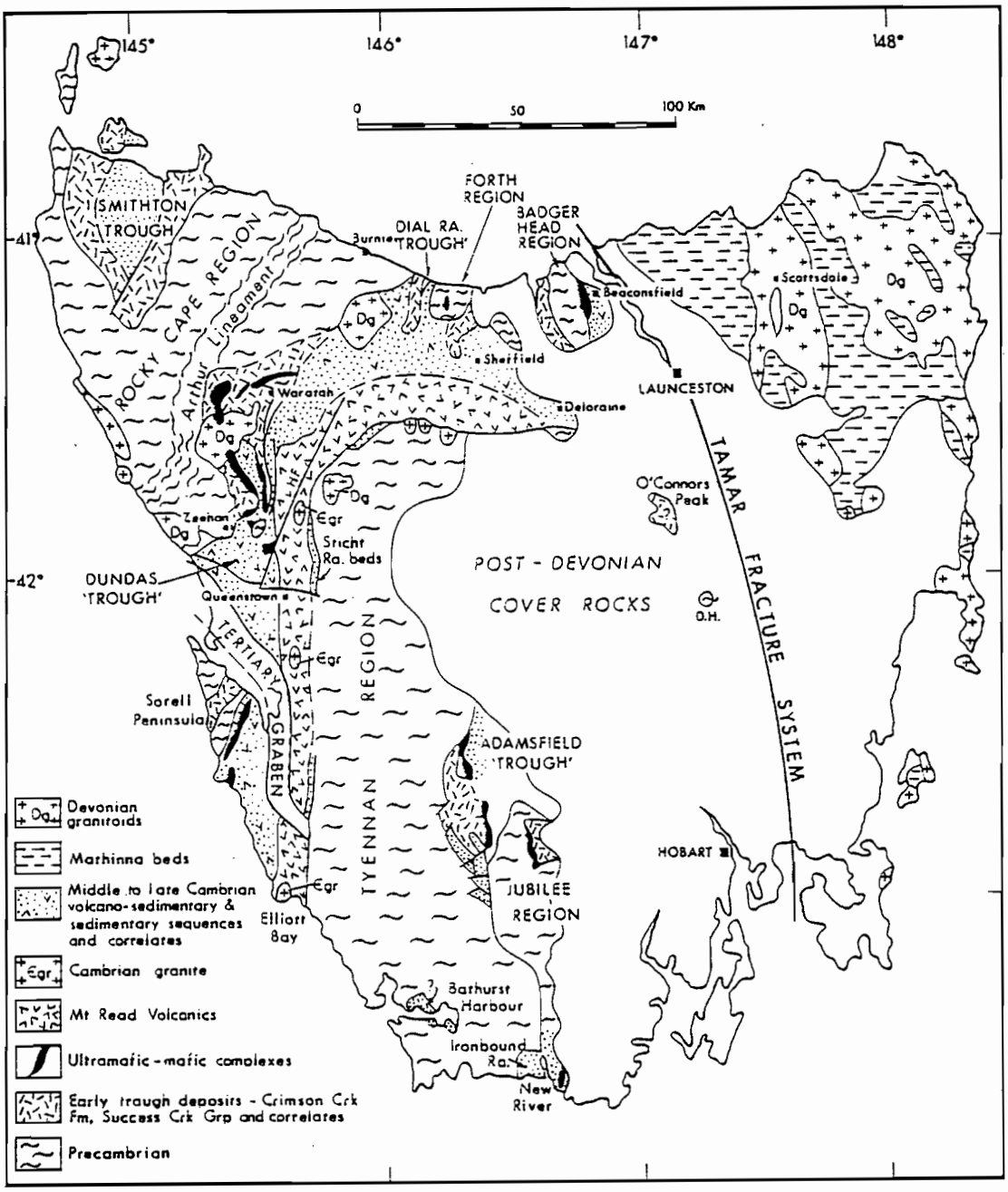

Figure 1.1: Simplified geological map showing the distribution of the Mount Read Volcanics. (after Corbett and Turner 1989)

The majority of the Mount Read Volcanics have undergone lower greenschist metamorphism. This has produced a quartz-sericite-chlorite-pumpellyite-epidote-actinolite assemblage throughout most of the volcanic belt. Localized hydrothermal alteration in the Cambrian was also an important alteration process in the Mount Read Volcanics.

In terms of economic value, the Mt Read Volcanics host at least five major ore bodies plus numerous other less significant zones of mineralization. The major ore bodies include Mt. Lyell, Rosebery, Hercules, Que River and Hellyer, all of which are generally considered to be formed as part of volcanogenic massive sulphide systems. As well as Cambrian mineralization a lesser proportion of the mineralization found in the Mount Read Volcanics formed during the Devonian. This Devonian mineralization can be spatially related to the position of Devonian granite intrusions (Williams et. al. 1989).

The Mount Read Volcanic belt is cut longitudinally by a major fault system termed the Henty Fault (figure 1.2). To the south and east of the fault, the volcanic sequence is divided into three groups.

A basal volcano-sedimentry sequence of shales, vitric tuff, volcanogenic turbidites, and minor quartz sandstone is termed the "Western Sequence". Intrusive bodies of quartz-feldspar porphyry or extrusive quartz-feldspar-phyric lavas occur throughout the Western Sequence.

Overlying or interfingering with the Western Sequence is a series of rhyolitic to dacitic, feldspar-phyric lavas, pyroclastics and intrusives which is termed the Central Volcanic Complex. Some porphyritic andesitic lenses occur within the sequence in the Queenstown area and a sub-volcanic granite intrudes the sequence at Mt. Darwin.

A volcano-sedimentry sequence of rhyolitic quartz-feldspar-phyric lavas, tuffs, breccias, shales and volcaniclastics overlie both the Western sequence and the Central Volcanic Complex. This sequence has been named the Tyndall Group. In places it unconformably overlies the Precambrian basement and appears to have formed in north-south grabens developed within or at the flank of the pre-existing volcanic sequence.

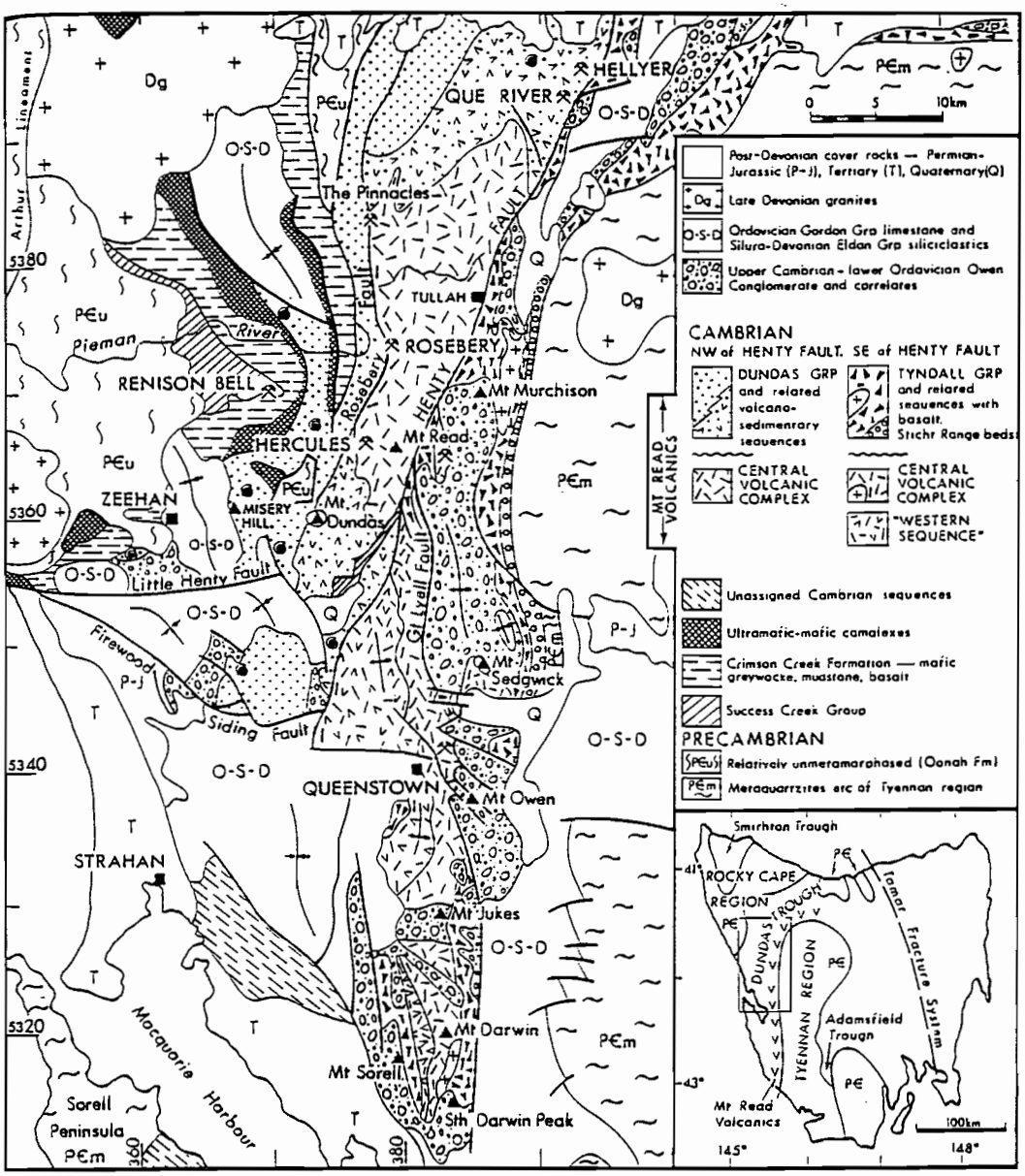

Figure 1.2: General geology of central western Tasmania showing the Mount Read Volcanic belt between Hellyer and Mt. Darwin. (after Corbett and Solomon 1989)

The Volcanic sequence to the north and west of the Henty fault is much simpler, consisting of a sequence of feldspar-phyric lavas and pyroclastics predominantly of dacitic to andesitic composition. Intrusive bodies of quartz feldspar porphyries, feldspar porphyries, and basaltic to gabbroic dykes occur throughout the sequence (Williams 1989). This sequence is considered to be part of the Central Volcanic Complex. It differs from the Central Volcanic Complex on the south-eastern side of the Henty fault by consisting predominantly of dacitic to andesitic volcanics with fewer of the rhyolites and virtually none of the potassic rhyolites seen on the south-eastern side.

The basal part of the Central Volcanic Complex north-west of the Henty fault is predominantly rhyolitic to rhyodacitic in nature, and hosts the Rosebery and Hercules ore bodies. It is this area which is of particular interest to this study.

Section 1.2: Geology of the Rosebery-Hercules Area

The Koonya prospect is hosted in the same sequence as the Rosebery and Hercules deposits. Considerable work has gone into defining the stratigraphy in the Rosebery area but there is still controversy over interpretation of the units, conditions of formation and, in some cases, the position of stratigraphic boundaries. The major formations in order from oldest to youngest are: Footwall pyroclastics, Host rock, Black shale, Quartz-phyric epiclastics and then the Mount Black Volcanics. Each unit is briefly described below.

1.2.1 Footwall Pyroclastics (≤400 m)

The basal unit in the Rosebery area is the Footwall Pyroclastics. Green (1983) described the rocks as vitric-crystal lapilli tuffs with albite and/or potassic feldspar phenocrysts often containing relict flattened pumice fragments. The units generally have 5-15% feldspar phenocrysts in a groundmass of quartz, albite and potassium feldspar. Common secondary minerals are chlorite, carbonate and epidote while sericite is ubiquitous. Green (1983) consider the units to be dominated by ignimbrites with the degree of welding varying from non-existent to strong.

More recent work by Allen (1988a) and Clifford (1988) has cast some doubt on the origin of the footwall volcanics. Allen (1988a) has made two major suggestions concerning the origin of the volcanics, these being that;

a) some part of both the Hanging wall and Footwall pyroclastics are lavas.

b) a substantial volume of the Hanging wall and Footwall pyroclastics are massive, fine grained, pumiceous rhyolite/dacite breccias which have some characteristics of both lavas and pyroclastics but are typical of neither.

Work by Clifford (1988) involved a detailed study of the Rosebery mine footwall. He concluded that the footwall consisted of four types of units, these being;

1. Stratified mass-flow re-sedimented debris
2. Massive units of non-welded pyroclastic debris
3. Thinly bedded, fine grained tuffaceous sediments
4. Lavas.

Both Allen (1988a) and Clifford (1988) consider the footwall to have accumulated in a subaqueous environment.

1.2.2 Host Rock (0-70m)

The host rock sequence consists of siltstones, slate and lenses of crystal tuff (Brathwaite 1974) conformably overlying the Footwall Pyroclastics. Mineralogically the sequence is dominated by quartz, sericite, and chlorite with lesser carbonate, pyrite and albite (Eastoe 1973). The host rock also contains disseminated fine grained pyrite and some bedded pyrite/sulphide lenses. The base of the host rock sequence is often masked by alteration. The lateral extent of the host rock is uncertain. It is well developed at the Rosebery mine and is inferred to occur elsewhere on the Rosebery mining lease as discontinuous lenses of sediment.

1.2.3 Black Shale (0-30m)

This unit is dominated by thinly laminated, grey to black shales with lesser interbedded thin crystal tuffs, and thin graded turbiditic sandstone horizons (the sand grains being derived from a metamorphic terrain) (Green 1983). Compositionally, the black shale consists of quartz, sericite, chlorite and minor organic material. The black shale occurs mainly in the Rosebery mine area where it is locally strongly eroded. Rafts of black shale are found in hanging wall epiclastics in the Hercules area (Lees 1987).

1.2.4 Quartz-phyric Epiclastics [or Hanging wall Pyroclastics] (≈500m)

This term has been suggested by Lees (1987) to replace Brathwaite's (1969) "Massive Pyroclastics". In the Rosebery mine area this sequence is dominated by units containing both quartz and feldspar phenocrysts but lacking potassium feldspar phenocrysts (Lees 1987). Breccia units are common. Alteration is generally limited to minor sericitization of feldspars with virtually no development of quartz-sericite schists which are common in the footwall pyroclastics.

The base of the quartz-phyric epiclastics contains numerous black shale fragments eroded from the underlying black shale. The abundance and size of shale fragments and quartz phenocrysts decreases southward so that east of Hercules the lower 250m of the quartz-phyric epiclastics is represented by plagioclase-phyric vitric crystal tuff with pumice fragments lacking quartz phenocrysts, very similar to the footwall pyroclastics (Lees 1987).

Green et. al. (1981), Green (1983) and Lees (1987) consider the quartz-phyric epiclastic sequence to have been deposited as a series of subaqueous density flows.

1.2.5 Mt. Black Volcanics (≈2500m)

Originally named by Brathwaite (1969), the Mount Black Volcanics were considered by Green (1983) to consist of two compositionally distinct sequences. The lower part of the sequence is dominated by monotonous rhyolitic and lesser dacitic flow banded to auto-brecciated lavas. The upper part of the sequence is dominated by andesitic, dacitic and minor basaltic tuffs and lava flows. The Mt. Black Volcanics appear to conformably overlie the quartz-phyric epiclastics and are terminated to the east by the Henty fault.

Section 1.3: Devonian Events

During the Devonian at least four major events occurred in the Rosebery area, namely regional deformation, localized deformation in related to movement on the Rosebery fault, regional metamorphism and, finally, intrusion of the Devonian granite complex plus the associated

metasomatism. All these events have had a direct effect on the Koonya prospect. As mentioned previously the main effect of the regional deformation was to produce a cleavage throughout the volcanic sequence, as well as causing some recrystallization of the volcanic belt.

1.3.1 The Rosebery Fault

A major thrust fault occurs just to the west of Rosebery. It separates the Dundas Group on the west, from the Footwall pyroclastics, on the east (figures 1 and 1.2). From mapping and drillhole intersections the Rosebery fault is known to dip at between 35° to 40° to the east and have a minimum down dip displacement of one and a half kilometres (Corbett and Lees 1987).

In terms of structure, the Rosebery fault has had a significant effect on the Rosebery area. It has formed a strong cleavage zone which extends from the fault to past the Rosebery mine, overprinting (and thus post-dating) the regional Devonian cleavage. Within the Rosebery orebody, the effect of the Rosebery fault is represented by a series of thrust faults which have similar orientation and movement sense to the major fault.

The major demonstratable movement on the Rosebery fault post-dates the regional Devonian deformation, but pre-dates the Devonian granite intrusion. Earlier movements of the Rosebery fault may have occurred but they are obscured by later events.

1.3.2 Metamorphism

In the Rosebery area, the peak metamorphic temperature appears to have been in the range 350°C to 400°C (Green 1983). Brathwaite (1969) describes the metamorphic assemblages in the Rosebery footwall and hanging wall sequences as consisting of quartz-albite-sericite-chlorite-sphene. Lees (1987) considered that the main phase of metamorphism pre-dated the Devonian granite intrusion.

1.3.3 Granite Intrusion and Metasomatism

A very shallow east-west trending ridge of Devonian granite occurs between the Rosebery and Hercules mines (Leaman and Richardson 1988, Archer 1989). The ridge peaks just to the south of Koonya at an approximate depth of one kilometre below the surface (figure 1.3). Fluids expelled from the granite as it cooled have caused a variable degree of metasomatism in

areas close to the Granite ridge. The Rosebery fault has acted as a conduit for some of these granite related fluids. In the lower part of the Rosebery orebody, mainly F lens, the effects of the granite related metasomatism are quite marked with pyrrhotite replacement of sulphides being reasonably common.

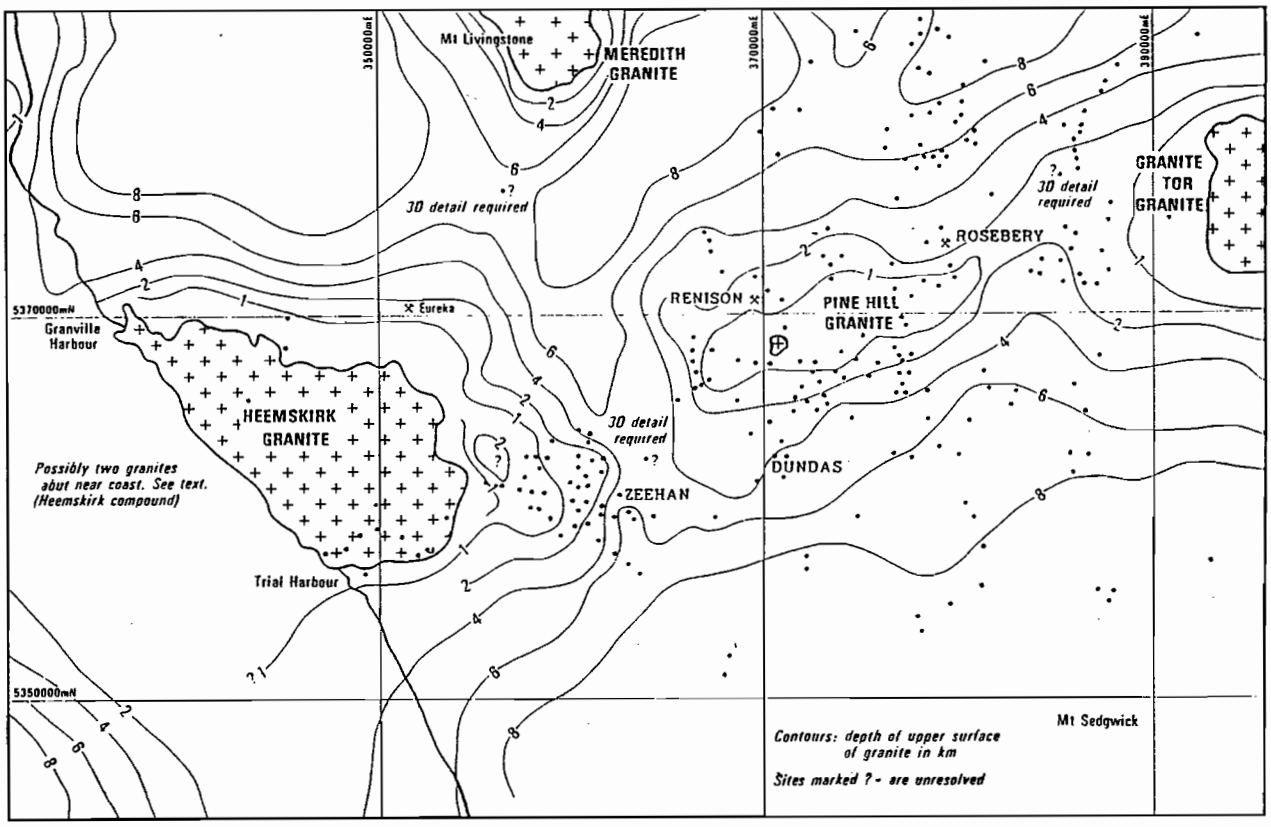

Figure 1.3: Provisional interpretation of the position of the granite ridge below the Rosebery region (after Leaman and Richardson 1988).

Chapter 2: LOCAL GEOLOGY

Five major rock-types have been recognised in the Koonya area. Two of the units are dominated by feldspar phenocrysts set in a fine-grained matrix, and have been termed the upper feldspar-phyric unit and lower feldspar-phyric unit. The other three rock-types are quartz-sericite(-pyrite) schists, a polymict breccia, and an unusual unit which is considered to represent slumped epiclastics.

Most of the surface of the Koonya prospect is covered by a thin (typically 0 to 6 metres thick) layer of glacial erratics which unconformably overlies the Central Volcanic Complex. These glacials consist mainly of fragments (up to boulder size) of siliceous conglomerate and volcanics. The majority of the Cambrian outcrop in the Koonya prospect occurs in bulldozed tracks. Only two rocktypes were identified during the surface mapping, these being quartz-sericite schists and the upper feldspar-phyric unit. A fact map of the prospect is shown in figure 2.1.

As well as surface mapping, a number of drillholes were logged and two sections, an east-west section and a north-south section, were constructed (figures 2.2 and 2.3 respectively). The drillhole positions are shown on the geological map (figure 2.1).

2.0.1 Quartz-Sericite(-Pyrite) Schists

Quartz-sericite schists occur in the upper part of all drillholes and crop out throughout the Koonya prospect (figures 2.1, 2.2, 2.3). A zone of quartz-sericite schists also occurs deeper in the north-south section (figure 2.3).

Typically the quartz-sericite schists are fine-grained units of quartz and sericite (≤0.01mm) with subhedral to euhedral pyrite grains (averaging 0.05mm to 0.2mm) disseminated throughout (plate 1). Often the unit contains tabular quartz aggregates or quartz-chlorite aggregates, typically 0.5mm to 2mm in length, which are considered to be feldspar pseudomorphs.

The quartz-sericite schists are intimately associated with mineralization. In the north-south section the schists crosscut the polymict breccia horizon. The interpretation for this unit is that it represents the alteration of feldspar-phyric volcanics, which were originally probably part of the upper feldspar-phyric unit.

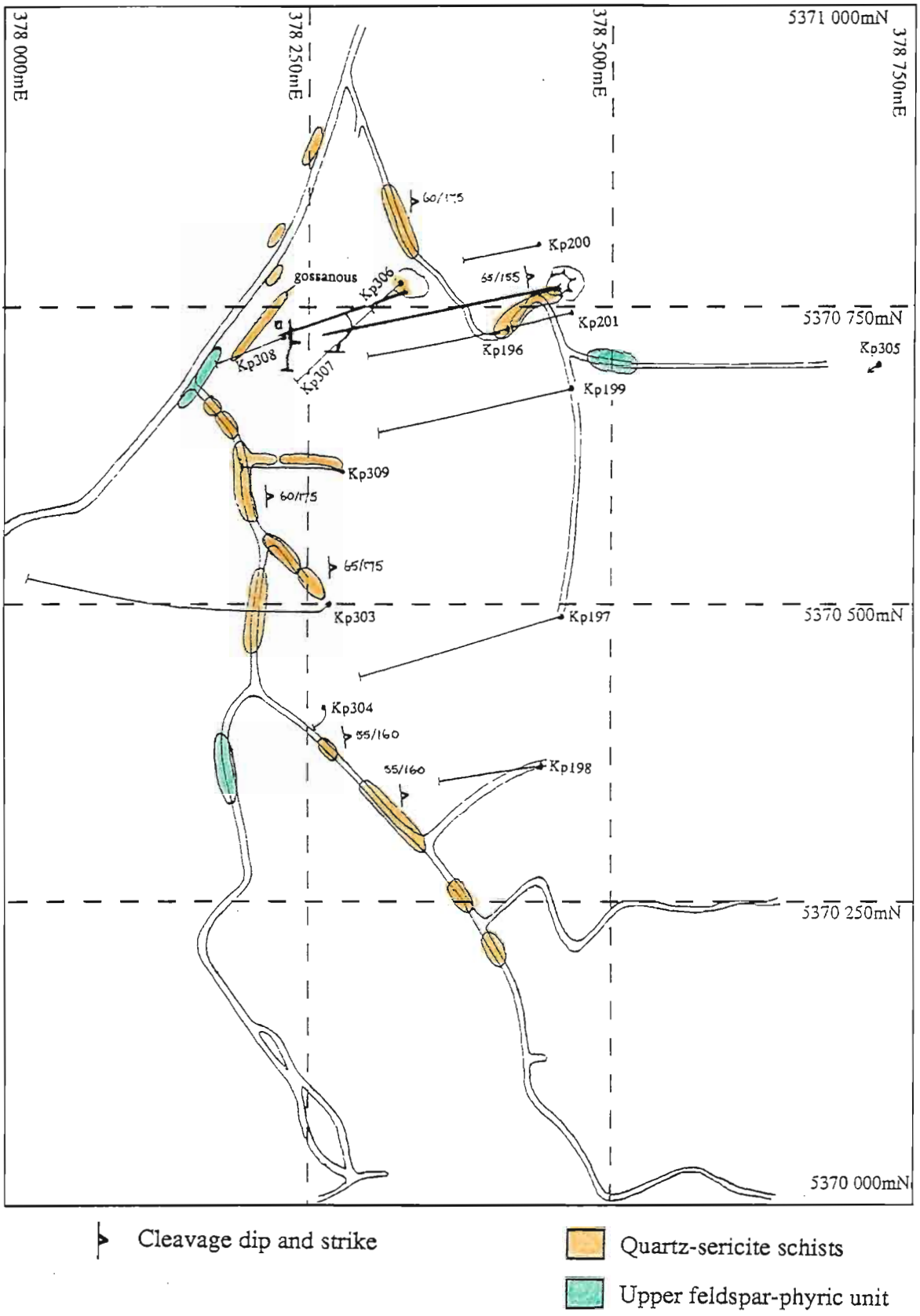

Figure 2.1: Surface map of the Koonya prospect showing the limited geology, drillholes, tracks and plan veiw of the two adits.

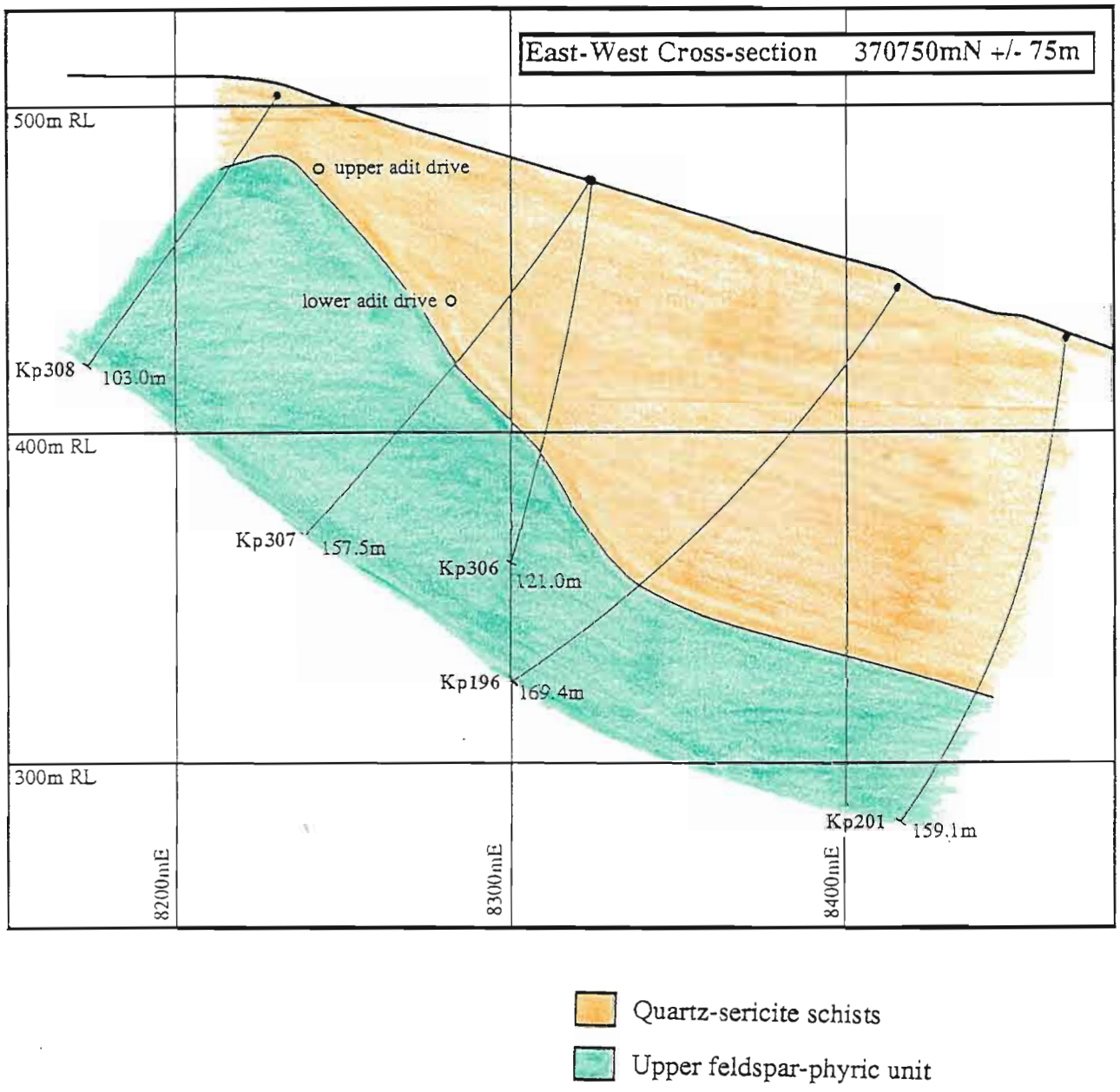

Figure 2.2: Geology of the east-west cross-section.

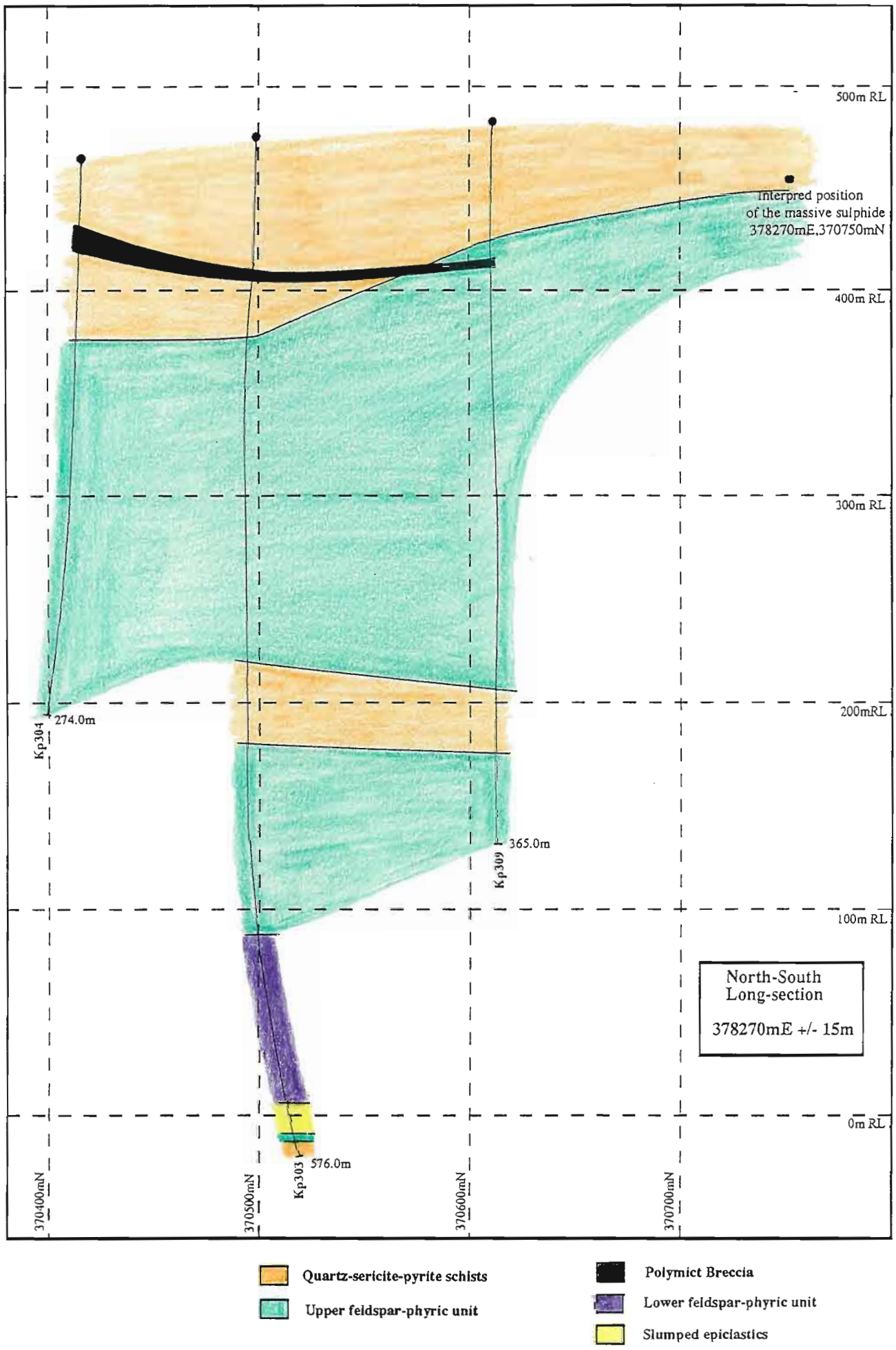

Figure 2.3: Geology of the north-south cross-section.

2.0.2 Upper Feldspar-phyric Unit

The upper feldspar-phyric unit is the dominant unit occurring in the Koonya area. It occurs in both the north-south and east-west sections as well as cropping out at the surface. In the north-south section the upper feldspar-phyric unit exceeds two hundred metres in vertical thickness.

The unit consists of 15% to 30% feldspar phenocrysts typically 0.5mm to 2mm in length, set in a fine-grained variably sericitic groundmass of quartz and feldspar (generally ≤0.01mm). Quartz phenocrysts are rare. The feldspar phenocrysts are dominantly albitic plagioclase. The feldspars typically are euhedral or subhedral with very few crystals that might be considered broken. In hand specimen the feldspar phenocrysts are evenly distributed throughout, but in thin section the feldspar distribution is patchy (plate 2) and in several places the phenocrysts have a glomeroporphryitic texture. The feldspar clusters or feldspar grains are often rimmed by quartz-feldspar aggregates which are slightly coarser than the groundmass. This texture is considered to be formed by devitrification around the feldspar edge (eg. MacKenzie et. al. 1982) which has later been recrystallized.

In several places the upper feldspar-phyric unit contains small lithic fragments. These lithic-bearing sections constitute only a small percentage of the upper feldspar-phyric unit. The lithic fragments typically constitute 1% of the lithic-bearing horizons but in some places abundances of 3% to 5% were observed. The lithic fragments are white to cream, subrounded to subangular, fine-grained, occasionally feldspar-phyric, and typically 5mm to 20mm in diameter. Most fragments are very similar in appearance.

As previously mentioned, the upper feldspar-phyric unit is variably sericitic. Close to the mineralized zone the groundmass of the unit may be almost entirely sericite. The feldspar phenocrysts are also variably altered to sericite but are rarely completely replaced. In other areas further away from the mineralization the upper feldspar-phyric unit contains virtually no sericite. The sericite is definitely an alteration of the same unit as the whole range of sericite alteration, from very strong to non-existent, was observed.

In plane polarised light some very distinctive textures can be observed in the upper feldspar-phyric unit, providing the sericitic alteration is not too strong. There are two types of textures, the first has a glass shard-like appearance, the second takes the form of fine banding (plates 3 and 4). In both cases the 'shards' or 'banding' are defined by slightly coarser quartz-feldspar aggregates in a very fine-grained (≤0.01mm) groundmass. The banding type structures occur

throughout the groundmass and appear to wrap around some phenocrysts (plate 4). The origin of the banding texture is uncertain but it is possible that it is flow banding.

The 'shard' like aggregates form small, often cuspate, delicate shapes. This texture can be interpreted as having two possible origins:

i) The 'shards' may be altered glass shards in a pyroclastic rock (unwelded due to the preservation of the delicate shard shapes).

ii) The other interpretation is that the texture is due to devitrification and alteration of an originally glassy lava (Allen 1988a). Allen (1988a) suggests that false shard textures may develop from selective alteration of perlitic fractured glass (see figure 2.4).

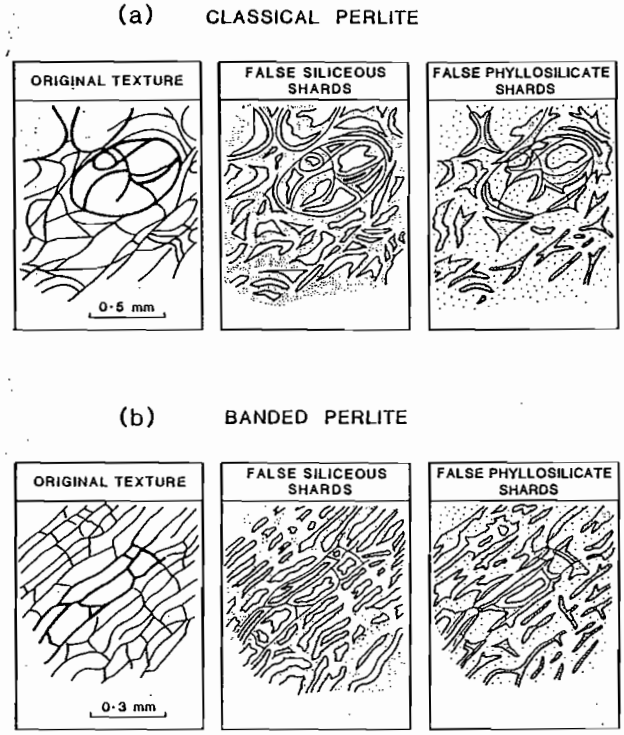

Schematic sketches summarized from thin sections, showing the relationship of (a) false nonwelded shards to the original texture in classical perlite, and (b) false welded shards to the original texture in banded perlite. To aid explanation, the portion of the original perlitic texture marked by heavy lines is repeated in the diagrams of false shard textures. The false shards may be preserved as siliceous segments between phyllosilicate-altered perlitic fractures (center), or as phyllosilicate-altered sections of the fractures themselves (right).

Figure 2.4: The development of various types of false shard textures in devitrified glassy lavas with perlitic fractures (after Allen 1988a).

Plate format: plate number: sample location, field of view, magnification, PP=plane polarised light XP=crossed polars RL=reflected light AL=arc lights

Plate 1: 307 zone B, 3.4mm, x20, XP Quartz-sericite-pyrite schist. The photomicrograph highlights the fine grained nature of much of this unit and the typical occurrence of sericite within the groundmass. Several pyrite grains can also be seen (opaque).

Plate 2: 307 120.7m, 15.5mm, x6.3, XP Relatively unaltered upper feldspar-phyric unit. The photomicrograph shows the fine-grained groundmass, the typical size and distribution of phenocrysts throughout the unit, and the slightly coarser grains within the groundmass which define the 'shard' and 'banding' textures.

Plate 3: 307 120.2m, 3.8mm, x20, PP 'Shard' textures in the relatively unaltered upper feldspar-phyric unit. In the upper centre of the photomicrograph a reasonably large cuspate shard can be seen.

Plate 4: 307 120.2m, 11.2mm, x8, XP Unusual 'banding' textures within the groundmass of the upper feldspar-phyric unit defined by coarser grained quartz and feldspar in a finer grained matrix. The lineations can also be seen around some feldspar phenocrysts.

Plate 5: 303 445.8m, 7.1mm, x12.5, PP 'Shard' textures in the lower feldspar-phyric unit. Small cuspate 'shards' can be seen throughout this unit.

Plate 6: 303 445.8m, 12.3mm, x6.3, XP The lower feldspar-phyric unit highlighting the size, shape and distribution of phenocrysts set in a fine-grained groundmass.

Plate 7: 303 537.6m, 26.5mm, x3.2, PP Slumped epiclastic unit. The photomicrograph is of a thinly bedded (≤5mm) unit in contact with a coarse-grained feldspar-phyric unit and containing a coarser-grained feldspar-phyric fragment (?) with an irregular boundary.

Plate 8: 303 537.6m, 26.5mm, x3.2, XP

The same field of view as plate 7 but under crossed polars.


1


2


3


4


5


6


7


8

Another feature of the relatively unaltered upper feldspar-phyric unit was observed in drillhole Kp303. In one 70 metre zone tubular pumice shards were observed. These fragments average 2mm to 5mm in diameter, are subrounded, and possess linear tube-like structures very similar to those described for pumice shards by Fisher and Schmincke (1984). The apparently limited occurrence of these pumice shards may be real, or may be due to the pumice fragments being obscured by alteration elsewhere.

The interpretation of the origin of the upper feldspar-phyric unit is difficult. The major facts relevant to the units origin are considered below:

Rims around phenocrysts, the very fine-grained groundmass and the shard textures all indicate that the rock was originally glassy.

Shard textures may indicate a pyroclastic or lava origin.

The lack of any relict perlitic fractures associated with the shards suggests they are pyroclastic in origin.

Banded textures are consistent with a lava origin.

Tubular pumice fragments (as observed in a significant zone in Kp303) suggest a pyroclastic origin.

The lack of broken phenocrysts suggests the unit is not pyroclastic.

The presence of lithic fragments is not consistent with a lava origin; however, the low abundance of lithic fragments is not typical of pyroclastics (Allen 1988a).

There is evidence to support both a lava or pyroclastic origin for the upper feldspar-phyric unit. If the unit is pyroclastic in origin it is definitely unwelded as the cuspate shard shapes are preserved. Allen (1988b) describes units very similar to the upper feldspar-phyric unit. He has termed these units 'pumiceous breccias' and considers them to be very unusual pyroclastics. In light of Allen's (1988b) findings, the interpretion placed on the upper feldspar-phyric unit is that it represents a sequence of very unusual pyroclastics.

2.0.3 Polymict Breccia

The polymict breccia was intersected in the three drillholes, Kp304, Kp303 and Kp309, in the north-south section (figure 2.3) but was not intersected in the east-west section. Because these intersections occur in a straight line it was impossible to use triangulation to calculate the dip or strike of the bedding.

The polymict breccia has a different appearance in each drillhole. From Kp304 to Kp303 and Kp303 to Kp309 there is a progressive decrease in grainsize, suggesting the clasts came from a southerly source. In all drillholes the polymict breccia seems to be weakly graded with fining occurring in an uphole direction.

In Kp304 the polymict breccia consists of pale pink to pink-red subangular fragments, generally 2mm to greater than 50mm in diameter, set in a chloritic groundmass. Several clasts appear to contain altered feldspar grains. The breccia is matrix supported and is 11.0m in vertical thickness. Both the clasts and the matrix are strongly altered to a quartz-chlorite assemblage.

In Kp303 the polymict breccia consists of white to black, strongly altered subrounded to subangular clasts, generally 1mm to 40mm in diameter, set in a fine-grained matrix. The more silicic clasts appear to contain altered feldspars. The strength of alteration obscures the clasts. The abundance of clasts is greater than in Kp304 but the unit is still matrix supported. The vertical extent of the breccia in Kp303 is approximately 2.9 metres.

In Kp309 the breccia consists of subrounded to subangular white, pale pink and lesser dark coloured clasts, typically 1mm to 10mm in size, set in a fine grained matrix. Ten to twenty percent of the unit consists of subhedral to euhedral feldspar grains. The unit is only just matrix supported with a high proportion of clasts. One large clast several centimetres in diameter occuring at the very base of the breccia is identical to many of the larger clasts in Kp304. The vertical extent of the breccia in Kp309 is 3.0 metres.

2.0.4 Lower Feldspar-phyric Unit

The lower feldspar-phyric unit consists of 10-20% feldspar and minor quartz phenocrysts, typically 0.15 to 1.0mm in length, set in a fine-grained quartz-feldspar groundmass. The majority of phenocrysts are euhedral or subhedral. Some grains have 'frayed' irregular edges and a few appear to be broken (see plate 6). In hand specimen the lower feldspar-phyric unit is a medium to dark green colour and the phenocrysts are difficult to see. The unit is only intersected in drillhole Kp303 between the depths 410.0m and 531.8m, a length of 122m (figure 2.3).

The lower feldspar-phyric unit differs from the upper feldspar-phyric unit in several key ways. The most noticeable difference is the much smaller size of the phenocrysts, the abundance of variably sized phenocrysts, the lack of glomeroporphyritic textures and the lack of coarser-

grained rims around feldspars phenocrysts. Another major difference is that the upper feldspar-phyric unit contains some lithic fragment-bearing zones but no lithics were observed in the lower feldspar-phyric unit. The lower unit does contain some clasts near the very base of the unit which Allen (1988c) considered to be altered pumice. Another major difference is that the lower feldspar-phyric unit is typically relatively unaltered throughout its length.

One similarity between the upper and lower feldspar-phyric units is the presence of 'shard' textures. The lower feldspar-phyric unit displays abundent 'shard' textures defined by slightly coarser-grained quartz-feldspar aggregates in a finer-grained groundmass (see plate 5).

As with the upper feldspar-phyric unit, the interpretation of this lower feldspar-phyric unit is difficult. The most likely interpretation of the lower feldspar-phyric unit is that it is pyroclastic in origin.

2.0.5 Slumped Epiclastics

The slumped epiclastic unit occurs only in drillhole Kp303 between the depths of 531.8m and 557.7m (figure 2.3). Its appearance varied throughout the zone with the unit consisting of a series of different lithologies slumped together in a random manner. The individual lithologies making up the slumped epiclastics include:

A thinly bedded (≤5mm) to massive fine grained lithology. The grain size is generally 0.01mm to 0.03mm with occasional quartz and feldspar grains up to 0.1mm. Some beds are quartz-feldspar rich and appear cream in colour while others also contain chlorite giving them a green appearance (plates 7&8).

An orange-cream feldspar-phyric fragment with very irregular boundaries, typically several centimetres in size. The feldspar phenocrysts are 0.05mm to 2mm in length and are set in a medium-grained (0.02mm to 0.15mm) groundmass of quartz and feldspar. Some grains within the groundmass have serrated edges and exhibit undulose extinction probably due to deformation (plates 7&8).

A grey-cream lithology with quartz and feldspar phenocrysts (0.2mm to 0.5mm) set in a medium-grained groundmass of quartz and feldspar (0.02mm to 0.15mm). This unit also contains some fine-grained patches up to 1mm in size which may be lithics (plates 7&8).

A dark green unit contains up to 30% euhedral feldspar phenocrysts (0.5mm to 2mm long) in a fine-grained groundmass.

In some places the unit contains subrounded to subangular, polymict lithic fragments up to several centimetres in length.

The major features suggesting slumping are the contorted nature of the boundaries between units, the random repetition of lithologies, small irregular patches (two or three centimetres in diameter) of brecciated material which occur in a number of places within different units, and finally the overall irregular appearance of the entire unit.

Section 2.1: Classification

Eleven wholerock and trace element analyses have been carried out on samples from the quartz-sericite-pyrite schists, upper feldspar-phyric unit and lower feldspar-phyric unit. Using the immobile elements titanium, zirconium, yttrium and niobium it is possible to classify the rocks (Winchester and Flyod 1977). Using this technique all the Koonya samples plot in the rhyolite field (figure 2.5).

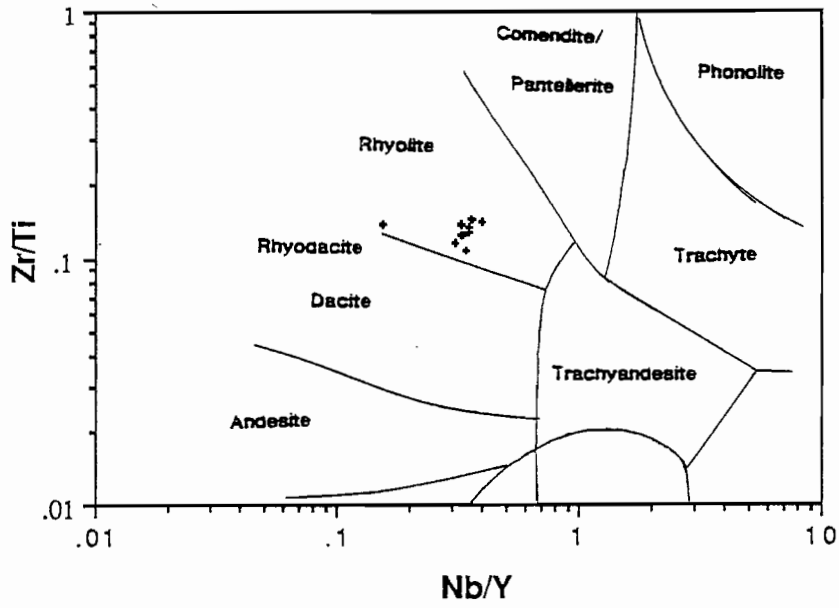

Figure 2.5: Immobile element plot for samples from the Koonya prospect (modified after Winchester and Flyod 1977).

Section 2.2: Structure

The dominant feature in the rocks outcropping in the Koonya prospect and intersected by the drillholes is a well developed cleavage. In particular, the quartz-sericite-pyrite schists show the strongest cleavage development with weaker cleavage development in the sericite altered zones in the upper feldspar-phyric unit. In the weakly altered parts of the upper feldspar-phyric unit and the lower feldspar-phyric unit the cleavage is very weak.

In a number of thin sections two cleavages were observed. One cleavage is reasonably weak and is obscured by a stronger cleavage. In the drillholes the dominant cleavage is typically developed at angles of 45° to 70° to the core axis. In outcrop the cleavage strike is 155° to 175° and the dip is 50° to 65° toward the east. The attitude of the cleavage is consistent with its being caused by the Devonian regional deformation (Corbett and Lees 1987). The second, weaker cleavage observed in thin section is probably associated with movement on the Rosebery fault.

Very little is known about the bedding at Koonya. The only place where bedding could be located was in the north-south section. The polymict breccia was intersected in all three drillholes in the section (figure 2.3). Unfortunately the two-dimensional nature of the drillholes in the section does not allow strike line constructions so the strike and dip of the bedding could not be determined. Mapping by Lees (1987) indicates that to the west of Koonya the bedding dips at approximately 60° to 090°, and to the north-west of Koonya the bedding dips at about 45° to 045°.

Within the polymict breccia and slumped epiclastics, weak graded bedding was observed. All grading consistently showed an uphole fining of the sequence. Assuming normal grading this corresponds to an upright facing for the sequence.

Chapter 3: MINERALIZATION

The mineralization at Koonya is mineralogically simple but its spatial arrangement is complex. Four styles of mineralization occur through the prospect: veins, bands, massive sulphide and disseminated sulphide. For the majority of the mineralized areas only five sulphides were recognized: pyrite, sphalerite, galena, chalcopyrite and small amounts of pyrrhotite. However, in one zone very minor amounts of arsenopyrite, tetrahedrite, bismuth, aikinite and hematite were observed. A wide range of textures were also observed, most of which are associated with deformation, recrystallization and annealing. Banding of sulphides was observed in association with the massive sulphide.

Three different horizons of mineralization have been recognized at Koonya. The uppermost mineralized horizon occurs in both the east-west (cross) section and the north-south (long) section. The other two mineralized horizons occur only in the north-south section. It is convenient to consider the uppermost mineralized horizon, which occurs in both the long section and cross section, as two separate zones, one in the cross section (the main lead-zinc zone) and one in the long section (the upper zone). This is because the styles of mineralization in the two sections are very different.

A major zone of mineralization occurs in the east-west section and has been collectively termed the 'main lead-zinc zone'. It consists of a thin, east dipping, massive sulphide layer with vein style mineralization continuing down dip (figure 3.1).

The three mineralized zones defined in the north-south section are separated from each other by over one hundred metres (vertically) of barren rock. They have been termed the 'upper zone', 'middle zone', and 'lower zone' (figure 3.2). The upper zone mineralization is the southerly extension of the main lead-zinc zone.

Section 3.1 The East-West Section

The main lead-zinc zone is generally less than ten metres in vertical extent and can be traced for several hundred metres. The mineralization occurs in two distinct forms, either as a thin sulphide-rich horizon (termed the 'massive sulphide' horizon) or as veins and disseminations (referred to as 'zone B'). Both these styles of mineralization will be described in detail. The zone B mineralization appears to be a down dip extension of the massive sulphide (figure 3.1).

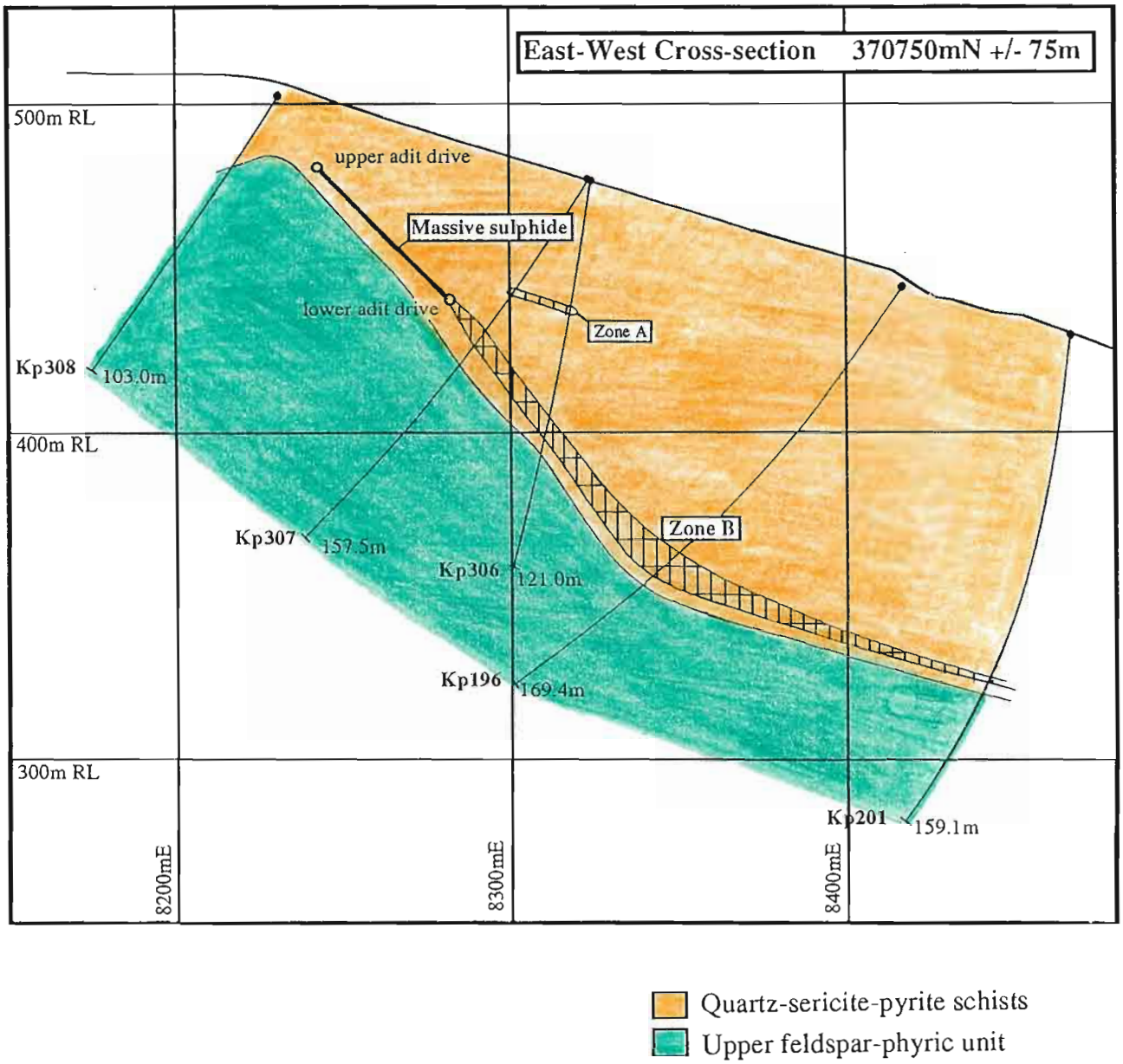

Figure 3.1: Mineralization in the east-west section

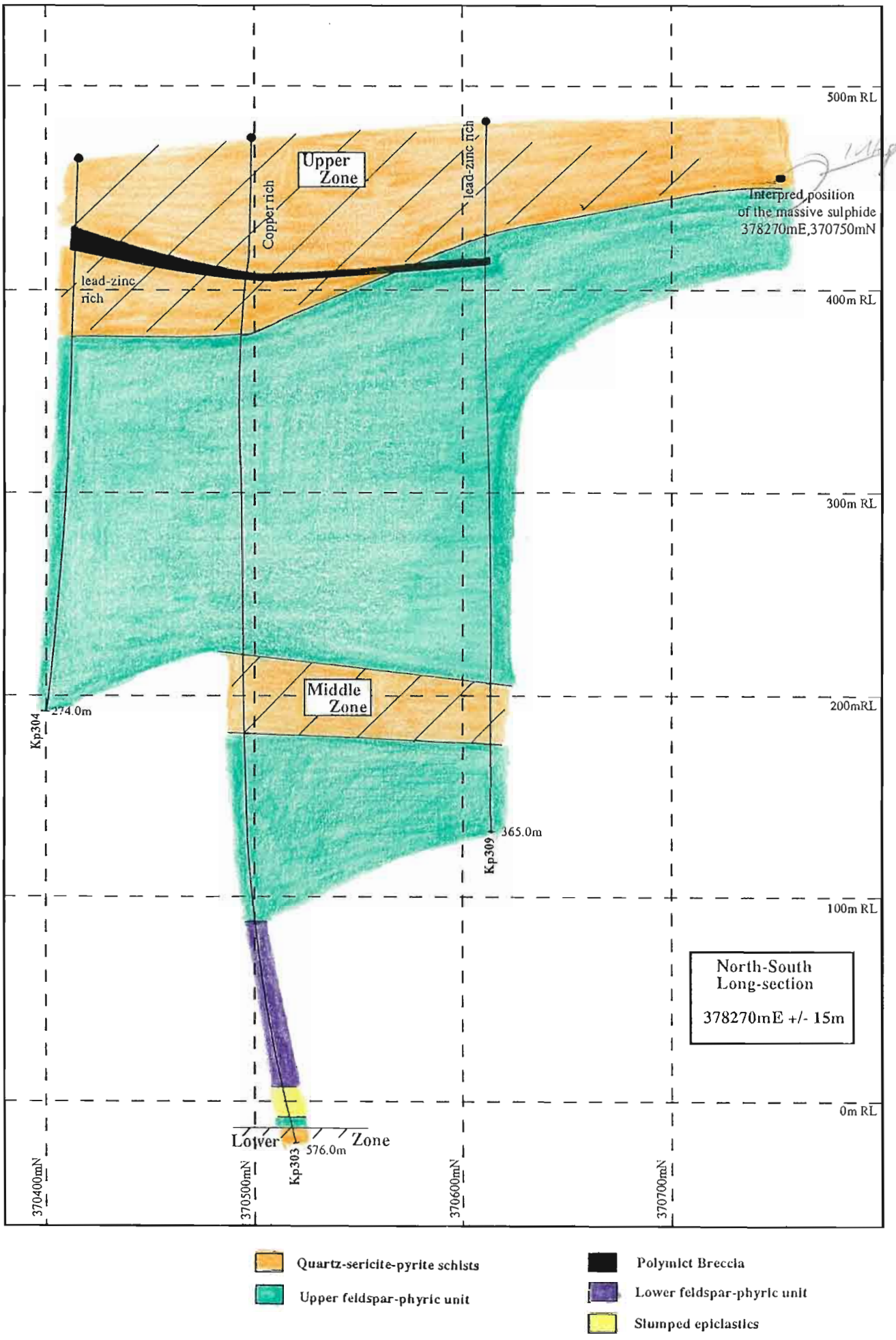

Figure 3.2: Mineralization in the north-south section

A limited zone of minor lead-zinc veining and disseminations also occurs in the east-west section above the main lead-zinc zone. This mineralization was only observed in two drillholes, Kp306 and Kp307, and is refered to as 'zone A'. The zone A mineralization will be discussed in the section on zone B as the mineralization styles are similar.

3.1.1 Massive Sulphide

The massive sulphide horizon is a narrow lens of reasonably high grade galena and sphalerite (3% to 30%). It is intersected by two adits (figure 3.1). In both cases the mineralization is 1 to 2 metres thick and 30 to 40 metres wide. The adits are separated by a down dip distance of about 50 metres. The massive sulphide is interpreted to extend between the two adits. In the top adit the mineralization strikes approximately 180° and dips 45° to the east. As well as intersections in the two adits, thin segments of the massive sulphide are intersected in two drillholes, Kp307 and Kp196. In Kp307 the mineralization is expressed as a 5 to 10 centimetre horizon at the very bottom of the mineralized zone. In Kp196 the extent of the massive sulphide is unknown due to removal of most of the ore zone for assay, however; both the high lead-zinc content (over 25% in places) and one sample from 123.4m suggest the presence of some massive sulphide in the deepest part of the mineralized zone.

3.1.1.1 *Mineralogy and Textures*

The mineralogy of the massive sulphide intersected in the adits is very simple, consisting of pyrite, sphalerite and galena. Chalcopyrite is also present as chalcopyrite disease in sphalerite but no grains larger than 0.02mm were observed. The dominant gangue mineral was quartz but minor chlorite is also present.

The sphalerite is homogeneous in colour (brownish-orange) and occurs as individual grains, generally <0.5mm in size, or as much larger aggregates. Most sphalerite contains chalcopyrite disease (plate 9). The chalcopyrite disease occurs mainly at the grain edges or in cleavage planes near the grain boundaries of the sphalerite, but the cores of the sphalerite grains are generally less affected. All chalcopyrite within sphalerite is approximately 0.0025mm or smaller.

Galena is reasonably abundant in the massive sulphide. It occurs in several different forms. The most obvious is large interconnected aggregates typically 0.1mm to 0.5mm in size. Sometimes galena in this interconnected form totally rims sphalerite grains (plate 12). This texture is interpreted to result from metamorphism (Mills 1976) rather than being indicative of a

primary paragenetic sequence. The second form of galena is as small, wispy, cuspate grains within sphalerite (plate 13). The third form of galena is tiny anhedral grains (generally ≤0.0025mm) disseminated through sphalerite. Both this texture and the previous textural styles are thought to indicate metamorphism of the galena and sphalerite (Mills 1976, Craig and Vaughan 1981).

Pyrite is the most abundant sulphide mineral in the massive sulphide samples. It generally occurs as subhedral to euhedral grains 0.05mm to 0.25mm in size although some grains may exceed 0.5mm. A less significant form of pyrite is as very small subhedral inclusions, often less than 0.0025mm, within sphalerite. Larger grains of pyrite, when contained in sphalerite or galena, often have strongly embayed margins indicating that they are being replaced by the galena and/or sphalerite (plate 10). This texture may be a result of two processes: either it reflects a paragenetic sequence in which the pyrite forms first, then is partially replaced by the galena and sphalerite, or it is a metamorphic texture related to the annealing of pyrite in the presence of sphalerite and galena (Craig and Vaughan 1981). The presence of this embayed pyrite in most of the other zones of mineralization suggests a metamorphic or annealing origin.

A rarer type of pyrite results from the annealing together of individual pyrite grains into a single larger grain. In several places where this annealing has occurred, another phase such as galena has been trapped in the cluster of pyrite grains so that the internal boundaries of the pyrite grains are visible. Another form of pyrite observed in one sample from the massive sulphide was a very limited late stage overgrowth of pyrite at the edges of some sulphide minerals facing onto quartz gangue. These overgrowths have a distinctly colloform nature although they are only 0.01mm to 0.02mm thick (plates 11 and 12).

The dominant gangue mineral in the massive sulphide is quartz. Quartz grains range from 0.01mm to 0.2mm in diameter. Many of the medium sized grains have irregular serrated edges and appear undulose. This texture is characteristic of low temperature deformation (Vernon 1976).

One of the major textures observed in the massive sulphide samples was banding. In most cases this banding occurred either between sphalerite/galena layers and pyrite, or sulphides and gangue. Generally the banding was not well developed and could have been either a primary feature or the result of deformation (plate 14, samples upperadit1, upperadit2). In Kp196 some well developed, possible primary banding was observed in the sample from 123.4m. This banding has been folded by later deformation (plate 14, sample Kp196 123.4m).

Plate 9: Upperadit 2, 0.23mm, x400, PP Chalcopyrite diseased sphalerite. The photomicrograph shows the edges of two sphalerite grains. The chalcopyrite disease is concentrated in cleavage planes at the edge of the sphalerite grains.

Plate 10: Upperadit 1, 0.83mm, x100, RL Embayed pyrite grains (yellow) within galena (light grey) and sphalerite (dark grey). This texture is common throughout most of the mineralization.

Plate 11: Upperadit 2, 0.093mm, x1000, RL Tiny colloform pyrite growths associated with gangue within the massive sulphide. A thin overgrowth of pyrite can be seen on the pyrite grain on the right side of the photomicrograph.

Plate 12: Upperadit 2, 0.37mm, x200, RL Galena (light grey) rimming a sphalerite grain. On the right side of the photomicrograph small colloform pyrite (yellow) growths at the edge of the sphalerite mass can be seen.

Plate 13: Kp196 123.4m, 0.86mm, x100, RL Wispy, cuspate, irregular galena grains (light grey) and anhedral galena masses within sphalerite.

Plate 14: Upperadit 1 / Upperadit 2 / Kp196 123.4m, 80mm, --, AL Three handspecimens of the Koonya massive sulphide. Weak banding can be seen in the two samples on the left. The sample from Kp196 shows strong banding of sulphides, which appears to have been folded in several places by later deformation.

Plate 15: 307 zB2a / 307 zB2, 50mm, --, AL The second style of veins observed in the zone B mineralization. These veins are very irregular and appear to replace generally chloritic, quartz-sericitic rocks. Sample 307 zB2 contains a small 'island' of the host rock within the vein.

Plate 16: 306 76.3m / 307 zB3, 50mm, --, AL Typical veins from the zone B mineralisation with chloritic edges and sphalerite-galena-pyrite-quartz±chalcopyrite centres.

Plate 17: 307 zB2, 0.66mm, x100, XP An intricate intergrowth texture between sericite and galena (opaque) that occurs in the second type of veining defined in zone B.


9


10

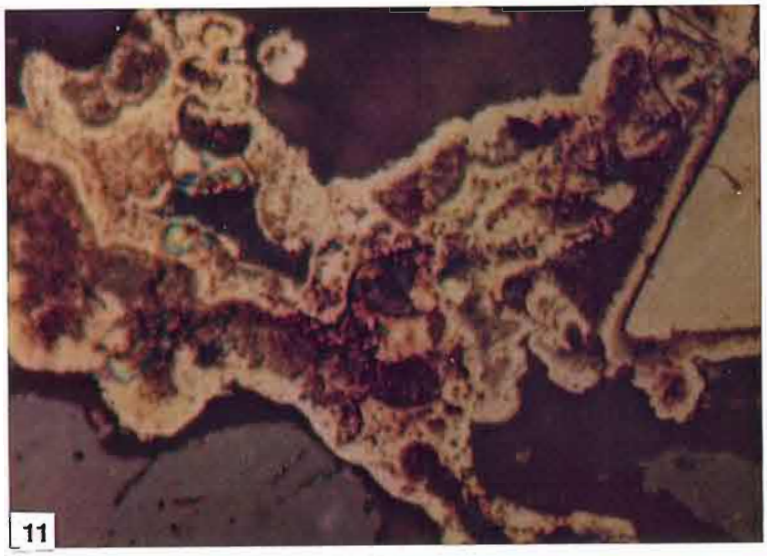
11

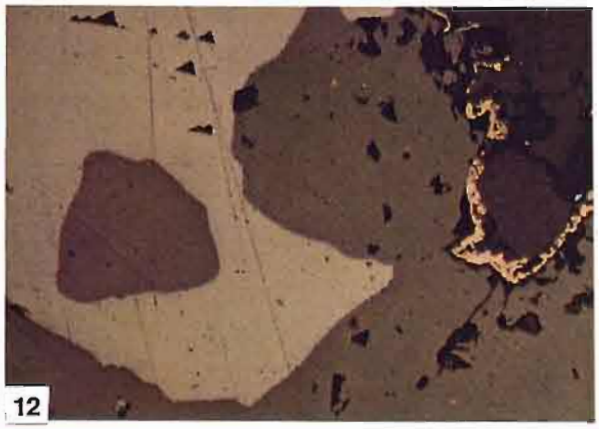
12

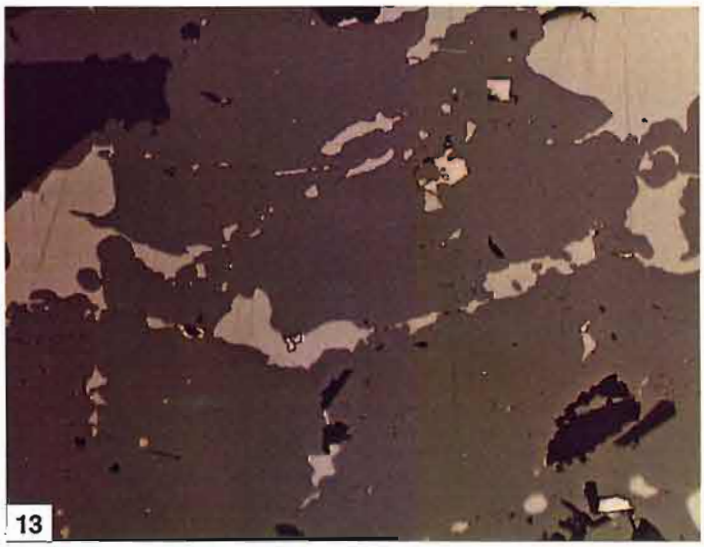
13

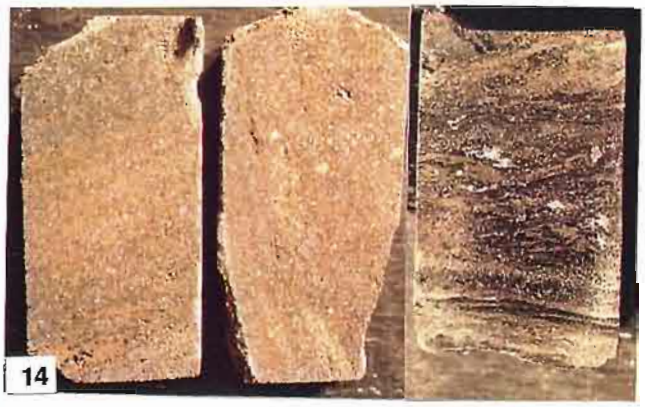
14


15


16


17

3.1.2 Zone B

Zone B is a narrow horizon (less than 10 metres in vertical extent) of vein style and disseminated lead-zinc. Strike line constructions reveal that the strike of the zone B mineralization changes as it extends away from the massive sulphide. The dip and dip direction change from 45° to 090° at the top of the massive sulphide to 40° to 150° below the mineralized intersection in drillhole Kp196. This can be seen on the east-west section as a flattening of the dip between Kp196 and Kp201 (figure 3.1).

Two distinctly different types of veins were recognized in zone B. The first type is characterized by chloritic edges and pyrite-sphalerite-galena-quartz±chalcopyrite through the rest of the vein (plate 16). This type of vein is generally folded and partially sheared into the dominant cleavage. The second type of vein is very irregular and appears to replace the rocks, often containing islands of host rock within the vein. These veins are much less common and their relationship to the cleavage is not clear (plate 15).

The zone A mineralization is very restricted in its extent (figure 3.1). It consists of thin lead-zinc-pyrite±chalcopyrite veins, similar to the first style of veining recognized in zone B, as well as lesser disseminations.

3.1.2.1 *Mineralogy and Textures*

Most of the zone B (and zone A) mineralization is dominated by a sphalerite-galena-pyrite assemblage with minor chalcopyrite and pyrrhotite.

The sphalerite occurs as anhedral grains or masses, and often contains chalcopyrite disease or tiny inclusions (≤0.0025mm) of disseminated pyrrhotite. In one sample, Kp305 148.3m, the tiny pyrrhotite inclusions were clustered at the sphalerite grain boundaries (plate 18). This migration of pyrrhotite to the grain boundaries is probably a result of metamorphism of the sphalerite (Craigh and Vaughan 1981 report similar textures for chalcopyrite). The sphalerite in this sample consistently showed triple point junctions of approximately 120°. This texture is interpreted as resulting from annealing of the sphalerite (Mills 1976).

The galena in the zone B samples shows a similar range of textures and forms as in the massive sulphide, that is, anhedral grains and masses, wispy cuspate grains and tiny inclusions in sphalerite. Galena rimming sphalerite grains was also observed. As previously mentioned, most of these textures are considered to be due to metamorphism. In one sample, Kp305

148.3m, the cleavage planes in the galena masses have clearly been deformed (plate 19). In the second type of veining in zone B, an interesting intergrowth texture with irregular thin 'channels' of sericte laced through galena was noted (plate 17). The significance of this texture was not understood.

Chalcopyrite does occur in both the zone B and zone A mineralization, mainly as chalcopyrite disease. However in one sample, Kp307 zA2, grains of anhedral chalcopyrite exceeding 0.1mm in size were observed.

The range of pyrite occurrence in the zone B and zone A mineralization is similar to that observed for the massive sulphide. In particular, the strong embayment of pyrite within sphalerite and/or galena is present in almost all of the samples. Several fractured pyrite grains were also observed in more strongly deformed samples. Pyrite also occurs as disseminated grains throughout zones B and A. This disseminated pyrite is typically 0.02mm to 0.2mm in size and generally euhedral, although some smaller grains are subhedral to anhedral.

Section 3.2 The North-South Section

Three distinct zones of mineralization were intersected in the north-south section. These mineralized zones are referred to as the upper zone, middle zone and lower zone based on the depth at which they occur. Figure 3.2 shows the position of the mineralized zones in the north-south section. The upper zone is the most complex and it shows strong metal zonation.

3.2.1 Upper Zone

The upper zone occurs in the top part of the north-south section. In Kp309 the upper zone extends to a depth of approximately 57m and in Kp303 and Kp304 it extends down to depths of 98m and 89m respectively (figure 3.2). The upper zone represents the three dimensional extension of the main lead-zinc horizon, but the styles of mineralization are very different in the two zones. The upper zone is discordent to the bedding and is seen to crosscut the breccia horizon in the north-south section (figure 3.2).

Plate 18: 305 148.3m, 0.086mm, x1000, RL Tiny pyrrhotite grains (yellow) occurring along the edges of individual sphalerite grains within a sphalerite mass.

Plate 19: 305 148.3m, 1.59mm, x50, RL Deformed cleavage planes in an anhedral galena mass. A fractured pyrite grain (yellow) can also be seen.

Plate 20: 309 22.9m, 12.7mm, x6.3, XP

A strongly sheared and folded thin quartz-sphalerite vein.

Plate 21: 303 89.2m, 27.6mm, x3.2, XP

A folded chlorite fragment within deformed chalcopyrite-pyrite mineralization.

Plate 22: 303 53.9m, 0.8mm, x100, RL This photomicrograph shows several pyrite grains (cream-yellow) annealing to form a larger pyrite grain. It also shows embayed pyrite grains within chalcopyrite masses (darker yellow).

Plate 23: 303 89.2m, 0.21mm, x400, RL The interesting textures often seen between chalcopyrite (darker yellow), pyrite (light yellow to pinkish yellow), arsenopyrite (light bluish-grey) and tetrahedrite (darker grey).

Plate 24: 303 274.3m, 25.7mm, x3.2, PP

A sheared sphalerite-chlorite vein from the middle zone.

Plate 25: 309 302.1m, 27.6mm, x3.2, PP Disseminated patches of sphalerite plus sericite in a quartz-sericite groundmass. Several patches have tabular shapes and may represent replacement of feldspar grains.

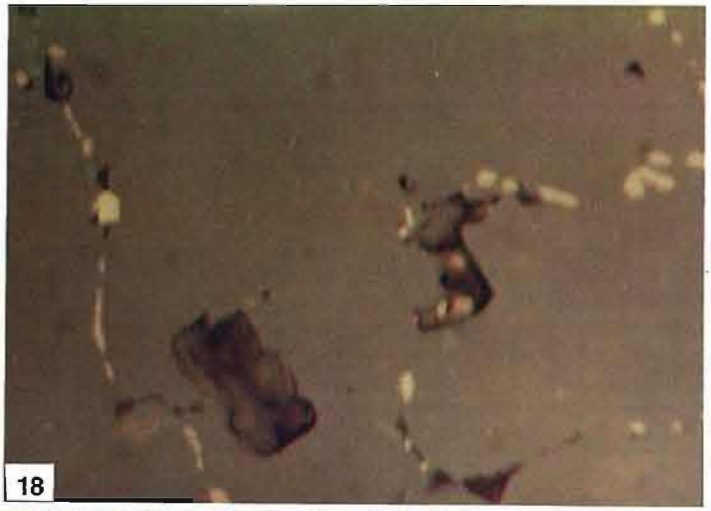
18


19

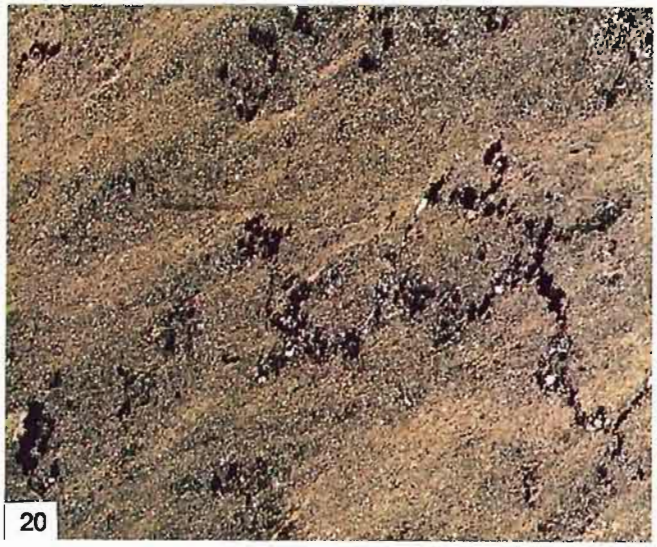
20


21

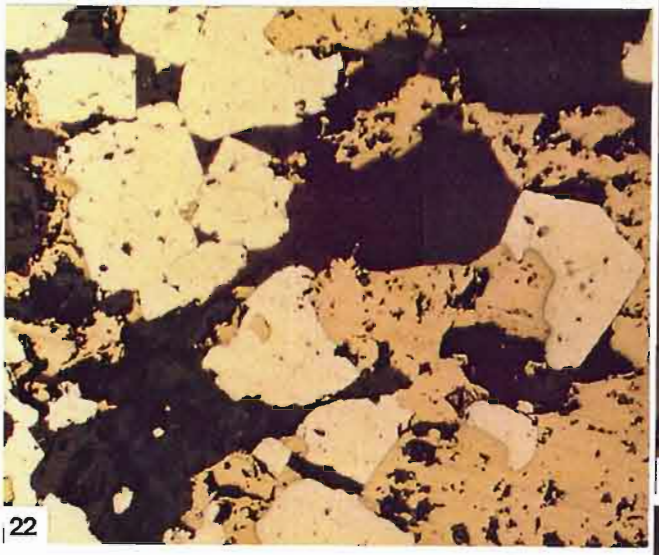
22

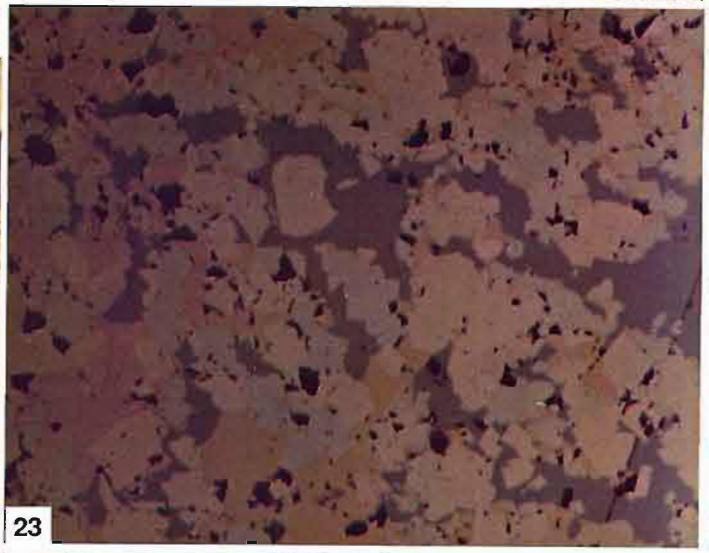
23

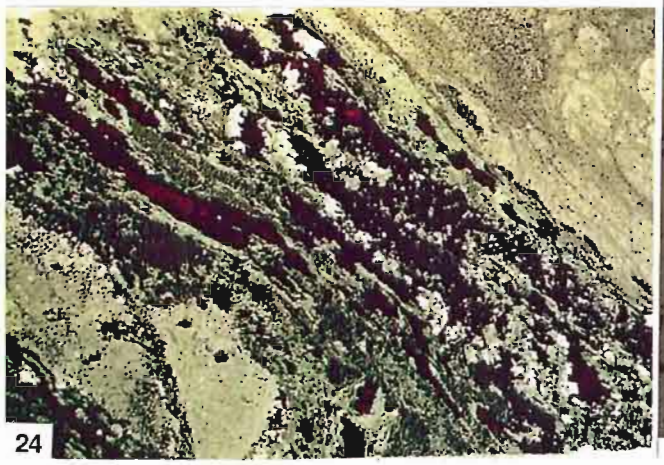
24


25

The upper zone exhibits various mineralogies suggesting an overall metal zonation along the horizon. In drillhole Kp303 the mineralization is relatively copper-rich with only minor lead and zinc (less than 0.1% combined Pb+Zn). This is in contrast to mineralization in the drillholes on either side of Kp303 which are relatively lead-zinc-rich (grades exceeding 0.5% combined Pb+Zn) and copper-poor.

In all three drillholes intersecting the upper zone the greatest concentration of mineralization occurs at or very near the bottom of the zone.

3.2.2.1 *Mineralogy and Textures*

The mineralogy of most of the upper zone is simple, with galena, sphalerite, chalcopyrite, pyrite and pyrrhotite being the only sulphides present.

Sphalerite was observed in all samples from the upper zone. In the copper-rich zone the sphalerite occurs as occasional disseminated grains riddled with chalcopyrite disease. Craigh and Vaughan (1981) indicate that such high concentrations of chalcopyrite disease cannot be due to exsolution. This suggests that the chalcopyrite is replacing the sphalerite. In the lead-zinc-rich zones sphalerite occurs either as disseminated grains or in thin (≤0.1mm) quartz-sphalerite veins. The sphalerite generally shows strong evidence of folding and partial deformation into the cleavage (plate 20). Tiny inclusions of pyrrhotite (≤0.0025mm) are commonly disseminated throughout the sphalerite. Some of the sphalerite observed in the lead-zinc-rich sections contains minor chalcopyrite in the form of chalcopyrite disease.

The concentration of galena is generally limited throughout the upper zone. In the copper-rich zones it occurs as small grains ≤0.1mm in size. In the more lead-zinc-rich mineralization it occurs as small grains or tiny inclusions in sphalerite. In one sphalerite-rich sample, Kp309 22.9m, the galena occurred either as tiny grains at the edge of the sphalerite grains or in very thin cracks within the sphalerite. This texture is probably a result of deformation and/or metamorphism of the sphalerite (Mills 1976, Craigh and Vaughan 1981).

Chalcopyrite is mainly restricted to the Kp303 drillhole although some chalcopyrite was observed in Kp304. Chalcopyrite in Kp309 appears to occur mainly as chalcopyrite disease in sphalerite. In the copper-rich zones the chalcopyrite is associated with pyrite, generally forming veins or concentrated patches through pyritic zones (up to 0.10 metres wide). In the areas of highest concentration the chalcopyrite occurs as anhedral masses. At lower concentrations,

small anhedral grains of chalcopyrite are often found in contact with pyrite grains. The highly irregular shapes of the chalcopyrite veins suggest they have been deformed. One sample, Kp303 89.2m, contains a strongly folded chlorite patch in a chalcopyrite-pyrite-rich zone (plate 21).

Pyrite is by far the most common sulphide phase in the upper zone. The highest concentration of pyrite occurs in drillhole Kp303 associated with the copper-rich mineralization. Pyrite grains range from 0.05mm to 0.5mm in size but average 0.05mm to 0.2mm. The grains are generally euhedral but some of the smaller grains may be subhedral to anhedral. The concentration of pyrite in any 20 centimetre segment of core ranges from 1% to >80%. In the more concentrated sections, larger pyrite grains were observed; these appeared to be annealed aggregates of smaller pyrite grains.

One sample, Kp303 89.2m, contained a much more diverse mineral assemblage than the other samples from the upper zone. The main ore minerals were chalcopyrite and pyrite, however lesser amounts of arsenopyrite, a mineral of the tenantite-tetrahedrite series (probably tetrahedrite on the basis of a qualitative microprobe analysis), hematite, a bismuth-lead-copper sulphosalt and native bismuth were also observed. Microprobe analysis suggests the bismuth sulphosalt is aikinite ($CuPbBiS_3$).

The arsenopyrite occurs as small grains associated with tetrahedrite and pyrite within an anhedral chalcopyrite mass. This intergrowth is unusual and may indicate replacement or perhaps breakdown of another unknown mineral phase (plate 23). The aikinite occurs as small irregular grains and is closely associated with tiny grains of native bismuth. These bismuth minerals occur within an anhedral mass of chalcopyrite. The hematite generally appeared to be associated with gangue although it was found intergrown with small euhedral pyrite within an anhedral mass of chalcopyrite

The paragenetic sequence represented by this sample appears to be: an initial phase of pyrite, a later phase of chalcopyrite, fine-grained pyrite, tetrahedrite, arsenopyrite and the bismuth minerals, then the last phase of hematite and associated gangue. However, some care must be taken when interpreting the paragenesis because some of the textures are likely to be due to metamorphism.

It is interesting to note that a very similar mineral assemblage to that observed in sample Kp303 89.2m has been observed at Rosebery with tetrahedrite, arsenopyrite, aikinite, native bismuth and other bismuth sulphosalts occuring in chalcopyrite-pyrite-rich ore (Brathwaite 1974, Green

et al. 1983, Huston and Large 1988). This suggests the metal source and/or fluid conditions at Koonya may have been similar to those that occured at Rosebery.

3.2.2 Middle Zone

The middle zone is intersected in two drillholes, Kp303 and Kp309 in the north-south section. In both drillholes the middle zone is dominated by disseminated sphalerite-rich mineralization with variable pyrite. A few veins, containing sphalerite and minor galena with chloritic or sericitic edges, were observed throughout this zone. In most one metre assays the sphalerite content is an order of magnitude greater than the galena content (appendix 2). In both drillholes weak lead-zinc mineralization does extend deeper than shown in Figure 3.2, but is only patchy.

3.2.2.1 *Mineralogy and Textures*

Sphalerite was a major component of the middle zone mineralization and occurs as disseminations or within veins. The disseminated sphalerite grains are anhedral and generally 0.1mm to 1.0mm in size. An unusual form of disseminated sphalerite was observed in samples from Kp309 in which sphalerite and sericite appeared to be pseudomorphing feldspar grains (plate 25). Veins ranged from thin, strongly deformed sphalerite-quartz veinlets to thicker deformed sphalerite-pyrite±chlorite±quartz±sericite veins (plate 24). The sphalerite ranged from being almost entirely free of small inclusions of other minerals to being either weakly chalcopyrite diseased or containing tiny pyrrhotite inclusions (≤0.0025mm).

Galena is much less common than sphalerite in the middle zone. Several disseminated grains of galena were observed but it was generally observed within veins. The only galena observed in thin section occurred as small wispy cuspate grains approximately 0.05mm in size.

Pyrite in the middle zone varied from concentrations of about one percent to greater than ten percent. The pyrite grains are mainly disseminated through the rock as subhedral to euhedral grains 0.01mm to 0.1mm in size. Pyrite within veins was generally coarser (0.05mm to >0.2mm). Pyrite grains occurring in sphalerite or galena were often embayed and partly replaced. As mentioned previously, this may represent a paragenetic or metamorphic texture.

The dominant textures observed in the mineralization were deformation of the sulphides. This was observed as shearing of individual disseminated grains into the cleavage, shearing plus contortion of thinner sphalerite-quartz veins, and shearing of thicker sphalerite-chlorite-galena

veins. Another texture observed was disseminated patches of sphalerite and associated sericite with markedly tabular shapes. It is possible that this texture represents a replacement of feldspar by sphalerite and sericite.

3.2.3 Lower Zone

The lower zone is the deepest of the mineralized zones. The only intersection is in drillhole Kp303 at a depth of 568m. The mineralization occurred over the bottom eight metres of the drillhole (568m-576m). The lower zone mineralization was not studied in detail but it is dominated by disseminated sphalerite and galena. Several thin veinlets of sphalerite and pyrite were also observed. No thin sections or polished blocks were made of the mineralization so the mineralogy could not be described in detail.

Section 3.3: Timing of Mineralization & Fluid Temperature

3.3.1 Fluid Temperature

No direct evidence for fluid temperatures (eg. from fluid inclusions) was obtained, but it is possible to get some idea of the depositional temperature for the massive sulphide from the mineral assemblages and metal ratios.

The temperature of the fluid depositing the massive sulphide can be estimated from the mineralogy. There is virtually no copper in the massive sulphide, but in the upper zone, the three-dimensional extension of the massive sulphide, a zone of chalcopyrite-rich mineralization containing bismuth minerals was observed. By analogy with the nearby Rosebery mineralization and work by various authors (eg. Large 1977, Large et. al. 1988) the copper-bismuth-bearing mineralization suggests fluid temperatures of 270°C or more. However the massive sulphide, the extension of the upper zone mineralization, contains virtually no copper indicating that the depositional fluid was incapable of transporting significant copper by the time it reached the massive sulphide horizon.

Calculations from Large et. al. (1988) indicate that for conditions expected for a volcanogenic massive sulphide fluid at a temperature of 250°C, the copper concentration in solution should be about 2 ppm compared to about 1000 ppm for zinc. Higher temperature fluids would carry more copper. Therefore the low levels of copper in the Koonya massive sulphide relative to the upper zone would suggest a lower temperature of formation ($\leq$250°C).

A second piece of evidence suggesting depositional temperatures of between 250°C and 200°C for the massive sulphide is provided by the zinc ratio distribution (discussed shortly).

There is a third piece of evidence that gives an indication of fluid temperature. The presence of a high concentration of manganese very near the massive sulphide mineralization suggests deposition from a lower temperature fluid ($\leq$250°C). This is discussed in more detail in the section on alteration geochemistry.

3.3.2 Timing of Mineralization

The Koonya mineralization clearly pre-dates the regional cleavage associated with the Rosebery fault. This is obvious from the strong deformation and cleavage development within the mineralization and associated alteration halo. Based on the amount of annealing within the mineralization it also seems probable that the mineralization pre-dates either or both the regional Devonian metamorphism and/or the thermal metamorphism related to the Devonian granite intrusion.

The relationships of the mineralization to the cleavage precludes the possibility of formation of the mineralization from being related to fluids derived from the Devonian granite which clearly post-dates the deformational event (Lees 1987).

Section 3.4: Zinc Ratio Distribution

The zinc ratio or zinc number is defined as 100Zn/(Zn+Pb). In descriptive terms, it is the percentage of zinc relative to the combined lead-zinc content of the mineralization.

Recent work by Huston & Large (1987) based on deposits in the Mount Read Volcanics has shown that the major Cambrian volcanogenic massive sulphide deposits have zinc ratio distributions different to that of other styles of mineralization, both Cambrian and Devonian in age. They interpret the zinc ratios of these volcanogenic sulphides as indicating saturation of the hydrothermal fluids forming the deposits with respect to lead and zinc. Huston and Large (1987) also show that for fluids saturated in lead and zinc the zinc ratio is dependent on temperature and salinity but independent of oxygen fugacity, pH and activity of H_2S.

As discussed previously, four zones of mineralization have been recognized at Koonya, these being the:

- Main lead-zinc zone, east-west section
- Upper zone, north-south section
- Middle zone, north-south section
- Lower zone, north-south section

The main lead-zinc zone and the upper zone are part of the same mineralized horizon but it is useful to consider them separately. The zinc ratio distributions for these different zones has been calculated, and each will be discussed in turn.

3.4.1 The Main Lead-Zinc Zone

It is the main lead-zinc zone that is of primary interest to this study as it contains the massive sulphide horizon intersected in the two Koonya adits. There are two styles of mineralization within the main lead-zinc zone at Koonya. Firstly, there is the massive sulphide intersected by the Koonya adits, and secondly, veins and disseminations, collectively termed 'zone B', intersected in drillholes down dip of the massive sulphide. The available data for both zones has been collated and the zinc ratio distributions calculated.

3.4.1.1 Massive Sulphide

The zinc ratio data for the massive sulphide mineralization comes from sampling of the Koonya adits carried out in the 1950's and 1970's. A histogram of the zinc ratios for the adits is shown in figure 3.3. As can be seen in the histogram, the majority of the data has zinc ratios of 50 to 70. The mean value is reasonably high (61.4) and the standard deviation fairly small (10.5).

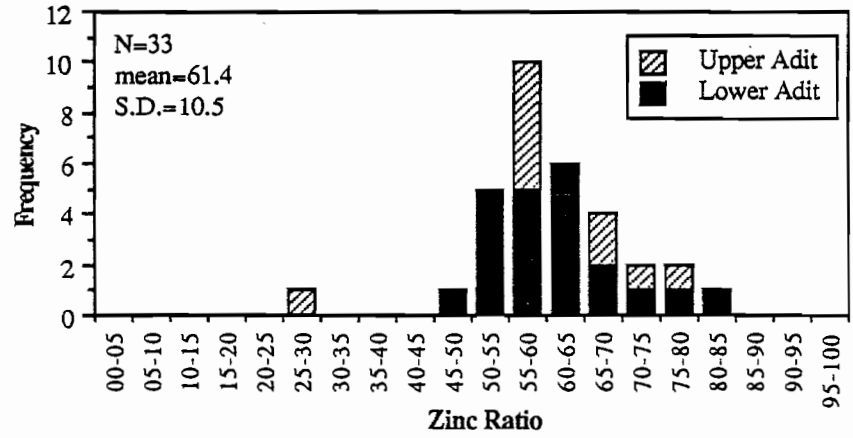

Figure 3.3: The zinc ratio distribution for the upper and lower Koonya adits. All samples exceed 3% combined lead+zinc.

The Koonya adits zinc ratio histogram has been compared to that of several other types of deposits, namely Cambrian volcanogenic massive sulphides, Cambrian vein systems and Devonian vein systems from the Mount Read Volcanics (figure 3.4). The similarity between the Koonya massive sulphide and volcanogenic massive sulphides is readily observed. In particular the zinc ratio distribution is very similar to that of South Hercules, with a similar mean value but a slightly larger standard deviation.

The fact that the Koonya massive sulphide has zinc ratios very similar to those of volcanogenic massive sulphides does not necessarily mean that the Koonya massive sulphide formed as an exhalative sulphide deposit. Rather it indicates that the hydrothermal fluid forming the mineralization was saturated with respect to lead and zinc at temperatures of approximately 200°C to 250°C.

Utilizing data from Huston & Large (1987) a zinc ratio of between 50 and 70 suggest that the fluid conditions were between 200-250°C and 0.5-1.0 molar weight percent NaCl equivalent (see table T3.1).

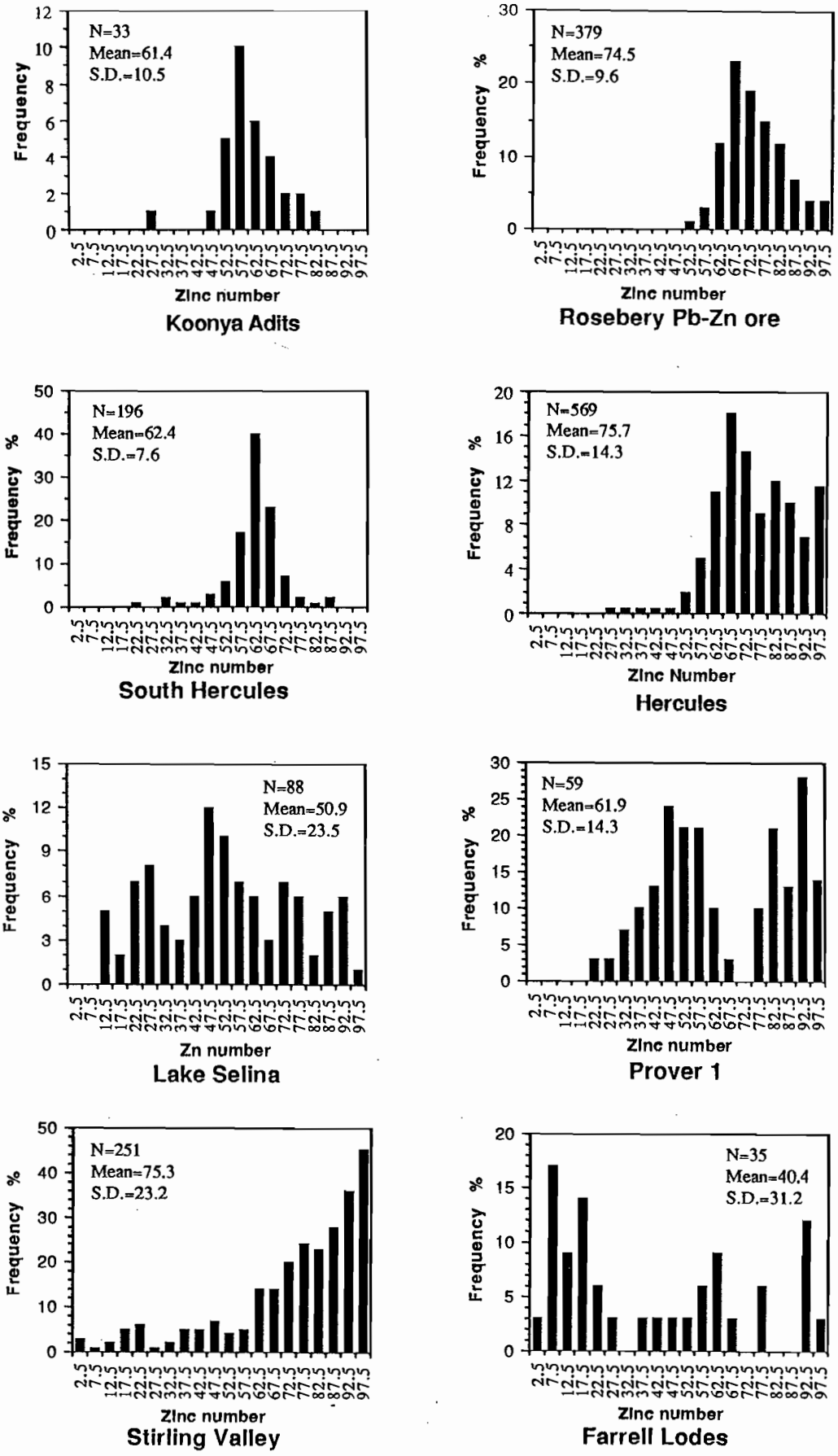

Figure 3.4: Zinc ratio histograms for various types of mineralization in the Mount Read Volcanics compared to the Koonya massive sulphide.

The Rosebery, Hercules and South Hercules deposits are considered to be Cambrian volcanogenic massive sulphides. Prover1 and Lake Salina are Cambrian lead-zinc vein style deposits. Farrell lodes and Stirling Valley are Devonian vein style deposits. [The histogram for South Hercules is from Khin Zaw (1989) and the other histograms are from Huston and Large 1987.]

temperature (°C)	Salinity (equiv. NaCl)				
	0.25m	0.50m	1.0m	1.5m	2.0m
25	99	99	98	98	98
50	97	97	97	97	97
100	93	91	91	92	93
150	86	83	83	85	87
200	73	66	62	65	68
250	61	58	68	77	83
300	34	24	15	11	9

Table T3.1: **The zinc ratios calculated by Huston and Large (1987) for fluids of varying temperatures and salinities. The values in the smaller oblong represents the most likely range of conditions to have formed the Koonya massive sulphide.**

3.4.1.2 Zone B

Down dip from the Koonya massive sulphide, intersected by various drill holes (Kp305, 306, 307, 196, 199, 200 and 201), is a vein and disseminated style of mineralization previously referred to as zone B (figure 3.1). A limited number of assays are available for each drillhole that intersects zone B. Histograms of the zinc ratio for the old drillholes (Kp196, 199, 200 and 201) and the new drillholes (Kp305, 306 and 307) as well as an overall histogram for zone B have been plotted (figure 3.5). The drill hole Kp308 also intersects zone B, but the mineralization is within the weathered zone. Under weathering conditions zinc is very mobile, so weathering will decrease the zinc ratio of the mineralization. For this reason the data from Kp308 has been disregarded.

The overall zinc ratio distribution obtained is distinctly different from that of the Koonya massive sulphide, however it does show some of the features of the massive sulphide distribution. In particular it is worth noting that very few of the zinc ratios are below 50. In this respect the zinc ratio distribution of this vein style mineralization is similar to that of a volcanogenic massive sulphide rather than a Cambrian or Devonian vein system. However, the zinc ratio distribution of the zone B mineralization is not nearly as constrained as that for a volcanogenic massive sulphide.

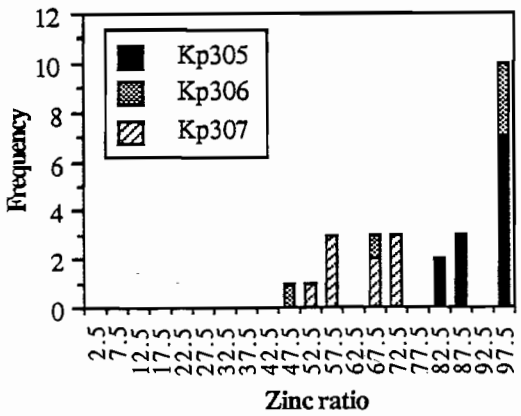

Zinc ratio histogram for the newer drillholes in 'zone B'

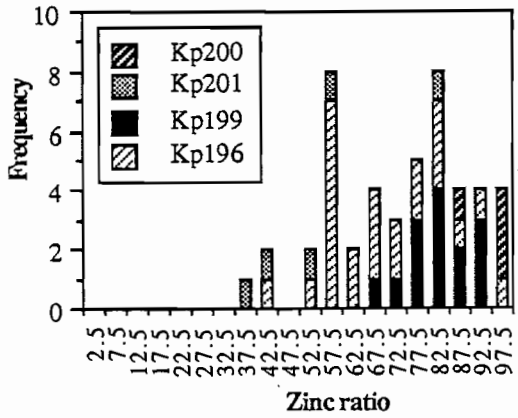

Zinc ratio histogram for the older drillholes in 'zone B'

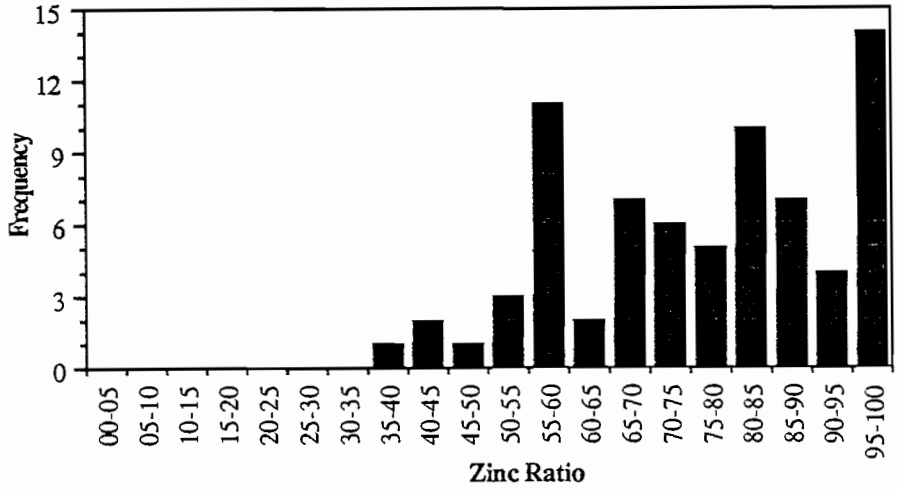

Overall zinc ratio histogram for 'zone B'

Figure 3.5: Zinc ratio distribution for the zone B mineralization

Two distinct possible explanations exist for the zinc ratio distribution obtained for zone B:

The first explanation could be that the fluid was saturated and the mineralization was deposited over a range of temperatures from 250°C to below 200°C. Temperatures below 200°C would produce the high zinc ratios observed. This explanation is quite feasible especially if the metal bearing fluid was subject to mixing with seawater (for example if it were at the edge of the mineralizing system).

The second explanation is that the hydrothermal fluids forming the mineralization was variably under-saturated in lead. This would also produce the higher zinc ratios observed for the zone B mineralization. One possible problem with this explanation is that the massive sulphide immediately up-dip from zone B appears to have been formed from lead saturated fluids.

3.4.2 Upper zone

The mineralization in the upper parts of drillholes Kp 303, 304 and 309 has previously been described in some detail. This horizon is the three-dimensional extension of the main lead-zinc horizon seen in the east-west section. For the most part, the mineralization consists of disseminations and veins. Only some portions of the upper zone in each drillhole have been assayed. The zinc ratio distributions of the sampled sections within each hole have been plotted. The data for the individual drill holes has then been combined into an overall zinc ratio histogram for the Upper Zone (figure 3.6).

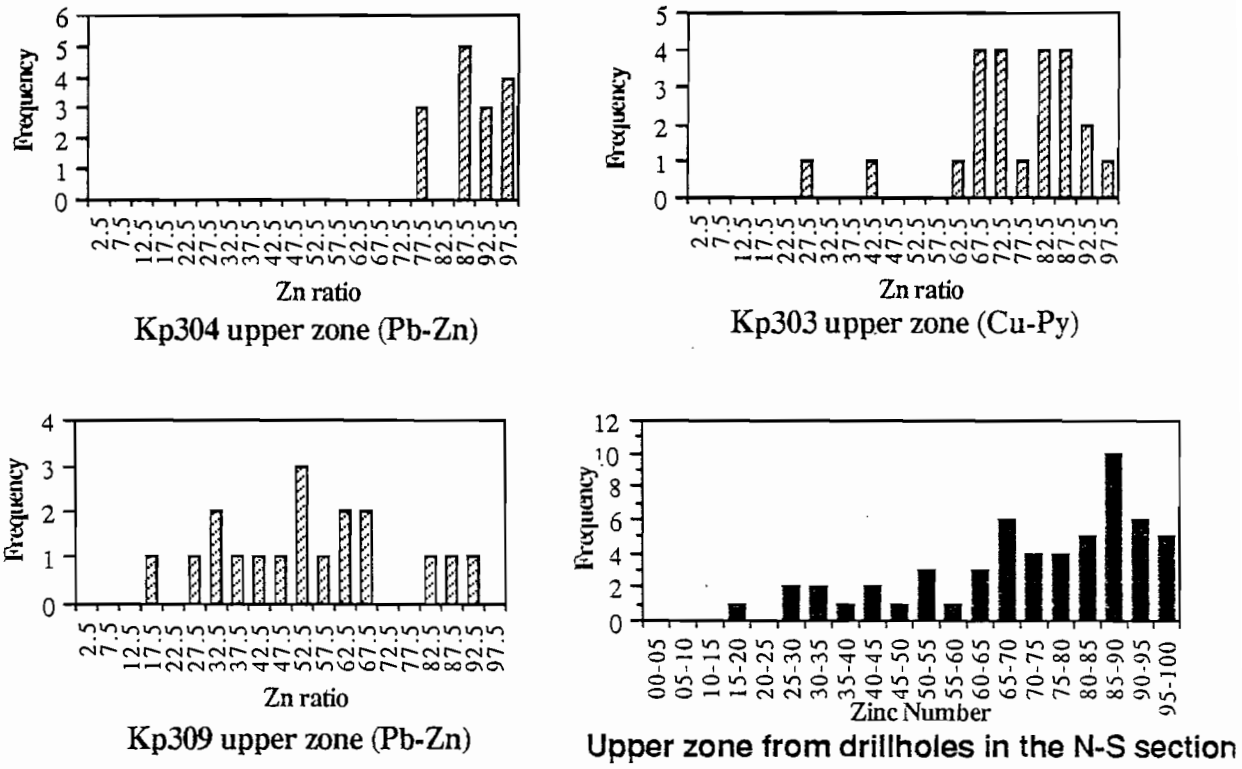

Figure 3.6: Zinc ratio distribution for the upper zone mineralization

The zinc ratio distribution for Kp303 and Kp304 are dominantly greater than 50. The zinc ratio values for Kp304 are tightly clustered while those for Kp303 show a greater spread. In contrast, the zinc ratio distribution for Kp309 is more spread out with a significant number of values below 50.

The mineralization in Kp303 is dominated by copper and pyrite with minor bismuth minerals. This mineral assemblage is considered to be indicative of higher depositional temperature (>250°C). Huston and Large (1987) show that for saturated fluids at this temperature the zinc ratio should be reasonably low (see table T3.1). However, it was found that the zinc ratios for Kp303 were actually reasonably high (between 60 and 100). This strongly suggests the fluids forming the copper-rich mineralization were under-saturated with respect to lead.

The mineralization in Kp304 has a very high (75 to 100), tightly constrained zinc ratio distribution. This type of distribution can be interpreted in two ways as previously discussed:

a) under-saturation of the hydrothermal fluid with respect to lead

b) deposition from saturated fluids with temperatures below 200°C

The presence of some copper (generally considered to be a higher temperature phase) in the mineralization would suggest that fluid temperatures were in excess of 200°C. This further suggests that the hydrothermal fluids were under-saturated with respect to lead.

In Kp309 the zinc ratio distribution for the upper zone mineralization shows a large spread of values ranging from 15 to 95. In many ways this distribution is similar to that seen for Cambrian or Devonian vein systems (refer to figure 3.4). The zinc ratio distribution could either be due to:

a) a large range in the of temperature of deposition (probably >200°C)

b) variable under-saturation to saturation of the fluid with respect to lead.

The second alternative, variable under-saturation, seems the most likely to have occurred.

A two-dimensional model of the upper zone and massive sulphide horizon can be envisaged. In this model the Kp303 mineralization is deposited from a fluid under-saturated with respect to lead, the mineralization in Kp309 is deposited from a fluid variably under-saturated with respect to lead and the massive sulphide is deposited from a saturated fluid. This gives an overall fluid zonation from south to north of:

under-saturated lead $\rightarrow\rightarrow$ variably under-saturated $\rightarrow\rightarrow$ saturated lead.

3.4.3 Middle Zone

The Middle zone is intersected by two drillholes, Kp303 and Kp309. A stacked column histogram has been plotted to show the zinc ratio distribution of each drillhole as well as the overall distribution for the Middle zone (figure 3.7). The data for Kp303 comes from depths of 256m-297m, while the data for Kp 309 comes from depths of 284m-325m.

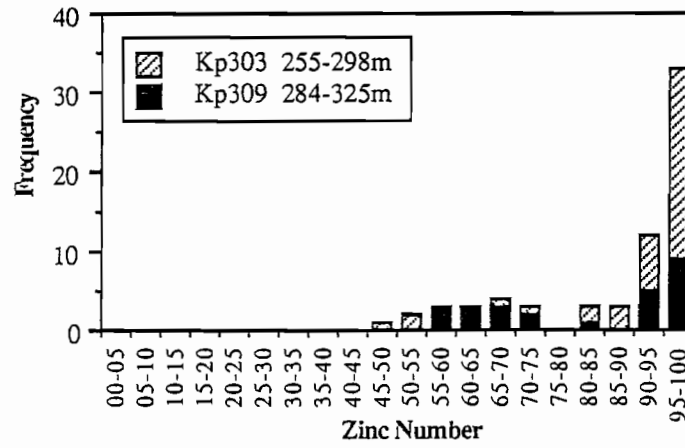

Figure 3.7: Zinc ratio distribution for the middle zone mineralization

Both drillholes show a fairly similar distribution with the majority of the data occurring at high zinc ratios. In many cases, the lead content of a sample is only a few hundred ppm or lower, while the zinc content may range from 0.1% to in excess of 1.0%.

Two possibilities exist to explain this type of zinc ratio distribution. These are, that deposition occurred from;

a) a lower temperature (≤200°C) saturated fluid;

b) a fluid under-saturated with respect to lead.

It is impossible to be sure which explanation is correct.

3.3.4 Lower Zone

The Lower zone is only intersected in one drillhole, Kp303. Only 8 metres of the zone was drilled before the hole was stopped, thus only a few zinc ratio values are available. Although only 7 values were obtained, the zinc ratio distribution is fairly tightly clustered between 70 and 90. This again suggests deposition from either lower temperature fluids (≤200°C) or fluids under-saturated with respect to lead.

Section 3.4 Lead Isotopes

Lead isotopes are one of the most powerful tools for determination of the relative age of lead bearing mineralization. A large data base exists for the Mount Read Volcanics on both Cambrian and Devonian mineralization (eg. Gulson & Porritt 1987). The lead isotope technique has been used on samples from the Koonya prospect in order to determine whether the lead was concentrated in the deposit in the Cambrian or Devonian.

3.4.1 Theory

The lead isotope technique is based on the fact that the ^{206}Pb, ^{207}Pb and ^{208}Pb isotopes are formed by the decay of the radioactive elements uranium and thorium. Throughout geological time, the concentration of ^{206}Pb, ^{207}Pb and ^{208}Pb has been changing; however the level of ^{204}Pb has remained constant. Thus at any point in geological time, the ratio of the radiogenic lead isotopes relative to the amount of ^{204}Pb will be different to that at any other time. The variation of the ratio of radiogenic lead against ^{204}Pb with time, is called the 'Growth Curve'.

If lead were to become concentrated in a certain area, such as an orebody, the ratio of decay elements relative to the ^{204}Pb is decreased by several orders of magnitude. This means that the change in the ratio of radiogenic lead (^{206}Pb, ^{207}Pb and ^{208}Pb) to ^{204}Pb is insignificant, effectively freezing the lead isotope signature to that at the time of lead concentration. Because the radiogenic lead isotopes are constantly changing with time for all lead at normal concentrations, orebodies formed at different times will preserve different lead isotope signatures. Thus by studying the lead isotope signatures of different deposits, some idea of the time at which the orebodies formed can be gained.

Gulson & Porritt (1987) have measured the lead isotopes of a number of deposits in the Mount Read Volcanics which are known to be either Cambrian or Devonian in age. From this they have constructed lead isotope fields for a number of the major deposits. As expected, their diagrams show a marked difference in the lead isotope signatures of the Devonian and Cambrian deposits. By comparing the lead isotope signatures of a deposit in the Mount Read Volcanics of unknown age to those that are known, it is possible to determine whether the lead is Cambrian or Devonian.

3.4.2 Results & Discussion

A total of fourteen lead isotope analyses have been carried out by the CSIRO Division of Exploration Geoscience (Dean and Carr 1989) on samples from the Koonya prospect, the majority of which come from the main lead-zinc mineralized zone. Three of the samples were analysed in 1986-87 and the other eleven were analysed in 1988. The samples are listed in Table T3.2 and the results plotted in Figure 3.8.

	location	type	mineralization	zone
1	upper adit	new	massive sulphide	
2	Kp306 76.1m	new	Pb-Zn vein	
3	Kp306 77.3m	new	Pb-Zn vein	main
4	Kp307 66.3m	new	Pb-Zn vein	lead-zinc
5	Kp 196 113.4m	old	Pb-Zn vein	zone
6 to 9**	Kp196 113.4m**	repeats	Pb-Zn vein	
10	Kp196 120.1m	old	Pb-Zn vein	
11	Kp201 111.3m	old	Pb-Zn vein	
12	Kp201 111.3m	repeat	Pb-Zn vein	
13	Kp303 91.7m	new	Cu-Py vein zone	Upper zone
14	Kp303 260.5m	new	Pb-Zn vein	Middle zone

Table T3.2: Lead isotope samples

As can be seen, the bulk of the data (10 analyses) is clustered in the lower part of the Rosebery 95% confidence ellipse. Four samples have $^{206}Pb/^{204}Pb$ ratios that differ significantly from the majority of the Koonya samples.

One of the older analyses has a significantly lower $^{206}Pb/^{204}Pb$ ratio than the other samples. Four repeat analyses of this sample are tightly clustered in the Rosebery ellipse (represented by the open box symbol labeled Kp196 113.4m). This marked difference between the repeat analyses and the original, indicates that the original result was incorrect and thus should be ignored.

One of the new analyses (labeled as Kp303 91.7m in figure 3.8) has a significantly higher $^{206}Pb/^{204}Pb$ ratio than the other Koonya samples. This is a very low lead sample with only 321ppm lead. As discussed by Gulson, Large & Porritt (1987), low lead samples, particularly those below 500ppm, are subject to significant radiogenic decay even if the host rock contains only a few ppm of uranium. The lower the lead concentration, the more significant the shift toward higher $^{206}Pb/^{204}Pb$. The presence of only 2 to 4 ppm uranium would be enough to have shifted the $^{206}Pb/^{204}Pb$ ratio of sample Kp303 91.7m from a signature similar to Rosebery to its present $^{206}Pb/^{204}Pb$ ratio. This would suggest that the $^{206}Pb/^{204}Pb$ ratio observed for this sample is in fact due to radiogenic decay effects on a low lead sample.

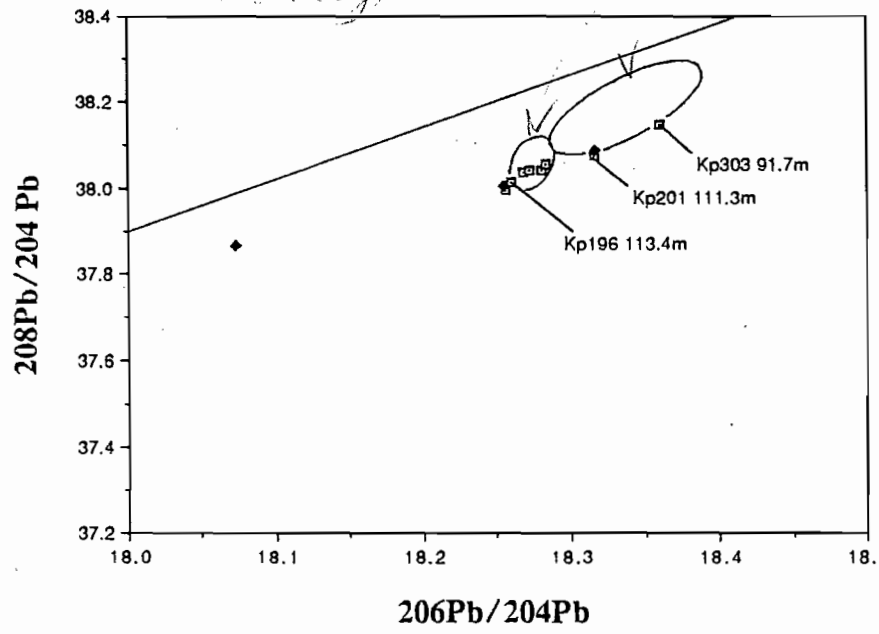

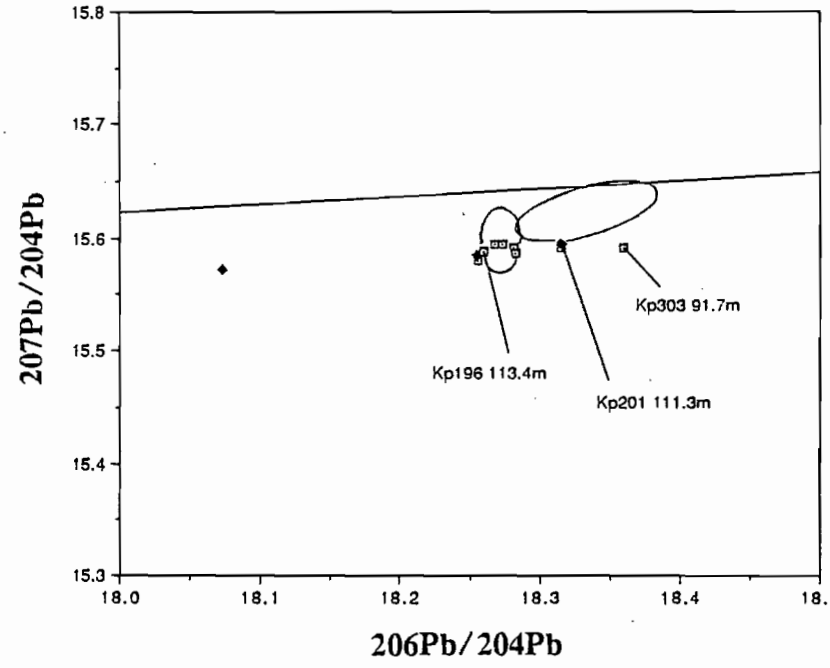

Figure 3.8: Lead isotope diagrams for the Koonya samples. The open squares represent new analyses and the black diamonds represent old analyses. The sample Kp196 113.4m is the average of four repeat analyses. (modified after Dean and Carr 1989)

Two samples, both an old and a new analysis of Kp201 111.3m (labeled in figure 3.8), plot very close together with a $^{206}Pb/^{204}Pb$ ratio somewhat higher than the bulk of the Koonya analyses. Unfortunately, the lead concentration of these samples is not known so it is uncertain whether this higher ratio represents a spread in the original lead isotopes or whether it is due to decay effects on a low lead sample.

As noted before, the majority of samples from Koonya have a lead isotope signature very similar to that of Rosebery. Thus, like Rosebery, the lead in the Koonya mineralization is likely to have been concentrated in the Cambrian.

Although the lead may have originally been concentrated in the Cambrian, it is still possible to have formed the Koonya mineralization in the Devonian by dissolving, transporting and re-precipitating the lead and zinc from a Cambrian deposit by Devonian metamorphic or granite related fluids. However this process is unlikely, especially because the mineralization seems to pre-date the granite intrusion.

The lead isotope signature of the Koonya deposit can be compared to other nearby deposits (see figure 3.9). These comparative samples are from:

a) Four samples, all from different drillholes, from the Rosebery Lodes prospect, a Cambrian exhalative Baritic Pb-Zn horizon.

b) Three samples from the Salisbury prospect, a Devonian vein system in the Rosebery fault zone.

c) Two samples from the Chamberlain prospect, another Devonian vein system in the Rosebery fault zone.

The two Devonian systems, Salisbury and Chamberlain, plot near the Devonian deposits, well away from the Koonya data. This indicates that Devonian deposits in the immediate area of Koonya do have a markedly different lead isotope signature to that of the Cambrian deposits confirming that it should be easy to differentiate Cambrian lead from Devonian lead in the Rosebery area.

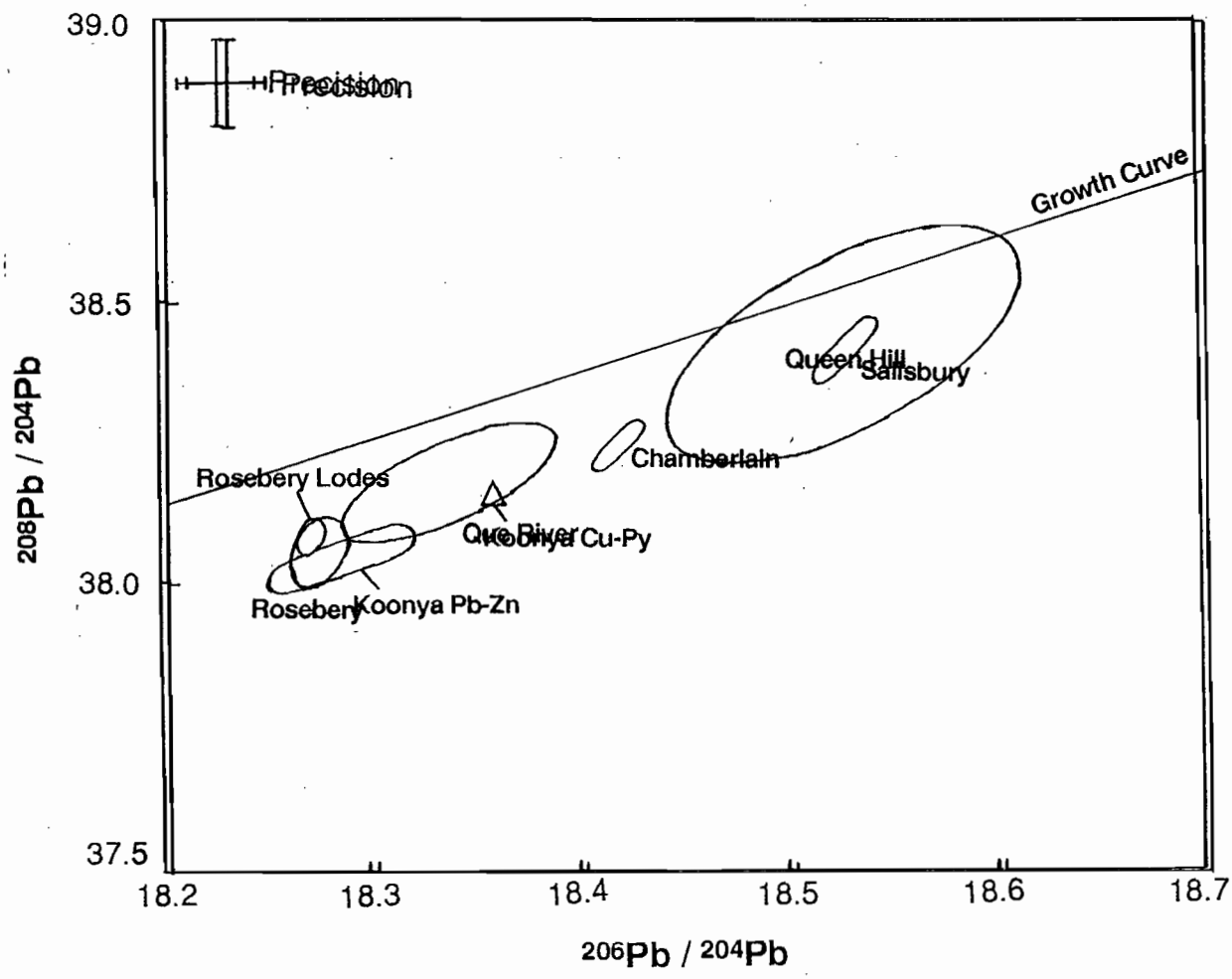

Figure 3.9: Comparison of the Koonya lead isotopes to nearby mineralization. (modified after Dean and Carr 1989)

The lead isotope signature of the Rosebery Lodes deposit is of particular interest, as it has been suggested that the Koonya mineralization is simply part of an alteration pipe for the Rosebery Lodes horizon (Rutherford 1986). If this were true, then both the Koonya and Rosebery Lodes prospects should have the same lead isotope signature. As can be seen in Figure 3.9 the lead isotope signatures of the two deposits seem to differ slightly; however this difference is not large enough to be certain that it is significant.

3.4.3 Summary

The lead isotope signature of the Koonya mineralization is similar to the Rosebery lead isotope signature, with the majority of samples actually having the same signatures. Examination of two Devonian deposits in the immediate Koonya area have very different lead isotopic values. This indicates that the lead was concentrated in the Cambrian and not the Devonian.

The Koonya lead isotope signature appears to be slightly different to that of the Rosebery Lodes mineralization. This seems to indicate that the two mineralized zones are not part of the one mineralizing system as suggested by Rutherford (1986). However, because of the relatively small difference between the two lead isotope signatures, it is impossible to be certain that they are, in fact, different.

Section 3.6: Sulphur Isotopes

Sulphur isotopes have in recent times been used to try and determine sulphur source and, to a lesser extent, the temperature of formation of sulphur-bearing mineralization. They have also been used to gain some idea of the variation of fluid conditions at different stages of mineral deposition. Although a potentially powerful technique, sulphur isotopes are not always definitive and their interpretation may be slightly ambiguous. The purpose of analysing sulphur isotopes from the Koonya prospect was two-fold. Firstly, it was hoped to delineate the possible sulphur source. Secondly, some idea of the variation of sulphur within the different mineralized zones was desired.

3.6.1 Theory

The sulphur isotope value is the ratio between the two most common stable isotopes of sulphur, ^{32}S and ^{34}S (^{32}S is much more common than the ^{34}S). The equation used to calculate the sulphur isotope value ($\delta^{34}S$) is

$$\delta^{34}S = 1000x \left\{ \frac{(^{34}S/^{32}S)_{unknown}}{(^{34}S/^{32}S)_{standard}} \right\} - 1000 \quad \text{(Ohmoto and Rye 1979)}$$

with the results being quoted as 'per mil' or ‰. The sulphur isotope value of a species/mineral is always measured relative to a standard. The standard generally used is the Canon Diablo Triolite or (C.D.T.).

The $\delta^{34}S$ value of species within a fluid phase is dependent on a number of parameters, particularly temperature and sulphur species present. Different sulphur species present within the same fluid, such as H_2S and SO_4, will have different $\delta^{34}S$ values dependent on the species' physiochemical properties. This difference in affinity of $\delta^{34}S$ between different sulphur species, is called fractionation. Fractionation is dependent on temperature such that $\delta^{34}S \alpha 1/T^2$ (Ohmoto and Rye 1979).

There are two major sources of sulphur; magmatic or sea-water. Magmatic sulphur, such as sulphur in minerals within volcanic rocks, has a $\delta^{34}S$ of about 0‰ to 3‰, whereas magmatic fluids given off by a magmatic intrusive may have higher $\delta^{34}S$ values (upto 5‰) (eg. Ohmoto and Rye 1979, McGoldrich 1988, Solomon et al. 1988). The sulphur isotopic value of sea-water is considered to have varied with time. The $\delta^{34}S$ value for sulphate in Cambrian sea-water is thought to have been in the range of 29‰ to 33‰, with the lower value dominant in the middle and late Cambrian (Claypool et. al. 1980 in Solomon et al. 1988).

3.6.2 Result and Discussion

A total of twenty-six samples were analysed for their $\delta^{34}S$ value. Two further values were found listed in Solomon et al. 1988. The samples were taken from the four mineralized zones, these being the:

- main lead-zinc zone, E-W section
- upper zone, N-S section
- middle zone, N-S section
- lower zone, N-S section

Table T3.3 lists the sample locations, the $\delta^{34}S$ values, and the mineral separates used for the analyses. Although some samples are shown as containing only one mineral, it is very difficult to guarantee the purity of the sample. In many cases it was impossible to obtain a mono-mineralic sample due to the intimate association of the ore minerals, so combined mineral samples were taken.

location	mineral	style of mineralization		d34S value
adit	Sph	massive sulphide		12.6
adit	Py	massive sulphide		12.5
adit	mixed	massive sulphide		12.1
Kp307 zone A	Py	sulphide vein		12.6
Kp307 zone A	Sph	sulphide vein	main	13.2
Kp307 zone B	mixed	sulphide vein	lead-zinc	12.8
Kp307 zone B	mixed	sulphide vein	zone	12.7
Kp307 zone B	mixed	sulphide vein		12.4
Kp307 zone B	Gn+Sph	sulphide vein		12.5
Kp306 38.1m	Py	disseminated pyrite		13.1
Kp306 76.3m	Sph	sulphide vein		12.5
Kp196 123.4m	mixed	sulphide vein		12.8
Kp305 148.3m	mixed	sulphide vein		12.4
**unknown	Py	unknown		13
**unknown	Py	unknown		12.7
Kp303 53.1m	Ccp	ccp vein		12.6
Kp303 53.1m	Py	disseminated/vein Py		13.5
Kp303 71.1m	Ccp	Ccp vein		10.8
Kp303 71.1m	Py	disseminated/vein Py	Upper	12.9
Kp303 89.2m	Py+minor Ccp	disseminated/vein Py	zone	10.8
Kp303 94.2m	Py+minor Ccp	disseminated/vein Py		10.8
Kp304 81.2m	Py+minor Ccp	disseminated/vein Py		11.3
Kp304 88.1m	Py+minor Ccp	disseminated/vein Py		10.8
Kp303 264.8m	Py	sulphide vein		11.6
Kp303 265.8m	Gn+Sph	sulphide vein	Middle zone	11
Kp303 274.3m	Py	sulphide vein		10.5
Kp303 568.9m	Sph+py	sulphide vein	Lower	9.5
Kp 303 570.3m	Py	sulphide vein	zone	9.3

Table T3.3: Sulphur isotope values from the Koonya mineralized zones

(Gn=galena, Sph=sphalerite, Py=pyrite, Ccp=chalcopyrite, 'mixed'= Gn+Sph+Py)

(The samples marked '**unknown' are from Solomon et al. 1988)

The $\delta^{34}S$ values obtained for 13 samples (plus 2 others listed in Solomon et al 1988) from the Koonya main lead-zinc zone are strongly homogeneous with a restricted range of 12.1‰ to 13.1‰. This range falls within the variation which might be expected for fractionation between pyrite, sphalerite and galena. Because variation in fluid conditions causes a change in the $\delta^{34}S$ value, the tightly constrained range of the Koonya main lead-zinc zone suggests it was precipitated entirely under constant fluid conditions.

The nine samples from the upper zone fall in the range 10.8‰ to 13.5‰. Given the fact that the sampling depths covered a range of 40 metres vertically and a greater horizontal distance, the isotopic values are very consistent. The average value is slightly lower than that for the main lead-zinc mineralized zone but overall, both zones are not particularly different.

The 3 samples from the middle zone taken from drillhole Kp 303, have $\delta^{34}S$ values ranging form 10.5‰ to 11.6‰. This is slightly lower than for the main lead-zinc mineralization.

The last 2 samples were taken from the lower zone at in drillhole Kp303. The $\delta^{34}S$ values measured 9.3‰ and 9.5‰, which are the lowest $\delta^{34}S$ values obtained from Koonya.

The sulphur isotope values have been plotted as a histogram in order to highlight the $\delta^{34}S$ distribution of the different mineralized zones (figure 3.10). The overall $\delta^{34}S$ range of all the Koonya mineralization is 9.3‰ to 13.5‰ with a mean value of 12.0‰.

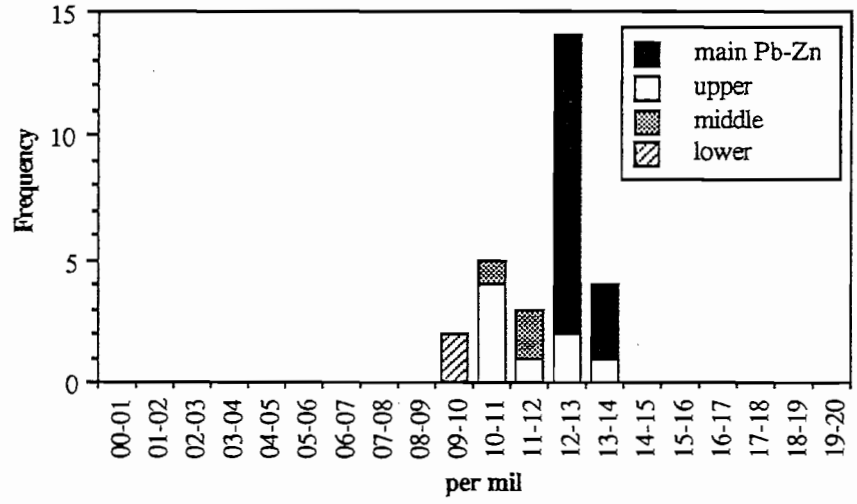

Figure 3.10: Sulphur isotope distribution for the different mineralized zones at Koonya

The sulphur isotope values obtained for the main lead-zinc zone, upper zone and middle zone are reasonably similar and it is quite possible that the sulphur in each zone had a similar source. The sulphur isotope values from the lower zone are slightly lower than for the rest of the mineralization but the difference is not very large, so may not be significant.

3.6.3 The Source of the Sulphur

A significant amount of data on $\delta^{34}S$ values exists for a number of deposits in the Mt. Read Volcanics. It is useful to compare some of these deposits to the Koonya mineralization.

Figure 3.11 shows the $\delta^{34}S$ distribution of the Koonya prospect compared to three Cambrian volcanogenic massive sulphides (Que River, Rosebery, Mt. Lyell) and two Devonian replacement deposits (Mt. Farrell and veins in the Zeehan area). Some other deposits and their $\delta^{34}S$ values are listed below.

Lake Selina, a Cambrian vein system, 9.8 to 10.9‰ (4 samples)
Rosebery Lodes, an exhalative Cambrian system a short distance north-east of Koonya, 10.9 to 18.6‰ (3 samples).
Hercules, an exhalative Cambrian system, 11.6 to 19.2‰ (12 samples)
Salisbury, a Devonian vein system a short distance from Koonya, 16.0‰ (1 sample).
Stirling Valley, a Devonian vein system, 8.6 to 8.7‰ (2 samples).

It is important to note the $\delta^{34}S$ range of the Devonian mineralization compared to the Cambrian. The $\delta^{34}S$ value of the Devonian mineralization examined ranged from 1‰ to 17‰ and the Cambrian $\delta^{34}S$ ranged from 4‰ to 19‰. The overlap between the two types of mineralization is obviously very large; therefore to try to classify the Koonya sulphur as being derived in the Devonian or Cambrian on the basis of sulphur isotopes would be very misguided.

There are a number of possible sulphur sources that could have provided the sulphur required to form the lead-zinc mineralization in the Koonya area. These are:

Devonian fluids derived from the nearby granite intrusion
Cambrian magmatic fluids derived from a nearby porphyritic intrusive (Lees 1987)
Magmatic sulphur leached from the volcanic pile by convecting Cambrian fluids
Cambrian sea-water sulphate or reduced sea-water sulphate.

The range of sulphur isotopes seen for Devonian deposits covers the range observed for the Koonya mineralization, so on this basis Devonian fluids cannot be discounted as having been the source for sulphur at Koonya. However, geological/structural relationships indicate the mineralization could not have formed from fluids from the Devonian granite intrusion.

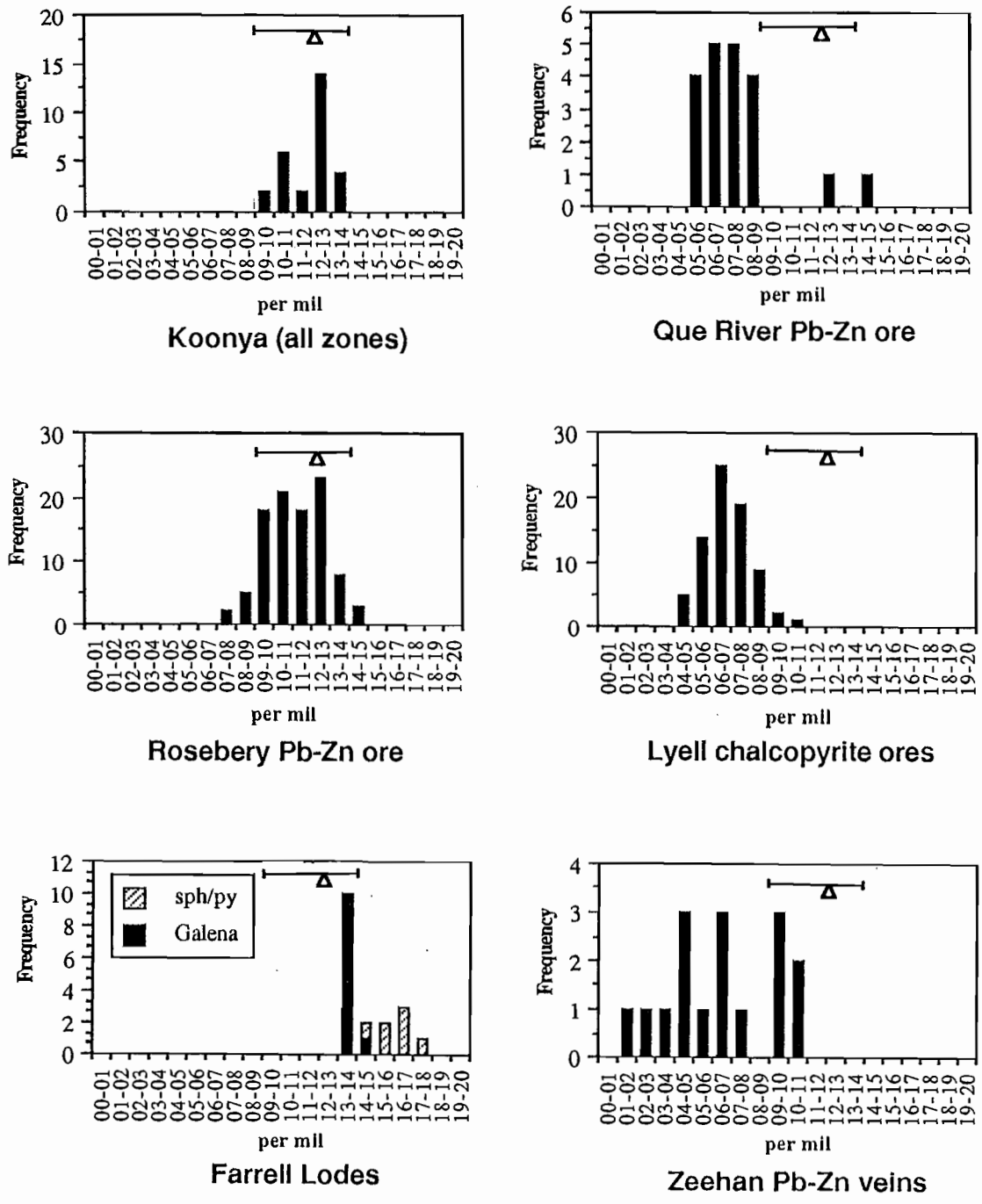

Figure 3.11: This diagram shows the $\delta^{34}S$ distribution for the Koonya mineralization compared to three Cambrian volcanogenic massive sulphide deposits (Rosebery, Que River and Mt. Lyell) and two Devonian vein systems (Farrell Lodes, Pb-Zn veins in the Zeehan area).

[Note: The data for Zeehan is from Both et al. 1969, the Farrell data is from Solomon et al. 1969 as is the data for Mt. Lyell, the Que River data is from McGoldrich 1988, and the Rosebery data is from Green 1984, Solomon et al. 1969 and Stanton & Rafter 1966]

The $\delta^{34}S$ values for Koonya indicate that the sulphur source was not dominated by magmatic sulphur, either from leaching or from fluids derived from a crystallizing magma. If magmatic sulphur was a major component, the $\delta^{34}S$ values would be expected to fall in the range of 0‰ to 5‰ and not 12~13‰ as observed for the main lead-zinc mineralized zone at Koonya. This does not totally exclude magmatic sulphur as being the source for some sulphur at Koonya but it does suggest that magmatic sulphur was not the major component of the total sulphur.

The other possible sulphur source is from Cambrian sea-water sulphate. If such sea-water were convected at low oxygen activities, then the sulphate would be converted to more reduced sulphur species such as H_2S or HS^-. Calculations based on fractionation curves show that if Cambrian sea-water sulphate ($\delta^{34}S \approx 30‰$) is reduced to H_2S or HS^- at a temperature of 350°C the $\delta^{34}S$ of the fluid would be approximately 12‰. If this fluid were to then rise, cool to 250°C and precipitate sulphides, the $\delta^{34}S$ values for the different sulphide phases would be;

$ZnS \approx 12\text{~}13‰$, $FeS_2 \approx 13‰$, $PbS \approx 11‰$ and $FeCuS_2 \approx 12‰$

Although this is a relatively simplistic model of the natural system, it does suggest that reduced Cambrian sea-water sulphate is likely to be the major source of sulphur for the Koonya mineralization.

3.6.4 Sulphur Isotope Geothermometry

Some attempt was made to use sulphur isotopes to determine the temperature of the fluid that precipitated the upper zone mineralization at Koonya. This was done by utilizing the different fractionation factors between chalcopyrite and pyrite. The difference (Δ) between the $\delta^{34}S$ values of two co-existing mineral phases (such as chalcopyrite and pyrite) is determined and the result put into a standard equation to calculate the temperature (Ohmoto and Rye 1979). The $\delta^{34}S$ values for both chalcopyrite and pyrite were measured for two samples taken from drillhole Kp303 at depths of 53.1m and 71.1m. The Δ values obtained were 1.0‰ and 2.1‰ respectively.

Unfortunately these Δ values are very different and correspond to a huge temperature difference. The failure of this technique to produce realistic results is probably due to both the difficulty in obtaining a pure sample and problems involved with only selecting grains precipitated at the same time.

Although the Δ values proved to be unusable, it is worth noting that the chalcopyrite-pyrite pairs do follow the fractionation trend with chalcopyrite possessing lower $\delta^{34}S$ values than the corresponding pyrite sample.

3.6.5 Summary.

The $\delta^{34}S$ values of the main lead-zinc zone, upper zone and middle zone at Koonya are 12.1 to 13.1‰, 10.8 to 13.5‰ and 10.5 to 11.6‰ respectively. The similarity in the sulphur isotope values indicates that sulphur source may have been the same for all three mineralized zones. The homogeneity of the $\delta^{34}S$ values within the main lead-zinc zone suggest it was deposited entirely under constant fluid conditions.

From observation of surrounding deposits it was concluded that Devonian or Cambrian mineralization could not be differentiated on the basis of sulphur isotopes. However, on the basis of geological relationships it was possible to narrow down the likely sulphur source to being reduced Cambrian sea-water sulphate. Magmatic sulphur was probably only a minor component of the sulphur in the fluid that formed the main Koonya mineralization.

An attempt to utilize sulphur isotope geothermometry failed to provide usable results, although the mineral pairs did follow fractionation trends.

Chapter 4: HYDROTHERMAL ALTERATION

Hydrothermal alteration in the Koonya area is extensive, and appears to be associated with several different events. Quartz, sericite, pyrite and chlorite are the dominant alteration phases, although other phases are locally common. Two distinctly different types of alteration occur throughout the Koonya prospect. These are:

i) alteration associated with mineralization

ii) a later phase of alteration

The alteration associated with mineralization is strongly feldspar destructive. It is dominated by a quartz-sericite-pyrite and lesser chlorite assemblage and is pre-cleavage or early syn-cleavage in origin. This type of alteration has been extensively studied as it dominates the east-west section in which the bulk of the drillholes lie.

The second type of alteration has a more varied mineralogy. Its most obvious assemblage is quartz. Later stage alteration is often associated with post-cleavage quartz or carbonate veining. This style of alteration is generally weakly feldspar destructive although it may mask the presence of feldspar phenocrysts in hand specimens.

Both types of alteration will be described in detail, as will the alteration veining that is seen throughout the prospect.

Section 4.1: Alteration Associated with Mineralization

Alteration associated with mineralization occurs in both the east-west and north-south sections. In both sections the alteration intimately associated with the mineralization is very similar, as both are dominated by a quartz-sericite-pyrite assemblage with variable amounts of chlorite. The alteration sequence in the east-west section has a very distinctive arrangement, which can be directly related to the position of the main lead-zinc mineralization.

4.1.1 East-West Section

The alteration sequence in the east-west section was determined from a series of seven drillholes (Kp 306, 307, 308, 196, 201, 200 and 199) as well as examination of the Koonya upper adit. The alteration sequence from the top to the bottom of the drillholes in the east-west section is very distinctive (figure 4.1). It can be summarized as follows:

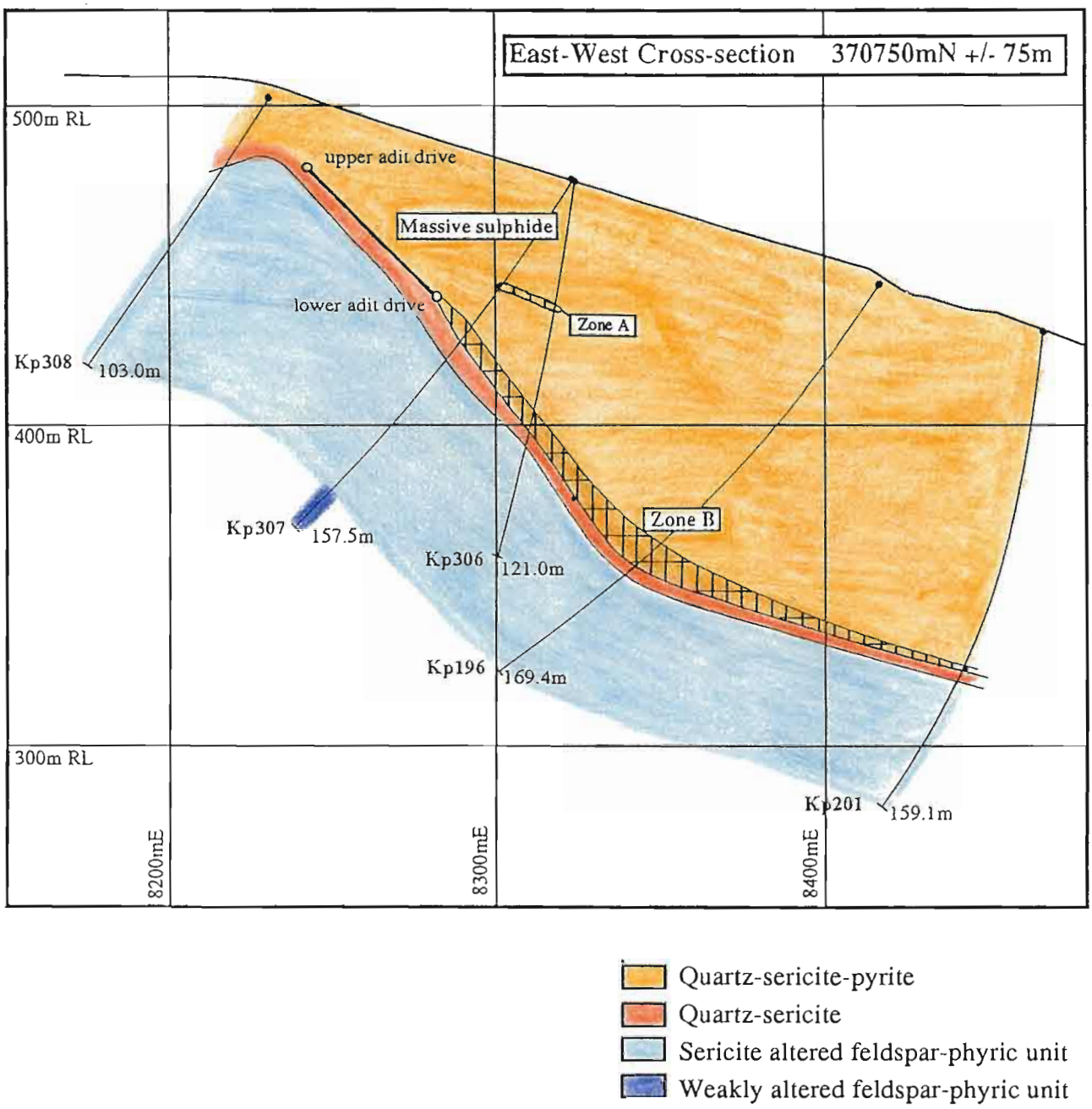

Figure 4.1: Alteration in the east-west section

Quartz-sericite-pyrite alteration with variable chlorite (plates 26,27,28). In this style of alteration the feldspars are destroyed, replaced by aggregates of small quartz or quartz-chlorite grains, which often retain the feldspar shape (plate 28). The quartz and sericite (and sometimes chlorite) form a fine-grained groundmass generally (≤0.01mm). Pyrite occurs as disseminated grains, averaging 0.05mm to 0.2mm in diameter, throughout the alteration. The concentration of pyrite is typically 1% to 5% but in several places it exceeds 50%. Chlorite occurs dominantly as a network of thin veins although it may also occur in the groundmass or as feldspar replacements. As the mineralization is approached it is common to see strong silicification of the groundmass causing a coarsening in the grainsize.

Immediately below the mineralization, a feldspar-destructive style of alteration characterized by a quartz-sericite-minor chlorite±pyrite assemblage occupies a zone extending several metres (generally >2m but <10m) before grading into sericitic alteration. The quartz and sericite form a fine-grained groundmass (≤0.03 mm) which is very similar to the alteration that occurs above the mineralization except that it generally contains less pyrite. Some pseudomorphing of feldspar by carbonate may occur in the deeper parts of this alteration zone.

Several metres to less than ten metres below the mineralization, the alteration changes to a strong sericitization of a feldspar-phyric unit (plate 29). The groundmass of this unit has been strongly altered to sericite, although in some places minor fine-grained (≤0.01mm) quartz can still be observed. The feldspar phenocrysts may be strongly sericitized but most are still partially intact. This zone of sericite alteration extends well below the mineralized horizon but its true extent is hard to determine due to the effects of later stage alteration.

Finally the sequence passes into a relatively unaltered feldspar-phyric unit, with some textural preservation within a fine-grained (≤0.01mm) groundmass (plates 2, 3, 4).

Plate 26: 307 29.0m, 14.4mm, x6.3, PP A very unusual alteration texture of oval shaped aggregates of quartz, often showing concentric layers with coarse-grained cores and finer grained edges, set in a fine grained chlorite-sericite-quartz groundmass.

Plate 27: 307 48.2m, 12.2mm, x6.3, XP Typical fine-grained quartz-sericite alteration. The larger patches of sericite may be feldspar replacements which have subsequently been deformed.

Plate 28: 307 zA, 13.8mm, x6.3, XP A fine-grained quartz-sericite-pyrite unit with larger tabular aggregates of quartz apparently pseudomorphing feldspar grains.

Plate 29: 307 86.0m, 12.8mm, x6.3, XP Strongly sericite altered feldspar-phyric unit. The sericite has almost completely replaced the groundmass and has partially attacked the feldspar phenocrysts.

Plate 30: 304 196.0m / 305 315.8m / 305 318.7m / 305 240.0m, 100mm, --, AL This shows several types of alteration associated with the later stage alteration. The sample on the far right is chlorite altered with flecks of chlorite throughout. The other three samples contain disseminated magnetite, causing the black colouration. The pink colouration in the middle two samples is due to carbonate but the phase causing the pink colour in the sample on the far right could not be identified.

Plate 31: 305 83.0m, 9.4mm, x9, PP A sheared, thin quartz vein interpreted to be pre-cleavage. In the bottom left of the photomicrograph several pyrite grains with chlorite pressure shadows can be seen.

Plate 32: 196 32.3m, 13.7mm, x6.3, XP Strongly sheared quartz-chlorite veins (pre-cleavage) in a sericitic groundmass. This sheared veining is common in the shallower parts of drillholes Kp196 and Kp201.

Plate 33: 307 48.2m, 14.0mm, x5.5, XP A syn-cleavage quartz vein. The quartz grains in the vein are aligned with their long direction parallel to cleavage.

Plate 34: 304 68.2m, 110mm, --, AL A post-cleavage quartz-chlorite vein and associated selvage (on the right side of the photomicrograph). The vein selvage can clearly be seen crosscutting the cleavage direction, which is highlighted by an alteration boundary (running diagonally from left to right on the left side of the photomicrograph).


26


27


28


29


30

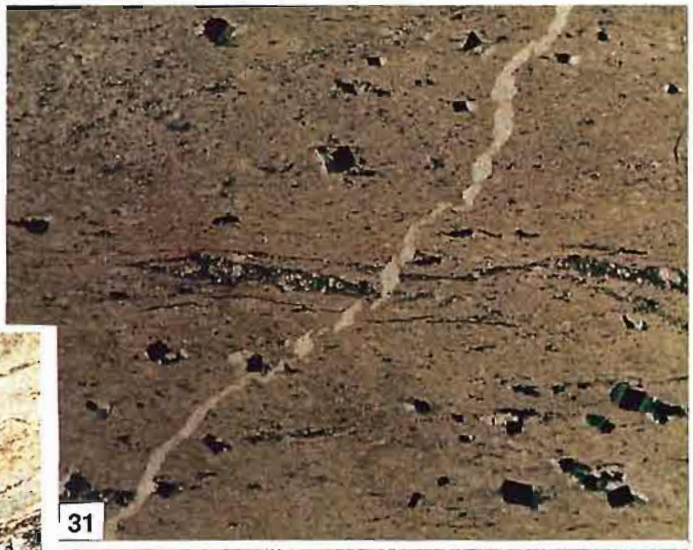
31


32


33


34

4.1.2 North-South Section

Three zones of mineralization occur in the north-south section, the extensive upper and middle zones and the limited lower zone, each of which has associated alteration (figure 4.2). Only the upper and middle zones were studied in detail due to the limited nature of the lower zone. The alteration associated with the upper and middle zones is similar to the alteration in the east-west section. A quartz-sericite-pyrite assemblage, with variable chlorite, dominates the alteration. This style of alteration is strongly feldspar-destructive and it is common to see quartz or quartz-chlorite pseudomorphs of feldspar phenocrysts in the less intensely altered areas. The intensity of the alteration is directly associated with the mineralization, with the most intensely altered areas occurring within the mineralization.

4.1.2.1 Upper zone

The alteration associated with the upper zone mineralization shows strong similarities to the alteration in the east-west section with the downhole pattern of the two mineralized zones being similar. In the upper zone the mineralization occurs in quartz-sericite-pyrite±chlorite altered rocks. Immediately below the termination of the mineralization the alteration changes to a quartz-sericite assemblage with only minor pyrite. This style of alteration extends only a few metres before passing downhole into sericite altered volcanics (figure 4.2). Throughout most of the upper zone the feldspar-phyric nature of the original rock-type can be discerned from the quartz and/or chlorite pseudomorphs of the feldspars.

4.1.2.2 Middle zone

The upper and lower boundaries of the middle zone quartz-sericite-pyrite alteration are gradational. The most intense alteration occurs in the more central areas of the middle zone, associated with the intense mineralization. In the less intensely altered areas, quartz and/or chlorite psuedomorphing of feldspar is common. In one section of the middle zone (in drillhole Kp309), disseminated sphalerite-sericite patches have tabular shapes suggesting that they may be replacing feldpars (plate 25).

Above the middle zone the alteration is very sericitic. This alteration passes rapidly downhole into quartz-sericite-pyrite alteration. Below the middle zone mineralization the quartz-sericite alteration grades into sericite alteration.

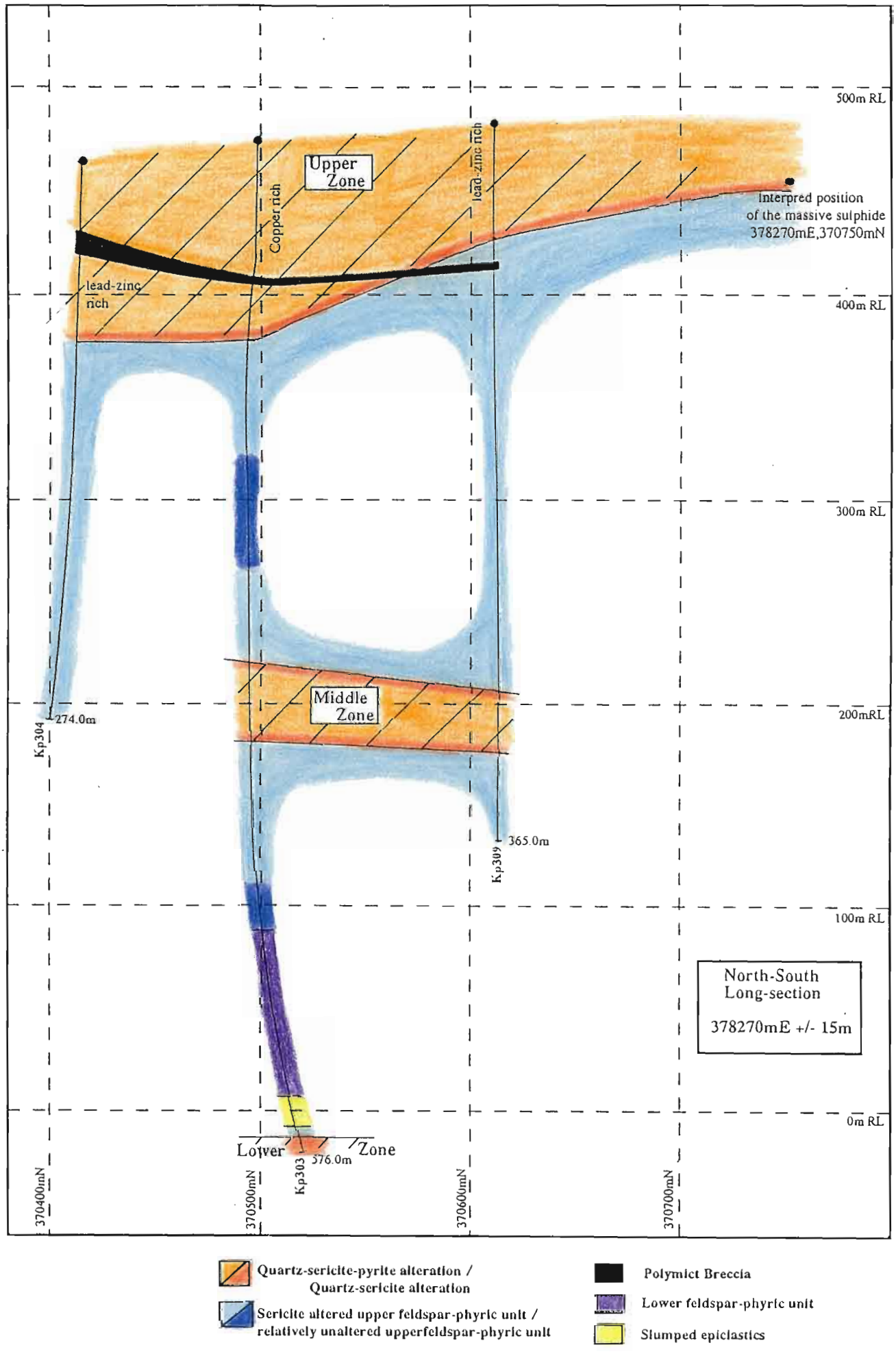

Figure 4.2: Alteration in the north-south section

Section 4.2 Later Stage Alteration

Later stage alteration is, spatially and mineralogically, more diverse than alteration associated with mineralization. It is found to some extent in all the drillholes in the Koonya area but has no obvious spatial association with any rock-type or mineralization. Silica seems to be the most abundant mineral associated with this alteration; however, sericite, carbonate, chlorite, minor magnetite, pyrite and possibly some type of feldspar were also observed. Generally this alteration is only partially feldspar-destructive. Later stage alteration is commonly associated with post-cleavage veining.

Although the quartz-sericite-pyrite alteration associated with mineralization is crosscut by some post-cleavage veining, it appears to be reasonably unaffected by late stage alteration.

Silicification is the most common phase of the later stage alteration with the intensity varying from moderate to very strong. Most silicification occurs on a scale of tens of metres, and is generally accompanied by a high frequency of post-cleavage quartz veining.

There are a number of other forms of late stage alteration. One of the hardest to quantify or describe is sericite-quartz alteration. In hand specimen it is very difficult to separate this style of alteration from sericite alteration associated with mineralization. The late stage quartz-sericite alteration was identified by its association with post-cleavage quartz veining and its more feldspar-destructive nature.

Another common phase associated with late stage alteration is chlorite. It occurs dominantly in zones one metre to several metres wide. These zones have boundaries that contain disseminated chlorite which intensifies towards the centre of the zone until the rock is almost entirely replaced by chlorite. Plate 30 (sample Kp304 196.0m), shows a sample from the chlorite flecked boundary of one of these chlorite altered zones.

The most obvious type of late stage alteration occurs in drillholes Kp304 and Kp305. This alteration takes the form of pink alteration patches or pale pink alteration through a dark, almost black, feldspar-phyric unit (plate 30 samples Kp305 315.8m, Kp305 318.7m, Kp305 240.0m). The black colouration is produced by very small amounts, $\approx$1%, of fine-grained ($\leq$0.03mm), disseminated magnetite in the groundmass of the rock. Trace amounts of disseminated pyrite are also present in the groundmass. The pink patches in several samples are attributed to patches of fine-grained carbonate. However, the mineral causing the pale pink alteration in some samples could not be identified. These styles of alteration are rarely feldspar-destructive.

The least significant from of late stage alteration is carbonate alteration. Carbonate alteration is feldspar-destructive, sometimes entirely pseudomorphing feldspar grains, and is usually associated with thin post-cleavage carbonate veins.

Section 4.3 Alteration Veining

Alteration veining is extensive throughout the Koonya area. The mineralogy of the alteration veins is quartz, chlorite, carbonate, quartz-chlorite or quartz-carbonate. Most veining is reasonably thin with the majority of chlorite or carbonate veins narrower than 10mm, and quartz veins less than 50mm wide. Four stages of veining have been recognized, one pre-cleavage, one syn-cleavage and two post-cleavage.

4.3.1 Pre-cleavage

Pre-cleavage veining occurs with the alteration associated with mineralization. The bulk of pre-cleavage veining occurs as chlorite, quartz or chlorite-quartz veins only a few millimetres wide (plate 31), although several thicker pre-cleavage quartz veins, characterized by their highly contorted nature and their diffuse margins, were observed. Thin chlorite or quartz-chlorite veins are often recognizable from their contorted and sheared appearance, however recrystallization of some veins, as well as alignment of these veins into the cleavage makes it difficult to determine a pre-cleavage or syn-cleavage origin.

The best examples of pre-cleavage chlorite or quartz chlorite veins occur in the lower parts of drillholes Kp196 and Kp201 in the east-west section (plate 32), or associated with mineralization in the middle zone (north-south section). Pre-cleavage alteration veins are intimately associated with the mineralization/alteration event.

4.3.2 Syn-cleavage

The second type of veining is syn-cleavage. These veins formed at the same time as the cleavage associated with the Devonian regional deformation. Syn-cleavage veins are generally thin (<5mm) and consist of quartz or quartz-chlorite (plate 33). Syn-cleavage veins have only been recognized in the altered zone in the east-west section.

4.3.3 Post-cleavage

Two distinct phases of post-cleavage veining have been recognized. The first consists of quartz (±chlorite, ±carbonate) veins generally ≤50mm thick (plate 34). The second consists of thin carbonate veins which crosscut the earlier post-cleavage quartz veining. Both are associated with the later phase of alteration and crosscut all other features in the rock. Some post-cleavage veining does occur through the alteration associated with mineralization, but is fairly restricted in extent. Plate 34 shows a post-cleavage quartz(-chlorite) vein crosscutting the cleavage.

Chapter 5: ALTERATION GEOCHEMISTRY

The main purpose of studying the alteration geochemistry at Koonya was to:

i) gain some information on the original composition of the altered rocks
ii) describe the enrichment or depletion of various elements associated with the alteration

In order to achieve this, a series of eleven wholerock and limited trace element analyses were carried out. The samples were taken in two separate sequences: five samples from drillhole Kp303 and six samples from drillhole Kp307.

The main emphasis of the geochemical study has been placed on the six samples from Kp307. These samples were taken as a downhole traverse through the alteration. The sample positions were carefully chosen to match the downhole alteration sequence previously described for the alteration related to mineralization in the east-west section. The relationship of the samples to the geology, mineralization and alteration is summarized in figure 5.1.

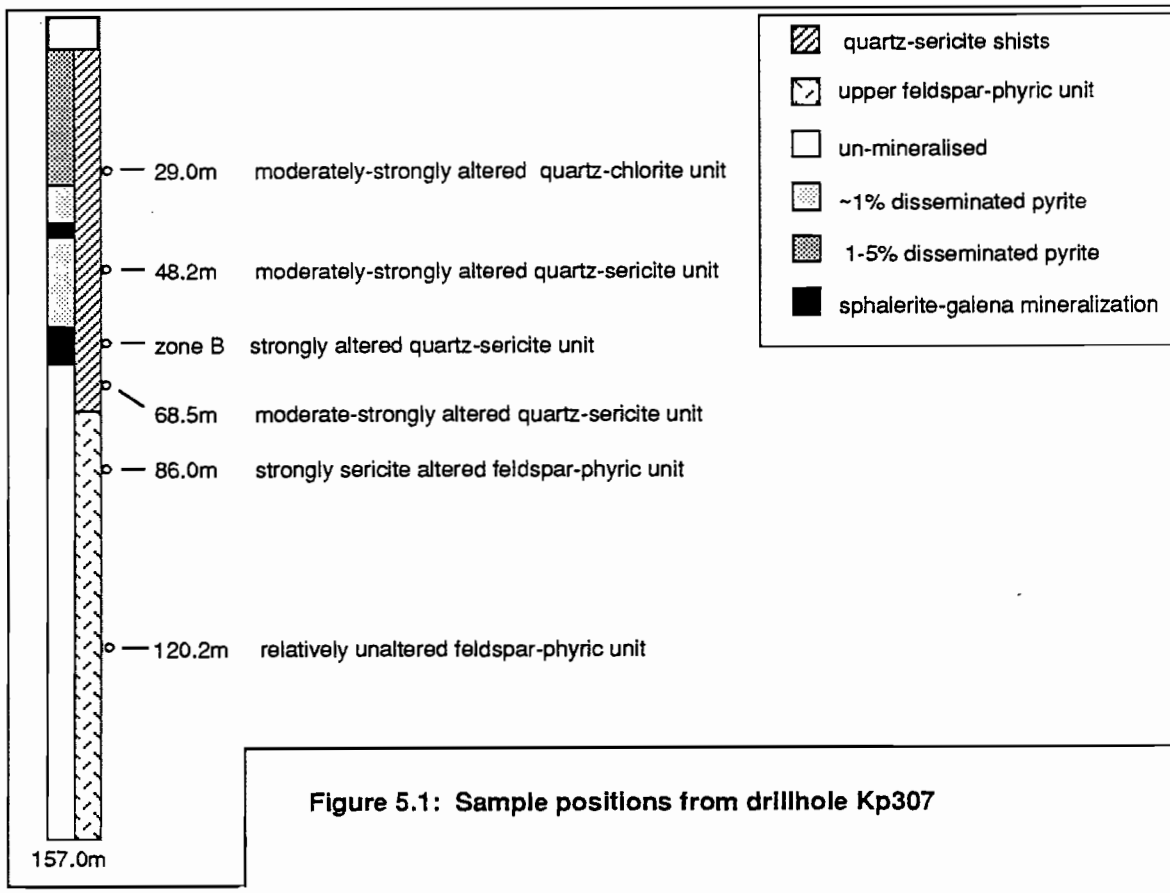

Figure 5.1: Sample positions from drillhole Kp307

	307 120.2	307 86.0	307 68.5	307 zone B	307 48.2	307 29.0	303 255.9	303 283.6	303 296.8	303 344.6	303 445.8
SiO2	76.29	65.14	72.31	66.81	73.23	65.15	58.7	67.38	71.87	61.74	74.89
TiO2	0.28	0.43	0.32	0.18	0.39	0.39	0.46	0.34	0.3	0.24	0.31
Al2O3	11.56	17.53	14.36	8.7	13.66	12.7	20.04	13.88	12.92	10.63	13.06
Fe2O3	2.06	2.64	2.49	7.32	3.37	9.94	3.04	8.39	2.68	4.31	2.35
MnO	0.11	0.14	0.96	2.09	0.45	0.6	0.25	0.39	0.72	3.45	0.04
MgO	0.55	2.87	0.85	0.69	1.03	1.84	2.54	1.17	0.95	1.32	1.7
CaO	0.81	1.43	0.1	0.1	0.08	0.08	1.61	0.05	0.88	5.08	0.27
Na2O	4.91	1	≤0.1	0.51	≤0.1	≤0.1	≤0.1	≤0.1	≤0.1	≤0.1	3.9
K2O	1.13	4.33	4.84	2.58	4.3	3.39	7.65	4.26	5.59	5.83	1.57
P2O5	0.06	0.06	0.05	0.01	0.06	0.06	0.05	0.05	0.04	0.03	0.03
Loss	1.94	4.5	3.31	6.01	2.89	5.2	5.85	3.51	3.59	7.88	1.77
Total	99.7	100.07	99.7	95.7	99.5	99.45	100.1	99.5	99.64	100.54	99.89
Zirconium	209	326	271	160	272	251	374	262	259	197	249
Niobium	10.5	15.5	13	-in-	13	13	17	12.5	12	10	13
Yttrium	32	47	33	-in-	42	38	53	36	33	65	37

Composition of samples from Kp307					
Feldspar quartz	feldspar sericite quartz minor chlorite minor MgCO3	quartz sericite minor pyrite minor chlorite	quartz sericite sulphides minor chlorite	quartz sericite pyrite minor chlorite	quartz sericite chlorite pyrite

-in-	indicates an interference occured during measurement

Table T5.1: Wholerock and trace element analyses for eleven samples from the Koonya prospect. The samples are labelled according to the drillhole number and the depth. Samples 307 120.2m and 303 445.8m are relatively unaltered while the other samples exhibit various degrees of alteration.

The five samples from Kp303 were taken from the following positions:

* Three samples from the mineralized Middle zone, one each from the top, centre and bottom sections of the zone (at depths of 255.9m, 283.6m and 296.8m respectively),
* an unusually altered sample from below the Middle zone (344.6m) ,and,
* a relatively unaltered feldspar-phyric sample (455.8m).

The main aim of taking samples from Kp303 was to provide an expanded data set for immobile element studies, and to get some comparison of rocktypes in the north-south and east-west sections.

The results of the wholerock and limited trace element analyses are listed in table T5.1. Two of the samples, 307 120.2m and 303 445.8m, are relatively unaltered, while all the other samples are variably altered.

Section 5.1: Immobile Element Studies

In an area as extensively altered as Koonya there is often a great deal of difficulty in determining the original lithologies of the altered rocks. This determination of original lithology is important as it may have a significant bearing on the interpretation of the alteration system and mineralization. In many cases the only clues to the original lithologies of strongly altered rocks are 'immobile elements'. Immobile elements, as the name implies, remain immobile during metasomatic alteration. Elements that are usually considered immobile include titanium, zirconium, yttrium, niobium and often aluminium (Pearce and Cann 1973, Winchester and Floyd 1977).

Probably the best way of using immobile elements is by considering the relationship between paired elements. A number of studies (eg. Pearce and Cann 1973, Whitford et al. 1989) have utilized the elements titanium and zirconium when studying alteration. A similar approach was initially adopted in studying the Koonya alteration. A diagram of titanium versus zirconium was plotted for all the analysed samples (figure 5.2a). It was found that the data exhibits a strong linear trend, with a correlation co-efficient of R=0.93. In descriptive terms, this straight line indicates that the ratio of titanium to zirconium is very similar for each sample but the concentration of the two elements varies systematically between samples.

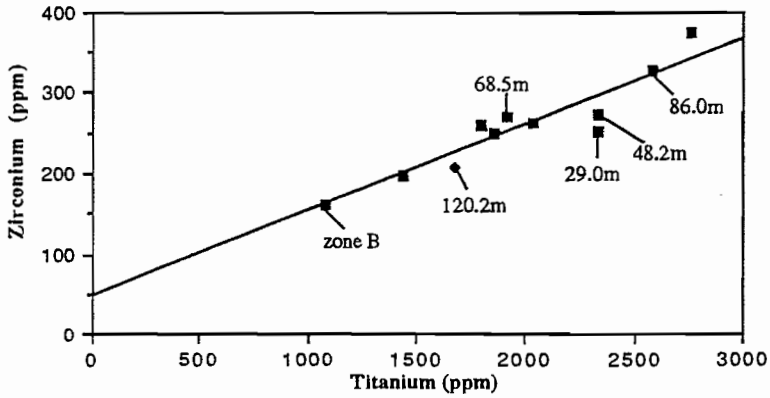

A plot of Titanium versus Zirconium

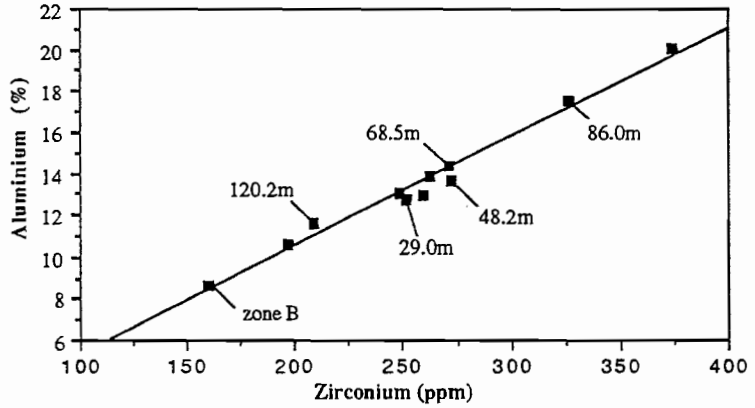

A plot of Zirconium versus Aluminium

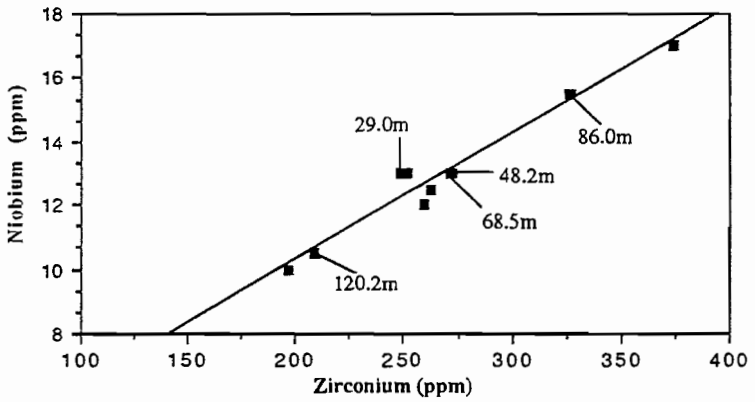

A plot of Zirconium versus Niobium

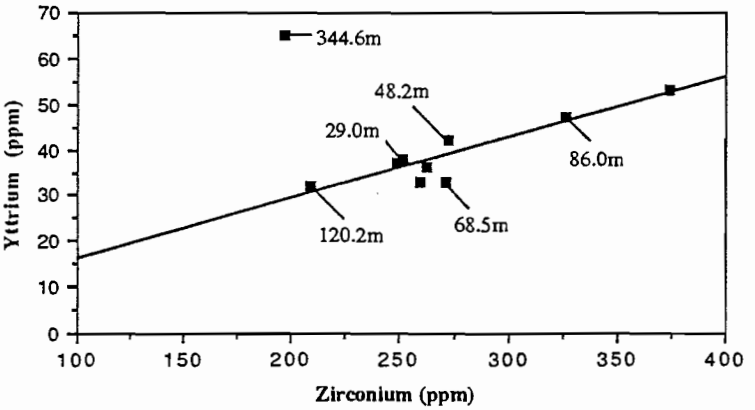

A plot of Zirconium versus Yttrium

Figure 5.2: Diagrams of the concentration of various immobile elements plotted against the concentration of zirconium.

The problem with using a titanium/zirconium diagram is the relatively poor precision in the determination of titanium in low titanium samples (4 to 10% error depending on Ti concentration). A more sensitive plot is obtained by plotting immobile elements such as aluminium and zirconium together. For this reason a diagram of zirconium versus aluminium was plotted (figure 5.2b). Again it was found the data exhibited a strong linear trend. The statistical correlation for this more sensitive plot was very high (R=0.99).

Two other elements which are generally considered to be immobile, yttrium and niobium, were also analysed for this study. Diagrams of zirconium versus niobium and zirconium versus yttrium were plotted (figure 5.2c&d). Once again straight line trends were observed. Statistically the correlation for niobium-zirconium and yttrium-zirconium are R=0.98 and R=0.91 respectively. However for the yttrium-zirconium data one sample, a strongly altered rock from Kp303 (labeled 344.6m on the diagram), plotted well away from the straight line trend. This sample appears to have been enriched in yttrium. Whether this enrichment is due to contamination or represents an enrichment in the rock is uncertain.

To determine if the immobile elements trends correlated with mobile elements a diagram of three immobile elements (Al, Ti and Zr) and seven mobile elements was plotted for drillhole Kp307. The result can be seen in figure 5.3. In this diagram the strong relationship between the immobile elements is very obvious however there is no discernible correlation between the mobile and immobile elements.

In order to examine the systematic variation of the immobile elements in terms of alteration, the depths at which various samples from Kp307 were collected have been labeled on all immobile element plots (refer back to figure 5.2). This allowed the observation of two important facts. The first was that the altered samples (29.0m 48.2m, zone B, 68.5m and 86.0m) plot well away from the relative unaltered sample (120.2m). Secondly, it was also noticed that the positions of each sample relative to the other samples is similar in all immobile element plots (particularly for the trends with the highest correlation co-efficients).

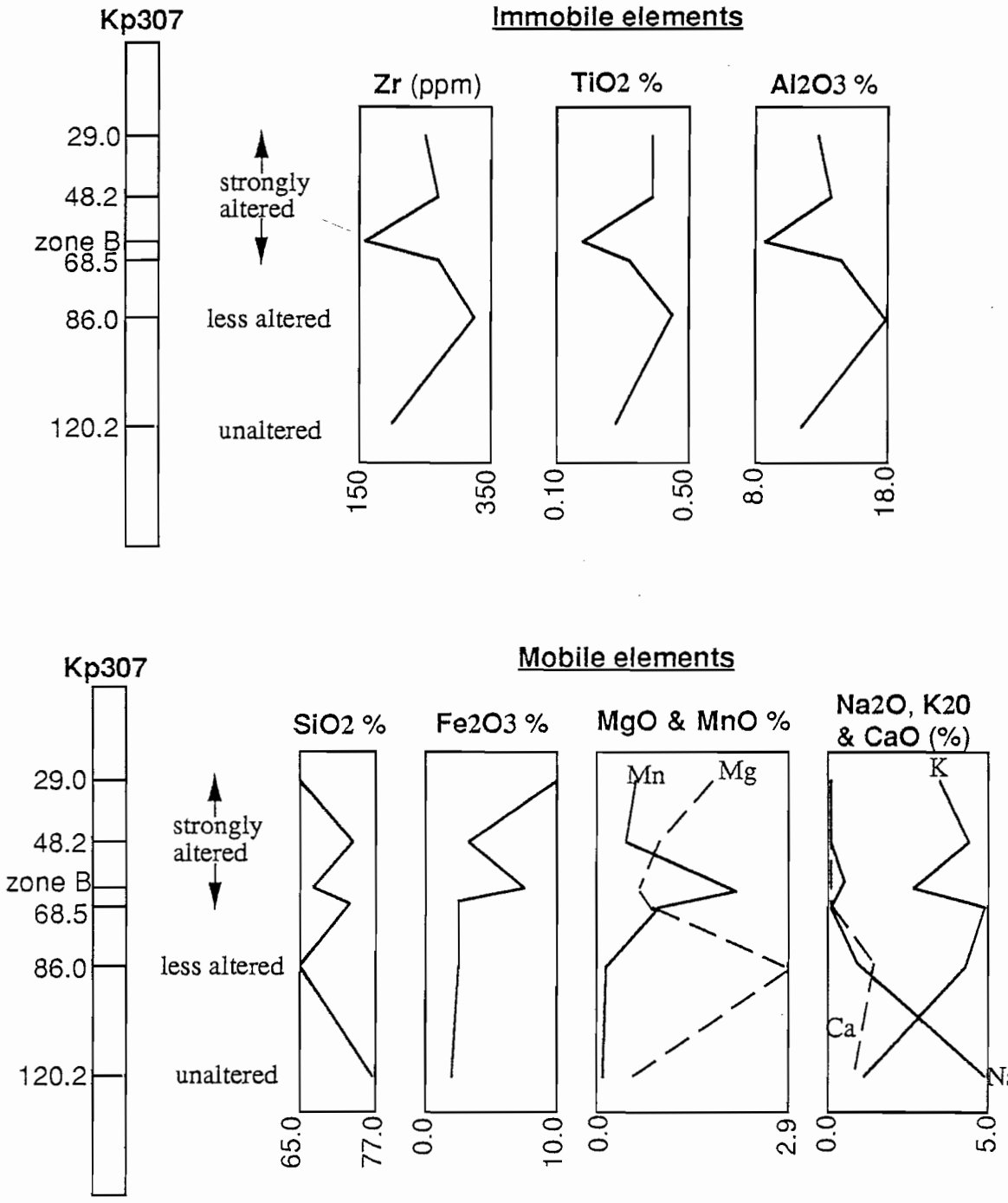

Figure 5.3: Downhole alteration plots showing the variation of certain mobile and immobile elements with depth in drillhole Kp307. It is interesting to note the similarity between the immobile element trends.

The observation that the samples appear to have similar relative positions can be quantified by examining the ratios of the concentrations of each immobile element between two samples. An example of the procedure is as follows. The concentrations of immobile elements in the relatively unaltered sample from Kp307 (120.2m) are compared to the concentrations of the immobile elements in the sample Kp307 (86.0m). The results are shown in table T5.2.

immobile element	Sample position		concentration ratio
	Kp307 86.0m	Kp307 120.2m	
Al (%)	17.53	11.56	1.52
Zr (ppm)	326	209	1.56
Ti (ppm)	2578	1679	1.54
Nb (ppm)	15.5	10.5	1.48
Y (ppm)	47	32	1.47

Table T5.2: Relative concentration of immobile elements between two samples

As can be seen from the data, the ratio of concentration of each immobile element is constant. This process was repeated for the other samples from Kp307 relative to the unaltered sample (120.2m) and in all cases the ratio of immobile elements between each pair of samples is approximately constant.

The constant ratio of all the immobile elements between samples and the lack of any discernable relationship between the mobile and immobile elements leads to one major conclusion. The protoliths for all the samples were geochemically very similar, but subsequent alteration has resulted in varying volume and/or mass changes, causing a proportional change in the concentrations of all immobile elements.

The extent of this volume/mass change can be estimated by comparing the concentration of immobile elements in altered rock to those of a relatively unaltered sample. Using sample 307 120.2m as the unaltered sample, concentration ratios obtained for the immobile elements in samples 307 zoneB and 307 86.0m are 0.76 and 1.50 respectively. In order to obtain a ratio of below one for 307 zoneB the volume/mass must have increased and to obtain an increased ratio in 307 86.0m the volume/mass must have decreased.

The magnitude of the volume/mass change in percentage terms is simply 100 times the inverse of the concentration ratio between the altered and unaltered samples minus 100 (eg. for 307 86.0m the concentration ratio is 1.50, so the volume change is 100x[1/1.50]-100 which equals -33%). The volume/mass changes for all the the altered samples in Kp307 have been calculated and are listed overleaf.

29.0m	-14%
48.0m	-22%
zone B	+32%
68.5m	-23%
86.0m	-33%

The two samples 307 zone B and 307 86.0m represent the greatest volume/mass changes seen in samples from Kp307. Such large volume changes, ±33%, are not unreasonable. Osterberg et al. (1987) described volume changes of a similar magnitude in samples from their study.

Section 5.2: Comparison of Koonya to the Mt. Read Volcanics

Large et al. (1986) demonstrated fractionation trends, based on element concentration versus the titanium/zirconium ratio, for a whole suite of elements for samples from the Mount Read Volcanics. McGoldrick et al. (1987) make use of these trends to examine alteration in the Que River area. A similar approach is appropriate for the Koonya data.

For each of the eight major elements a diagram of the element concentration versus the titanium/zirconium ratio has been plotted showing the eleven analysed samples. Most samples are displayed as diamonds but the relatively unaltered sample 307 120.2m is displayed as a cross. On each diagram the fractionation trend for the Mount Read Volcanics, as determined by Large et al. (1986), has been plotted. (see figure 5.4)

For all the major elements except K_2O the relatively unaltered sample plots within the fractionation trends. Whether this relative paucity of potassium feldspar in the relatively unaltered Koonya sample is due to alteration, or is reflecting original rock compositions, is uncertain.

The altered samples generally show a much more diverse range of compositions. Some samples show a distinct depletion in silica relative to the fractionation trends. Sodium is also strongly depleted in many of the altered samples. An enrichment of iron occurs in several altered samples which can be attributed to the abundance of pyrite in the samples. The only other element to show a significant spread of values away from the fractionation trend is aluminium, which shows both enrichment and depletion.

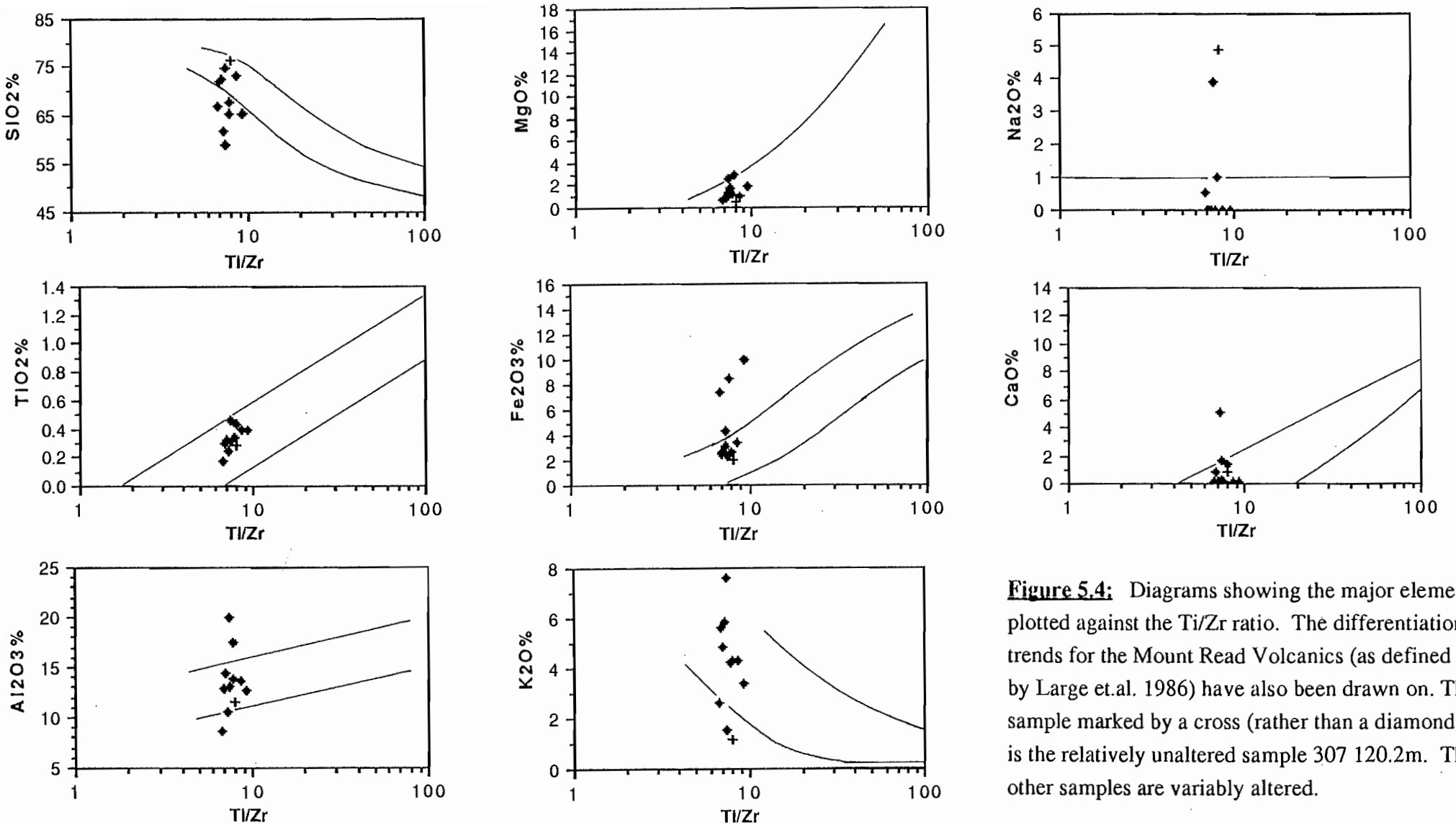

Figure 5.4: Diagrams showing the major element plotted against the Ti/Zr ratio. The differentiation trends for the Mount Read Volcanics (as defined by Large et.al. 1986) have also been drawn on. The sample marked by a cross (rather than a diamond) is the relatively unaltered sample 307 120.2m. The other samples are variably altered.

Section 5.3: Element Depletion/Enrichment During Alteration

To examine a table of geochemical analyses in order to determine the relative depletion or enrichment of certain elements in an alteration zone is a very subjective matter. A mathematical means of treating the data would be a superior technique to that of simple estimation. In this study, a mathematical technique proposed by Grant (1986) and modified by Huston (1988) has been used to determine the relative depletion/enrichment of various elements during alteration.

The method involves comparing the altered rocks to a relatively unaltered rock. This technique makes two major assumptions;

i) the unaltered and altered rocks were originally geochemically very similar; and
ii) the so called 'immobile' elements are immobile (in this case 'immobile elements' refers to Ti, Zr & Al).

As previously discussed, these two assumptions appear to be correct for the analysed samples from the Koonya area.

Huston's (1988) technique utilizes the immobile elements to determine the relative alteration between an altered and unaltered sample. Any net change of volume/mass during the alteration is compensated by comparing, and correcting for, the ratio between the concentration of immobile elements in the altered and unaltered samples. This technique is termed the isocon diagram. The procedure used is outlined below.

Each element to be included in the study is assigned a sequential number (Ni) herein called the scaling parameter. This study used values of Si=1, Ti=2, Fe=3, Mg=4, Mg=5, Al=6, Ca=7, K=8, Na=9, Zr=10. To get the best results the immobile elements were interspersed evenly through the mobile elements. Then for each element, a scaled concentration (Xi) is calculated by dividing the element concentration in the altered sample by the element concentration in the unaltered sample, and multiplying by the scaling parameter (Ni) for that element. Mathematically,

$$Xi=Ni(\text{altered}/\text{unaltered}).$$

The 'isocon diagram' can be drawn by plotting the scaled concentration (Xi) against the scaling parameter (Ni). A line of best fit (called the isocon) is then drawn through the immobile element points (Ti, Al, Zr) and the slope of the line (Mi) is measured. This procedure has been performed for the five altered samples from Kp307 (86.0m, 68.5m, zone B, 48.2m, 29.0m) by comparing them to the relatively unaltered sample from Kp307 (120.2m). The isocron

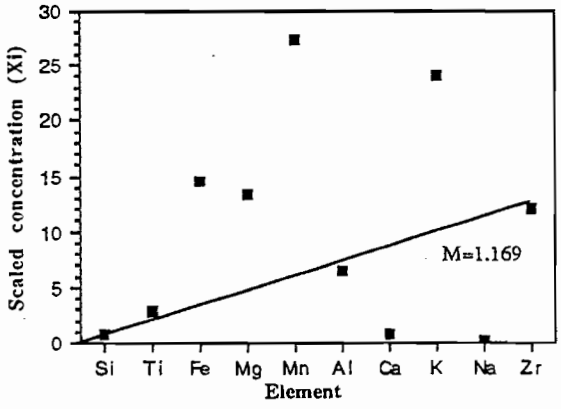

Isocon diagram for Kp307 29.0m

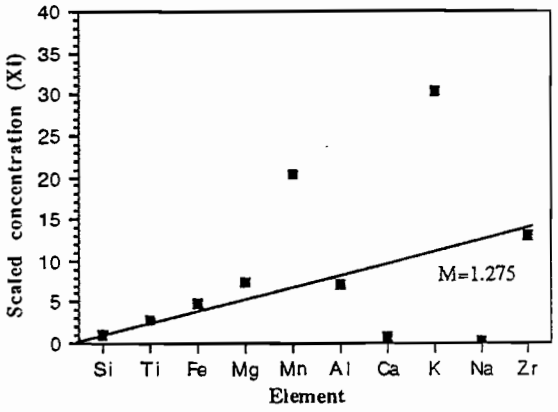

Isocon diagram for Kp307 48.2m

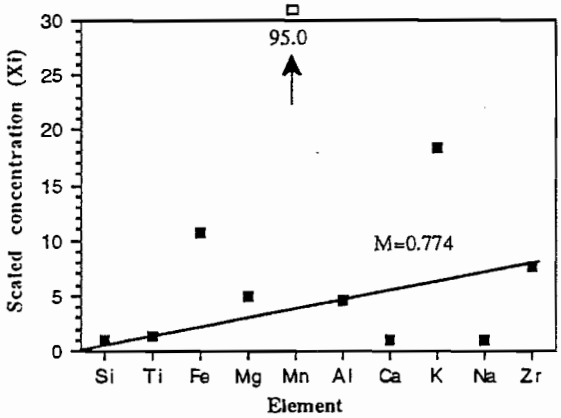

Isocon diagram for Kp307 zone B

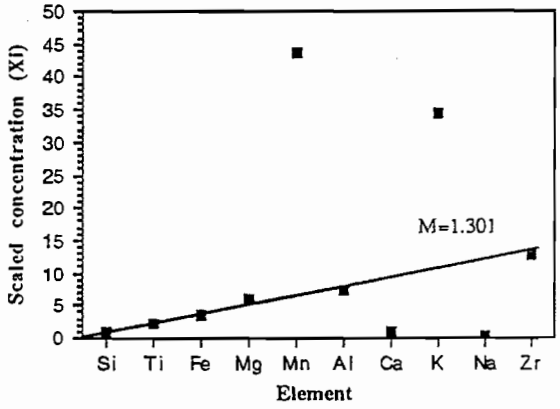

Isocon diagram for Kp307 68.5m

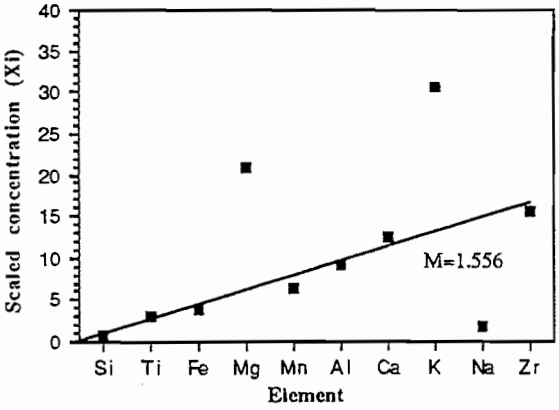

Isocon diagram for Kp307 86.0m

Figure 5.5: Isocon diagrams for the altered samples from Kp307 relative to the reasonably unaltered sample Kp307 120.2m. The value 'M' is equivelent to the slope of the isocon. elements that plot above the isocon have been enriched while elements below the isocon have been depleted during alteration.

diagrams for the samples are shown in figure 5.5. Any elements that plot above the isocron have been enriched, and any below the isocron have been depleted during alteration.

Further mathematical treatment of the isocon data allows calculation of the relative enrichment/depletion of the various elements in percentage terms. The calculations are carried out for each element using the equation,

$$Ci=100 (Xi/(MiNi)) - 100$$

where Ci is the relative percentage enrichment or depletion, Xi is the scaled concentration of the element, Mi is the slope of the isocron for the altered sample, and Ni is the scaling parameter for each element. The percentage enrichment-depletion has been calculated for the five altered samples from Kp307 and the data has been collated and plotted in figure 5.6.

5.3.1 Results

As can be observed from the diagram showing relative enrichment/depletion a number of elements have been added or subtracted relative to the reasonably unaltered sample (307 120.2m).

The most strongly depleted elements are sodium and calcium. These two elements are depleted in all samples except 86.0m. This one sample differs to the others because the feldspars are still partially preserved. This presence of plagioclase in sample 86.0m explains the slight enrichment in calcium and the slightly lower depletion of sodium relative to the other samples. The strong depletion of sodium in the altered samples is a feature common to many alteration zones, particularly those associated with massive volcanic sulphide deposits (eg Hashiguchi et al. 1983, Mc Goldrick et al. 1987).

Four of the five altered samples from Koonya show a significant depletion in their relative silica content. This appears to be due to sericitization or chloritization of the matrix (hence producing the depletion); however, quartz is often seen replacing feldspars in the same samples. The one sample that is relatively enriched in silica (307 zone B) has a strongly silicified groundmass.

Four elements have been significantly enriched during alteration. The elements are potassium, manganese, magnesium and iron.

The most consistently enriched element in all the altered samples is potassium. It varies from about 150% to 200% enrichment. In all samples this enrichment takes the form of strong

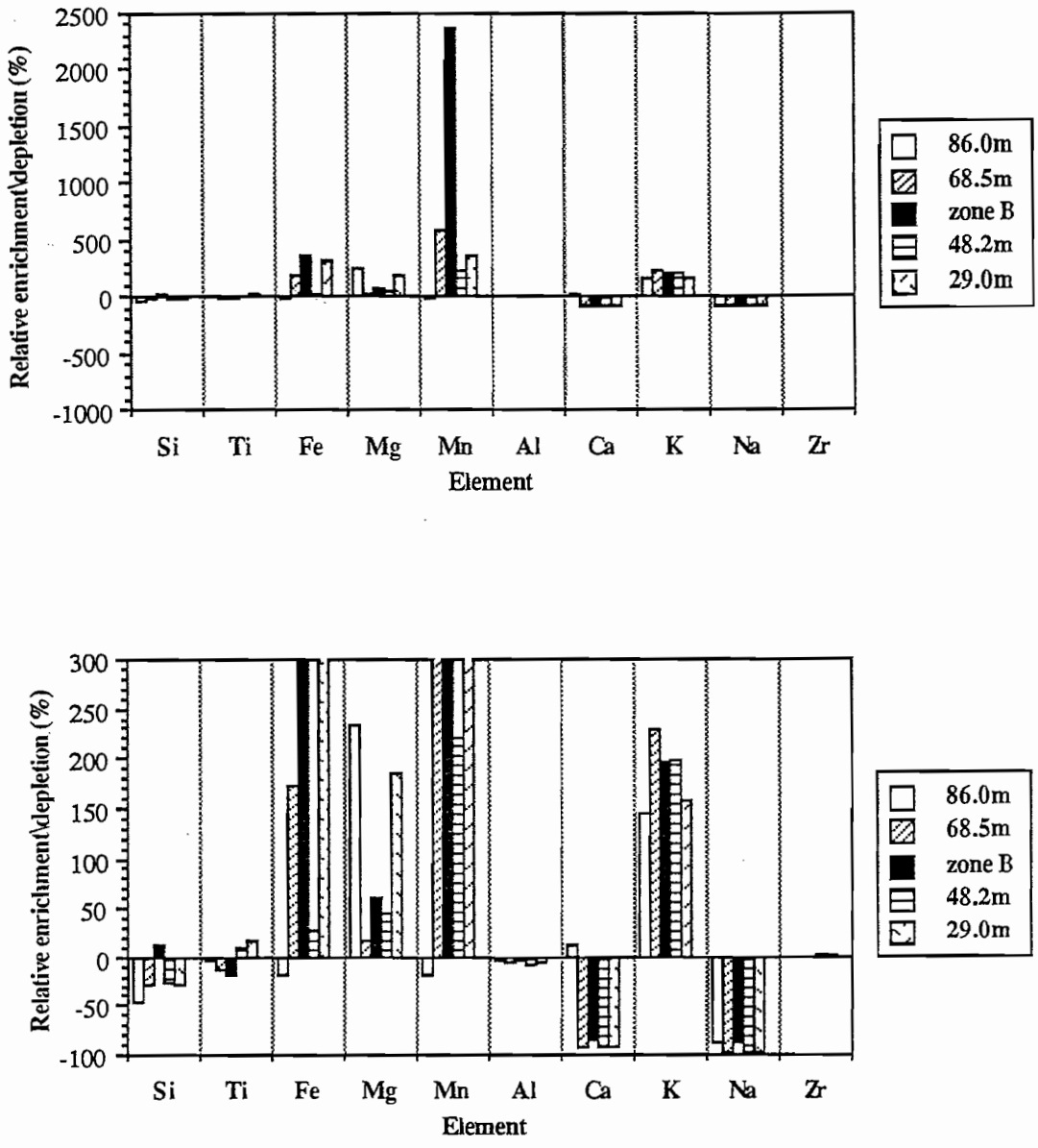

Figure 5.6: These two diagrams show the relative enrichment/depletion of elements in the five altered samples from Kp307 relative to the reasonably unaltered sample Kp307 120.2m. Both diagrams depict the same data but at a slightly different scale.

sericitization of the groundmass. It is interesting to note that, for a typical unaltered rhyolite from the Mount Read Volcanics (as defined by fractionation trends from Large et al. 1986) this enrichment would probably be non-existent due to the significantly higher levels of potassium in such a rock. However the low levels of potassium in the both the unaltered Koonya samples (compared to the previously mentioned fractionation trend) means that the presence of sericite alteration is associated with an enrichment in potassium.

Iron is variably enriched in the samples from Kp307. This enrichment, which ranges from 50% to several hundred percent can be directly related to the increased abundance of pyrite in the sample.

Magnesium is also variably enriched in Koonya samples. This can be directly related to the amount of chlorite in the sample (based on microprobe analysis of the chlorites; see chapter 7).

The element which shows the most significant enrichment in the altered samples from Kp307 was manganese. The strongest enrichment occurs in the sample from the mineralized zone (307 zone B). The two samples above and the sample immediately below the mineralized zone are also significantly enriched. Calculations based on chlorite composition and chlorite concentration (see chapter 7) indicate that the manganese in the three least enriched samples is contained entirely within chlorite. However, the highly enriched sample does not contain nearly enough chlorite to explain the levels of manganese observed. The majority of the manganese must be contained in some other phase. Acid tests revealed that the manganese could be present in the form of carbonate. It is also possible that some of the manganese may be contained in sphalerite (Green et al. 1981).

Very little previous literature describing manganese in alteration zones was found. Most information dealt with volcanogenic massive sulphide systems, although some mentioned porphyry copper systems.

Information on the Ely porphyry copper deposit described a metal zonation with a Cu-Mo-rich core, Pb-Zn-Ag-As-enriched edges and an outer zone of Mn (McCarthy and Gott 1978). This zonation corresponds to a temperature gradient becoming progressively cooler away from the core. In many volcanogenic massive sulphide systems increased levels of manganese were noted in exhalite horizons (Govett 1983) or associated with footwall alteration immediately adjasent to lead-zinc mineralization (Green et al. 1981, Govett 1983, Gair and Slack 1984, Whitford et al. 1989). Combining the descriptions of the occurance of manganese it appears that the element is associated with lower temperature alteration ($\leq$250°C).

Section 5.3: Summary

Samples were taken from both the north-south and east-west sections for geochemical analysis. The main emphasis was placed on studying alteration associated with mineralization particularly in the east-west section.

On the basis of immobile element studies it is concluded that before alteration the rocktypes at Koonya were geochemically very similar (and thus were probably the same lithology). Hydrothermal alteration has produced marked volume/mass changes of these originally similar units. These changes in volume/mass may exceed ±30% of the original volume/mass.

Compared to generalized fractionation trends defined for the Mount Read Volcanics by Large et al. (1986) the potassium in the relatively unaltered Koonya samples is lower than expected.

A study of altered samples from a downhole sequence in Kp307 showed that a number of elements have been depleted or enriched in the altered areas, relative to the unaltered rocks.

Depletion of Na occurs in all the altered samples. Calcium is depleted in the more intensely altered samples that show total feldspar replacement or destruction. Silica is also depleted in most of the samples.

Enrichment of four elements occurs. These elements are potassium (due to sericitization), iron (due to pyrite), magnesium (due to chlorite) and manganese. In three cases the enrichment in manganese could be attributed to the presence of manganese in chlorite but the mineral causing the extreme enrichment in the sample from the mineralised zone (307 zone B) was not positively identified.

Chapter 6 OXYGEN ISOTOPES

Oxygen isotopes are a useful tool for studying alteration systems. They may, in some cases, provide information on the source of the hydrothermal fluids that produced the alteration and can sometimes be used to study the water/rock interaction (eg. Beaty and Taylor 1982).

Section 6.1 Basic Theory

The oxygen isotope value (δO^{18}) is defined as

$$\delta O^{18} = 1000x \left\{ \frac{(O^{18}/O^{16})_{unknown}}{(O^{18}/O^{16})_{standard}} - 1 \right\} \quad \text{(Taylor 1979)}$$

and is quoted in units of per mil (‰). The standard commonly used is SMOW (standard mean ocean water).

In a hydrothermal alteration system, fluids of a certain δO^{18} exchange O^{18} with the minerals in the rock being altered. This process, called fractionation (Δ), is dependent on several factors, the most important two being: the particular mineral phase or phases present, and the temperature such that $\Delta\alpha 1/T^2$ (Taylor 1979, Kyser 1987). The fractionation between various minerals and water ($\Delta_{mineral/H2O}$) are listed below.

$\Delta_{quartz/H2O}$	$= 3.38x10^6/T^2 - 3.40$	(Clayton, O'Neil & Mayeda 1972)
$\Delta_{sericite/H2O}$	$= 2.38x10^6/T^2 - 3.89$	(O'Neil & Taylor 1967)
$\Delta_{chlorite/H2O}$	$= 1.56x10^6/T^2 - 4.69$	(Wenner & Taylor 1971)

If the exchange of O^{18} occurs between a fluid and a pre-existing mineral/rock the final δO^{18} value of the mineral/rock will depend on a number of factors including the δO^{18} of the fluid (δW), the initial δO^{18} of the mineral or rock (δRi), the water-to-rock ratio (W/R), and the fractionation factor (Δ) (Taylor 1979). If, however, a mineral is precipitated directly from a hydrothermal fluid it should be in equilibrium with the fluid δO^{18}, so is dependent on the fractionation factor alone (Kyser 1987).

The fractionation factor between two phases in isotopic equilibrium such as a precipitated mineral and the parent fluid can be considered to be a close approximation to the δO^{18} value of the fluid (δW) subtracted from the δO^{18} value of the mineral, i.e.

$$\Delta_{mineral/water} = \delta O^{18}_{mineral} - \delta W \quad \text{(Taylor 1979)}$$

6.1.1 Results

Ten samples from the Koonya alteration were analysed for their oxygen isotope values. Two sets of five samples were taken. The first five samples were taken from veins in the quartz-sericite-pyrite altered zone (from drillholes Kp306 and Kp307). The other five samples were wholerock samples taken from Kp307 (matching the upper five wholerock analyses taken from the same drillhole, figure 5.1 chapter 5).

The δO^{18} results for the ten samples are shown in Table T6.1. This table also lists the approximate concentration (weight percent) of individual oxygen bearing minerals within each sample. The vein compositions were determined by quantitative XRD (X-ray diffraction) analysis while the wholerock compositions were calculated from wholerock data and one sample was checked by XRD. Unfortunately, the composition of the vein sample from Kp307 48.3m could not be determined.

sample	comment	composition	dRf
WHOLEROCK			
Kp307 29.0m	moderately altered	60%qtz,23%mica,17%chl	9.78
Kp307 48.2m	moderately altered	65%qtz,26%mica,9%chl	11.22
Kp307 zone B	strongly altered	70%qtz,25%mica,5%chl	11.1
Kp307 68.5m	moderately altered	65%qtz,27%mica,8%chl	11.68
Kp307 86.0m	relatively unaltered	not calculated	12.02
VEINS			
Kp307 zone B	chlorite-quartz vein	50%qtz,25%chl,25%matrix	10.66
Kp307 zone B2	ore vein chlorite	95%chl,5%qtz	7.43
Kp307 zone B3	ore vein chlorite	90%chl,10%qtz	6.95(6.76)
Kp307 48.2m	chlorite-quartz vein	unknown	7.76
Kp306 76.3m	ore vein chlorite	95%chl,5%qtz	5.62

Table T6.1: Composition and oxygen isotope values for the Koonya samples

Section 6.2 Veins

A total of five vein samples were taken, three from mineralized veins and two from quartz-chlorite veins. Unfortunately problems were encountered with both quartz-chlorite vein samples. Sample 307 zone B was accidently contaminated with material from the rock hosting the vein, and sample 307 48.2m was totally used during the oxygen isotope analysis, so no composition could be obtained. Hence these two quartz-chlorite vein samples could not be used in further calculations.

It is possible to determine the δO^{18} of a fluid from vein minerals. By knowing the mineral composition of a vein and knowing the fractionation factors of each mineral, the fraction equation for the vein (Δvw) can be calculated (Gregory and Criss 1986). For example, a vein with a composition of 95% chlorite and 5% quartz will have a fractionation equation equal to:

$$\Delta vw = 0.95 \times (\Delta chlorite/H20) + 0.05 \times (\Delta quartz/H2O)$$

As mentioned previously, minerals precipitated directly from a hydrothermal fluid, such as those in a vein, should have δO^{18} values in fractionation equilibrium with the fluid. The value of δO^{18} for the fluid (δW) can therefore be determined by utilizing the fact that for equilibium fractionation:

$$\Delta vw \approx \delta O^{18}_{vein} - \delta W \qquad \text{(Taylor 1979)}$$
$$\therefore \quad \delta W \approx \delta O^{18}_{vein} - \Delta vw$$

where δO^{18}_{vein} is the measured δO^{18} value for the vein and Δvw is the fractionation factor of the vein calculated for an assumed temperature.

The δO^{18} value of the fluid that would be in equilibium with the three mineralized veins has been calculated for several assumed temperatures. The results have been compiled and tabulated in Table T6.2. It seems most likely that the lead-zinc veins, from which the samples were taken, formed from fluids with temperatures at or below 250°C (based on sulphide mineralogy, section 3.3). It is for this reason that the temperatures of 200°C and 250°C were modelled. Temperatures of 300°C and 330°C have also been modelled to provide contrast to the lower temperatures.

Temperature °C	δO^{18} of the fluid			Average dWi
	307 zone B2	307 zone B3	306 76.3m	
200	2.89	3.64	4.69	3.74
250	4.22	5.06	6.03	5.1
300	5.22	6.12	7.03	6.12
330	5.71	7.43	7.52	6.62

Table T6.2: Average δO^{18} of the fluid causing the alteration associated with mineralization (calculated from mineralized veins).

The average fluid compositions calculated were 3.74, 5.10, 6.12 and 6.62 ‰ for temperatures of 200°C, 250°C, 300°C and 330°C respectively. These calculations assume that the δO^{18} values for the altered rocks and veins have not been modified by a later event. Unfortunately, this is not likely to be the case at Koonya due to post-mineralization metamorphism and granite related metasomatism. This can be checked by utilizing the δO^{18} values measured for the wholerock samples and a calculated parameter called the water/rock ratio.

Section 6.3 Wholerock Oxygen Isotopes and the Water/Rock Ratio

The water/rock ratio is a concept based on the fractionation of oxygen isotopes between a fluid and rocks containing oxygen-bearing minerals. It is calculated by considering the initial δO^{18} value of the fluid (δWi), the initial δO^{18} value of the rock (δRi), the δO^{18} value of the rock after alteration (δRf) and the fractionation factor between the fluid and rock (ΔRW) (Taylor 1979). The water/rock ratio in simple terms is the proportion of atomic oxygen in a fluid, relative to the oxygen in the rock, required to change the rock from its initial δO^{18} to its final δO^{18} value. This equates to approximately twice the mass of water required for a given mass of rock (Taylor 1987).

In order to calculate the water/rock ratio a number of factors must first be determined, including δRi, δRf, δWi and ΔRW.

The initial δO^{18} value for the rock can be estimated by considering the typical oxygen isotope value for fresh rhyolites. Taylor (1968) records values of about 6 to 8‰ for dacitic to rhyolitic lavas and values of 7 to 9 % for rhyolitic pyroclastics. Thus a δRi value of 7.5‰ has been assumed for this study.

The final δO^{18} value of the rock (δRf) is the parameter that is measured in the wholerock oxygen isotope analysis.

The δO^{18} of the initial fluid can be estimated from the calculation made in the previous discussion of veins, i.e. 3.74, 5.10, 6.12 or 6.62 ‰ for temperatures of 200°C, 250°C, 300°C and 330°C respectively.

If the mineral composition of the rock is known, and mineral/water fractionation equation for each mineral is known, the fractionation equation for the rock (ΔRW) can be calculated (Gregory & Criss 1986). For example, a rock containing 60% quartz and 40% sericite would have the following fractionation equation:

$$\Delta RW = 0.6x(\Delta quartz/H2O) + 0.4x(\Delta sericite/H2O)$$

The fractionation equations for each rock sample have been calculated and are shown below.

307 29.0m $\Delta RW = 2.85x10^6 xT^2 - 3.73$

307 48.2m $\Delta RW = 2.96x10^6 xT^2 - 3.64$

307 zoneB $\Delta RW = 3.04x10^6 xT^2 - 3.59$

307 68.5m $\Delta RW = 2.96x10^6 xT^2 - 3.63$

307 86.0m not calculated due to difficulties in determining composition but should be similar to 307 zoneB

The final factor to be considered before calculating the water/rock ratio (W/R) is the type of fluid circulation system being considered. There are two major types of circulation systems, closed systems and open systems. In a closed system the fluid is recirculated continuously through the same rock so that both the δO^{18} of the rocks and the fluid are changed. In an open system the fluid makes one pass through the rock and is then lost from the system (Taylor 1987). At Koonya, a non-symmetrical arrangement of the alteration relative to the main lead-zinc zone suggest that the fluid circulation system was open; however, both an open system and a closed system have been modelled. The equations for the water/rock ratio are listed below (both are taken from Taylor 1979):

closed system $$W/R = \frac{\delta Rf - \delta Ri}{\delta Wi - \delta Rf + \Delta_R W}$$

open system $$W/R = \ln\left\{\frac{\delta Rf - \delta Ri}{\delta Wi - \delta Rf + \Delta_R W}\right\}$$

6.3.1 Expected Water/ Rock Ratios

Michard & Albarede (1986) in their study of hydrothermal vent fluids from the East Pacific Rise conclude that the likely water/rock ratios for the entire fluid system lie in the range 1 to 5. This is the typical range suggested by various authors for entire fluid-rock systems. However, at Koonya only part of the fluid-rock system is being studied, namely the alteration immediately associated with the mineralized zone. Beaty and Taylor (1982) in their study of the alteration pipe for the Amulet mineralization (a volcanogenic massive sulphide deposit) consider that the water/rock ratios exceed 100.

Some idea of the expected water/rock ratio of the Koonya alteration zone can also be gained from the intensity of the alteration as well as from analogy with Beaty & Taylor (1982). Immobile element studies of the Koonya alteration have shown that strong metasomatic alteration of the rocks has occurred (upto 30% volume/mass change). Such strong metasomatic alteration is the product of high (localized) fluid-to-rock ratios. A conservative estimate for the water/rock ratio would be about 20.

6.3.2 Calculated Water/Rock Ratios

The water/rock ratios have been calculated for the four quartz-sericite-pyrite altered samples for several assumed temperatures (table T6.3). The temperatures used matched those for the vein samples so that the fluid δO^{18} calculated from the veins for a given temperature could be used as δWi in the water/rock equation.

Temperature °C	Average dWi	WATER/ROCK closed\open			
		29.0m	48.2m	zone B	68.5m
200	3.74	0.76\-0.27	1.76\0.57	1.36\0.31	2.52\0.92
250	5.1	1.13\0.12	3.51\1.26	2.37\0.86	6.85\1.92
300	6.12	1.71\0.54	13.51\2.60	5.22\1.65	-ns-
330	6.62	2.40\0.88	-ns-	12.39\2.52	-ns-

Table T6.3: The water/rock ratios calculated for both open and closed systems using the average fluid δO^{18} calculated from veins. [note: -ns- indicates the δWi used in the calculation could not have produced the wholerock δO^{18} measured for that particular sample]

The calculations for the temperatures 200°C and 250°C result in water/rock ratios below 7 for closed systems and below 2 for open systems. This is in direct contrast to the expected water/rock ratios. This discrepancy can be explained by modification of the δO^{18} values set during the hydrothermal alteration by a later event. It means that veins cannot be used to estimate the original hyrdrothermal fluid δO^{18}.

6.3.3 Metamorphism/ Granite Related Metasomatism

It seems very likely that the later event that modified the alteration rock/vein δO^{18} values set during alteration was either regional metamorphism or metasomatism related to granite fluids (or both). Both these events have fairly high positive fluid δO^{18} values associated with them. The Devonian magmatic fluid probably has δO^{18} values in the range 7 to 8‰ (G. Green pers. comm.). The low temperature metamorphic event would have a similar sort of fluid δO^{18} range or possibly slightly higher (Taylor 1979). As the two events likely to produce later modification of pre-existing δO^{18} values have fluids of fairly high positive δO^{18}, an estimate of the maximum fluid δO^{18} for the earlier alteration/mineralization event can be calculated.

6.3.4 Estimate of Maximum Hydrothermal Fluid δO^{18}

At temperatures below 500°C later fluids with a high positive δO^{18} (such as +7‰) could only have increased the rock/vein δO^{18} produced by the earlier event. This means that the measured wholerock oxygen isotopes ($\delta Rf_{measured}$) must be the maximum value that could have been attained during the earlier event, that is:

$$\delta Rf_{early\ event} \leq \delta Rf_{measured}$$

Combining this with the fact that for relatively high water/rock ratios (3 for an open system or 10 for a closed system) the final δO^{18} value of a rock being altered by a fluid is approximately equal to $\delta Wi + \Delta RW$ (appendix 3 shows how this is derived), an equation for the δRf of the early event would be

$$(\delta Rf_{early} \approx) \delta Wi_{early} + \Delta RW \leq \delta Rf_{measured}$$

This assumes that the compostion of the rock has not been changed much during the later event. Re-arranging the equation:

$$\delta Wi \leq \delta Rf\ (measured) - \Delta RW$$

so the maximum value for δWi is:

$$\delta Wi\ (max) = \delta Rf\ (measured) - \Delta RW$$

Thus by calculating the rock-water fractionation (ΔRW) for different assumed temperatures the maximum value for the hydrothermal fluids δO^{18} can be estimated. These values have been calculated for temperatures of 200°C and 250°C (the likely temperatures for formation of the mineralization, see section 3.1).

The approximate value that could produce the δO^{18} values observed at a given temperature for all four samples was taken as the maximum fluid δO^{18} for that temperature. A slight increase of the maximum fluid δO^{18} was made in order to correct for the approximation made in the equations. The results are shown in Table T6.4.

temperature °C	$\Delta RW/\delta Wi_{(max)}$				Fluid dWi (max)
	29.0m	48.2m	zone B	68.5m	
200	9.01/0.77	9.59/1.63	10.00/1.10	9.60/2.08	~ 1.0
250	6.69/3.09	7.18/4.02	7.52/3.58	7.19/4.49	~ 3.1

Table T6.4: Estimate of the maximum fluid δO^{18} for the alteration associated with mineralization.

The alteration being studied is associated with the main lead-zinc zone. The mineralogy of the of this mineralized zone would suggest that it formed at temperatures below 250°C (see section 3.3). This corresponds to a hydrothermal fluid with a maximum δO^{18} value of 3‰. Because the wholerock oxygen isotope values set by the original hydrothermal event have been increased by the later event, the initial δO^{18} value of the early fluid was less than the maximum value calculated.

Section 6.4: Conclusion

The maximum fluid δO^{18} for the hydrothermal fluid causing the alteration associated with the main lead-zinc mineralized zone at Koonya was 3‰ but the actual fluid δO^{18} was probably less. Using information from Taylor (1979), this fluid δO^{18} is unlikely to be metamorphic or igneous in origin, but it does correspond to δO^{18} values observed for geothermal systems and connate waters. It is interesting to note that many of the Kuroko massive sulphide deposits, interpreted to have formed from circulating seawater, have δO^{18} values typically in the range of -1‰ to 3‰ (eg. Taylor 1979, Beaty and Taylor 1982, Taylor 1987). Thus it seems likely that the Koonya alteration/mineralization was formed from a circulating seawater system.

Chapter 7: CHLORITE

Chlorite is a common mineral in many hydrothermal alteration zones. In 1981, Walshe and Solomon proposed a six component chlorite solid solution model (since modified by Walshe 1986) designed to determine the temperature of formation of the chlorite from its composition.

Chlorite compositions associated with the alteration around the main lead-zinc zone in the east-west section at Koonya have been investigated in some detail in order to both utilize Walshe's (1986) model to determine temperature of chlorite formation, and to examinine the variation of chlorite compositions with differing alteration and cleavage relationships.

7.0.1 Analytical Procedures

Standard size thin sections were marked up, carbon coated, and then analysed using a Cameca SX500 microprobe. Three of four patches of chlorite spread out over each of twelve thin sections were analysed. Within each patch, a minimum of three analyses were carried out on different chlorite grains. All the data for a particular patch was reviewed, and any analyses that were significantly different to the other analyses, were discarded. The remaining analyses were then averaged to produce a generalised chlorite composition for the chlorite patch. The exception to this was thin section 307 zA2 which had a damaged carbon coating, so only two analyses could be obtained.

The majority of chlorites were analysed for the elements Si, Al, Fe, Mn, Mg, Ti and Cr; but some analyses included the additional elements Te, Ca, K, Na, Cl, S, P, Zn and Ni. In all cases, the only elements above the detection limits were Si, Al, Fe, Mn and Mg. This is important, as Walshe's (1986) chlorite model does not allow for the presence of any other elements (except Ti and Cr) in the chlorite's structure.

Section 7.1: Chlorite Composition

All chlorite samples analysed were taken from drillholes in the east-west section (namely Kp307, and to a lesser extent, Kp306). The majority of samples were from the quartz-sericite-pyrite altered zone (and are refered to as **qtz-alt**), however one sample (Kp307 86.0m) came from the sericite altered zone (refered to as **ser-alt**). The chlorite in the sericite altered sample occured as distinct patches associated with feldspar phenocrysts.

	SiO2	Al2O3	FeO	MnO	MgO	Total
307 zb1c1	23.23	21.27	26.98	4.29	9.17	87.55
307 zb1c2	22.19	20.64	28.33	4.31	8.72	86.45
307 zb1c3	22.6	20.23	28.99	4.11	8.58	86.77
307 zb1c4	23.09	19.66	29.78	4.38	8.33	84.97
307 zb2c1	22.83	20.23	29.47	3.95	8.65	85.15
307 zb2c2	22.98	19.76	29.63	3.82	8.7	84.94
307 zb2c3	23.41	19.48	29.85	4.33	8.55	85.75
307 zb2c4	22.27	20.27	30	4.15	8.19	84.97
307 zb3c1	22.82	20.82	33.98	4.51	5.9	87.55
307 zb3c2	21.68	20.9	33.66	4.49	5.66	86.45
307 zb3c3	22.12	20.98	33.46	4.53	5.64	86.77
307 za1c1	21.69	20.65	31.01	4.63	6.95	84.97
307 za1c2	21.61	20.89	31.54	4.3	6.73	85.15
307 za1c3	21.78	20.7	30.97	4.72	6.76	84.99
307 za2	22.67	20.61	29.06	4.59	8.41	85.34
307 za2	22.94	20.68	28.46	4	8.78	84.86
306 76.3c1	23.36	20.36	30.82	3.78	8.4	86.72
306 76.3c2	23.8	20.03	30.91	4.03	8.36	87.13
306 76.3c3	22.62	20.9	30.84	3.77	8.11	86.24
307 zb0c1	22.47	20.94	33.18	4.51	5.78	86.88
307 zb0c2	22.43	20.87	33.01	4.43	5.85	86.59
307 zb0c3	22.37	20.98	32.62	4.2	5.86	86.03
306 66.2c1	23.15	21	29.74	5.07	8.36	87.33
306 66.2c2	23.27	21.28	29.33	4.39	8.19	86.46
306 66.2c3	22.85	20.9	29.25	4.75	8.33	86.08
306 66.2c4	22.9	20.77	29.11	4.44	8.54	85.76
307 70.3c1	23.55	21.05	27.56	4.41	9.86	86.56
307 70.3c2	23.3	21.19	27.49	4.48	9.72	86.23
307 70.3c3	23.89	21.79	27.01	3.86	9.56	86.18
307 48.2c1	22.65	20.88	29.65	4.48	8.3	86.06
307 48.2c2	23.01	20.79	29.51	4.22	8.36	85.96
307 48.2c3	23.5	20.34	29.63	4.54	8.88	86.94
307 29.0c1	22.91	20.91	29.13	3.39	9.74	86.08
307 29.0c2	23.06	20.9	29.46	3.4	9.81	86.63
307 29.0c3	22.95	20.65	28.95	3.41	9.65	85.61
307 29.0c4	22.76	20.74	28.89	3.34	9.77	85.5
307 86.0c1	26.29	22	14.61	0.87	21.78	85.55
307 86.0c2	25.69	21.44	14.74	0.94	21.79	84.6
307 86.0c3	25.93	21.5	15.13	0.9	21.72	85.18
307 86.0c4	26.44	21.56	14.86	0.91	22.3	86.07

	type of chlorite	chlorite association
zb1c1	sheared egde of ore vein	
zb2c2	chl at ore vein edge	ore vein from the lower zone
zb1c3	chl within vein	
zb1c4	chl at ore vein edge	
zb2c1	chl at ore vein edge	
zb2c2	chl within vein	ore vein from the lower zone
zb2c3	chl at ore vein edge	
zb2c4	sheared egde of ore vein	
zb3c1	chl at ore vein edge	
zb3c2	chl within vein	ore vein from the lower zone
zb3c3	chl at ore vein edge	
za1c1	chl at ore vein edge	
za1c2	chl within vein	ore vein from the upper zone
za1c3	chl at ore vein edge	
za2	chl within vein	ore vein from the upper zone
za2	chl within vein	
30676c1	sheared egde of ore vein	
30676c2	chl at ore vein edge	ore vein from kp306
30676c3	chl at ore vein edge	
zb0c1	chl in chl vein	
zb0c2	chl in chl vein	pre-deformation chl vein
zb0c3	chl in chl vein	
30666c1	chl in qtz-chl vein	
30666c2	chl in qtz-chl vein	syn-deformation chl veins from kp 306
30666c3	chl in qtz-chl vein	
30666c4	chl in qtz-chl vein	
70.3c1	chl in qtz-chl vein	
70.3c2	chl in qtz-chl vein	syn-deformation chl veins
70.3c3	chl in qtz-chl vein	
48.2c1	chl in qtz-chl vein	
48.2c2	chl in qtz-chl vein	syn-deformation chl veins
48.2c3	chl in qtz-chl vein	
29.0c1	pressure shadow	
29.0c2	pressure shadow	syn-deformation chl pressure shadows
29.0c3	pressure shadow	
29.0c4	pressure shadow	
86.0c1	sheared feldspar?? replcement	
86.0c2	sheared feldspar?? replcement	associated with albite pre-cleavage?
86.0c3	sheared feldspar?? replcement	
86.0c4	sheared feldspar?? replcement	

Table T7.1: Chlorite composition and its association to the mineralization and deformation

Chlorites taken from the quartz-sericite-pyrite alteration included;

i) chlorite in lead-zinc-pyrite veins, both sheared chlorite and apparently unsheared, randomly orientated chlorite (possibly recrystallized), refered to as '**ore veins**', and
ii) thin chlorite veins/pressure shadows, both pre-cleavage or syn-cleavage, and either sheared or unsheared/recrystallized chlorite, refered to as '**chl veins**'.

The analytical results for the twelve thin section are shown in Table T7.1 as the weight percent oxide for the five detected elements (ie: SiO_2, Al_2O_3, Fe0, Mg0 and Mn0). This table also includes a description of the type of chlorite and the association in which the chlorite occurs. The chlorite compositions within a thin section are very homogeneous despite differences such as being sheared or unsheared.

Histograms of the chlorite composition for each of the five elements are presented in Figure 7.1 (as weight percent oxides). The distribution of the chlorite composition for SiO_2, Al_2O_3, and Mn0 are each shown as a single histogram with the three classes of chlorite (ore vein, chl vein, and **ser-alt**) depicted by different symbols (figure 7.1a, b & c). However the distributions of both MgO and FeO are depicted by two histograms (figures 7.1d&e and 7.1f&g respectively). The first histogram for both elements shows the difference between the **qtz-alt** (both ore veins and chl veins) and **ser-alt** samples on a large scale (figures 7.1d & f), while the second histogram shows the detailed variation between the 'ore veins' and 'chl veins' for the **qtz-alt** samples (figure 7.1e & g).

7.1.1 Chlorites from the Quartz-Sericite-Pyrite Alteration

The ore vein chlorites and the chl vein chlorites comprise the group of samples taken from the quartz-sericite-pyrite alteration zone (or the **qtz-alt** chlorites). The distributions of SiO_2, Al_2O_3 and MnO for the quartz-sericite-pyrite altered samples are tightly constrained within a limited range of values. (SiO_2=22.75±1.25, Al_2O_3=20.75±0.75, MnO=4.25±0.75) (figure 7.1a, b &c). This is in direct contrast to the distributions of FeO and MgO which have a much wider range of compositions (figures 7.1e & g). Both Al_2O_3, and SiO_2, are strongly temperature (Cathelineau and Niera 1985) dependant, but FeO and MgO are only vaguely temperature dependant (Walshe and Solomon 1981, Green 1983). The distribution of elements in both the 'ore veins' and 'chl veins' are very similar.

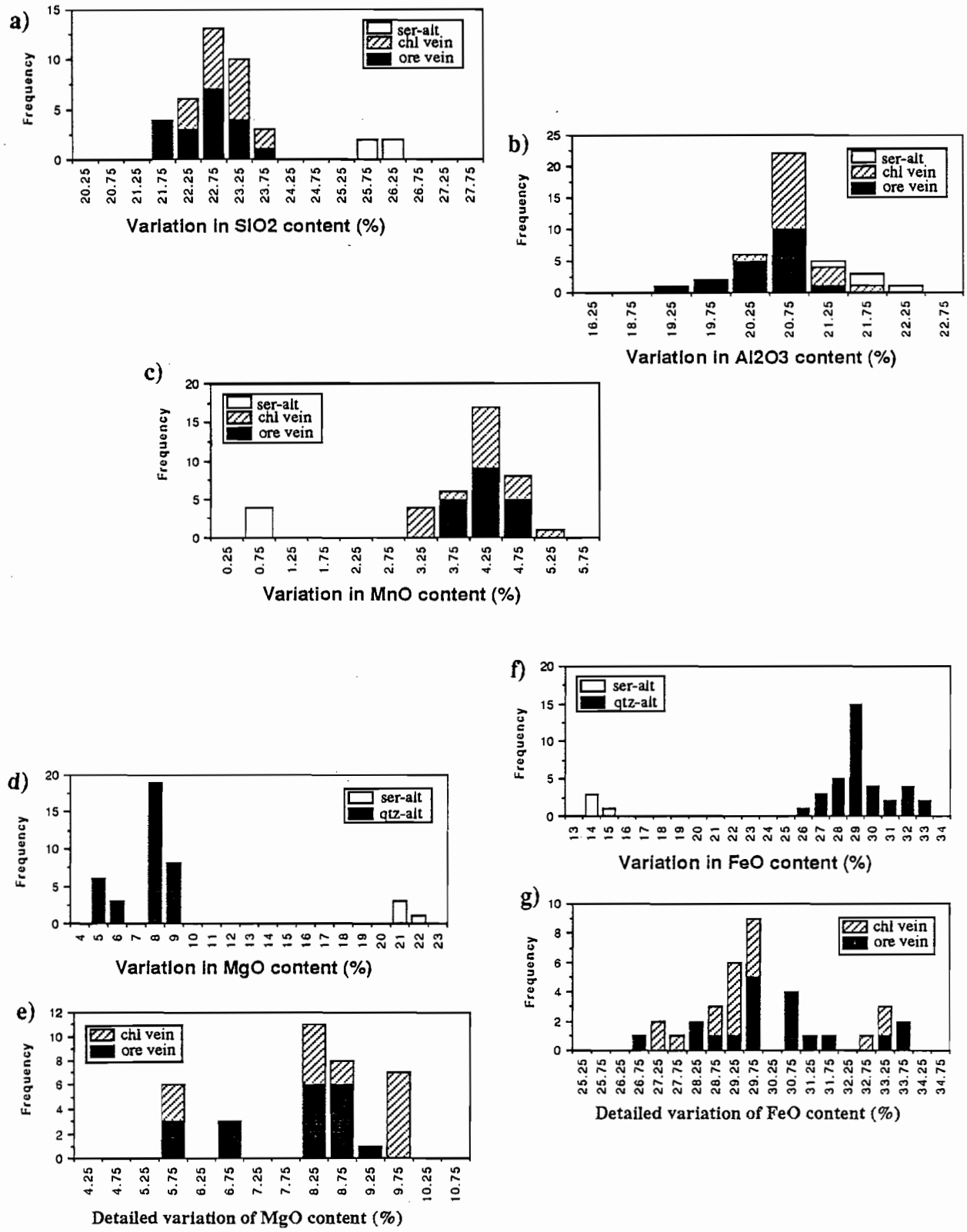

Figure 7.1: Variation of the concentration of different elements within the Koonya chlorites

There are several possible explanations for the observed distribution of the elements.

i) All chlorites were formed from fluids at similar temperatures (both pre-cleavage and syn-cleavage!).
ii) Early formed chlorites partly controlled the later compositions; however the similarity of Al_2O_3 and SiO_2 (both of which are strongly temperature dependent) within syn-cleavage and pre-cleavage chlorites suggests the temperatures for formation of all chlorites must have been similar.
iii) Chlorites have been re-equilibrized during metamorphism, homogenising the temperature dependent elements Al_2O_3 and SiO_2, but retaining some variations in FeO and MgO contents which are generally not considered to be strongly temperature dependent (Cathelineau and Niera 1985).

7.1.2 Manganese Content of the Koonya Chlorites

An interesting feature of the Koonya chlorites is their remarkably high MnO content. They form a tightly constrained group with an MnO content of 4.25±0.75 weight percent. At Rosebery, the highest MnO content recorded by Green (1983) is 1.79wt.%. Eastoe et al. (1987) described chlorite compositions from throughout the Mount Read Volcanics, but the highest MnO content they reported was approximately 3.0wt.% for chlorites in the Hercules area.

Polya et. al. (1986) report values of up to 1.8wt.% MnO in the Murchison Gorge area. They suggest that such high MnO contents are consistent with fluids (seawater) having leached the manganese from the volcanic pile.

Both the pre-cleavage and syn-cleavage chlorites have very high manganese contents, this suggests that either both events had very high manganese, which seems very unlikely based on the apparent rarity of high manganese chlorites, or the manganese content of the syn-cleavage chlorite is controlled by pre-existing chlorites and/or the surrounding rock.

Section 7.1.3: Quartz-Sericite-Pyrite Alteration Versus Sericite Alteration

One of the most obvious features of the chlorite compositions is that the **qtz-alt** , which includes both ore veins and chl veins (from the quartz-sericite-pyrite alteration) and **ser-alt** chlorites (from the sericite alteration) are significantly different. The largest differences are in the FeO and MgO contents, with lesser differences in the MnO and SiO_2 content, but virtually no difference in the Al_2O_3 content. These differences suggest that the fluids or physio-chemical conditions during forming the two types of alteration, quartz-sericite-pyrite alteration and sericite alteration, were reasonably different.

Section 7.2: The Six Component Chlorite Solid Solution Model and Metamorphism

Walshe and Solomon (1981) devised a model whereby the solid solution chlorite series was broken into six end members. By calculating the thermodynamics of each end member (or component) they developed a thermodynamic model for the chlorite solid solution series. Walshe (1986) has further refined this model.

The main purpose of the chlorite model is to determine the temperature of formation of chlorite co-existing with mineralization, and hence determine the temperature of ore deposition. Walshe's (1986) chlorite model can also be used to calculate other conditions such as oxygen fugacity (fO_2) and the activity of H_2S (a_{H_2S}) of the fluid from which it formed. The chlorite model gives fairly accurate results upto about 300°C, but temperatures above 320°C may be over-estimated by the model (Walshe, Hedges and Harrold 1986, B.Harrold pers. comm. 1989).

Walshe's (1986) chlorite model has been applied to the Koonya chlorites compositional data. By utilizing a computer program held by the Tasmania Mines Department (called 'chlorite'), the conditions of the chlorite's formation were calculated for both liquid-vapour and one kilobar (1Kb) pressures. In a number of cases, particularly for the 1Kb pressure, values were not obtained for the chlorite concerned due to the program's limitations.

A histogram of the distribution of temperatures calculated at both liquid-vapour and 1KB pressures for the Koonya chlorites is presented in Figure 7.2.

At liquid-vapour pressures, chlorites from the quartz-sericite altered zone have temperatures of formation that range from <295°C to >335°C with an average of 313°C (for 34 analyses).

However, the chlorites from the sericite altered zone have temperatures ranging from 359°C to 368°C (4 analyses). All temperatures obtained at liquid-vapour pressures appear to be too high to have formed with the associated lead-zinc mineralization (see section 3.3). Fluids at such temperatures at Koonya should have produced relatively copper-rich mineralization (as seen in drillhole Kp303), but the main lead-zinc zone is relatively copper-poor.

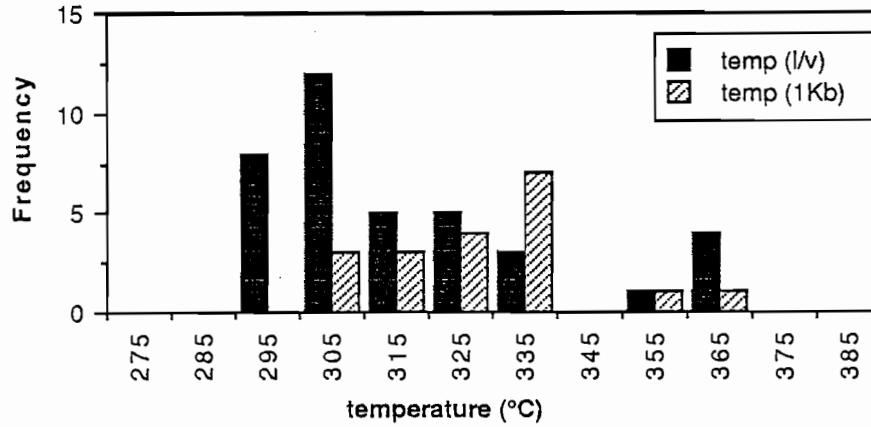

Figure 7.2: Temperatures calculated at both liquid-vapour and 1KB pressures using Walshes' (1986) six component solid solution model.

At a pressure of 1KB the chlorite composition from the altered zone corresponds to a temperature of between 310°C and 340°C, with an average of 328°C. The temperature has increased from that calculated for liquid-vapour pressures. The only value obtained at 1Kb for chlorite from the sericite altered zone, showed a decrease in temperature to about 353°C.

On the basis of chlorite composition and the temperatures derived from Walshe's (1986) model, it appears the chlorite is reflecting a metamorphic event rather than the alteration event associated with the chlorites formation. This assumption can be confirmed by examining the relationship between $\log(fO_2)$ and temperature, both of which are calculated by the chlorite model. If the chlorite has been re-equilibrized by a metamorphic event, the temperature and $\log(fO_2)$ should be directly related (G.Green pers. comm. 1989). A diagram of $\log(fO_2)$ versus temperature (figure 7.3) reveals that for the majority of the data, $\log(fO_2)$ and temperature are directly related (ie. lie on a straight line). The only points that lie well away from the line are those of the chlorite from the sericite altered zone.

It can be concluded that all chlorites from the quartz-sericite-pyrite altered zone at Koonya have been re-equilibrized during metamorphism. Using the results from Walshe's (1986) model at an assumed pressure of 1KB, the average temperature for the metamorphic event is 328°C.

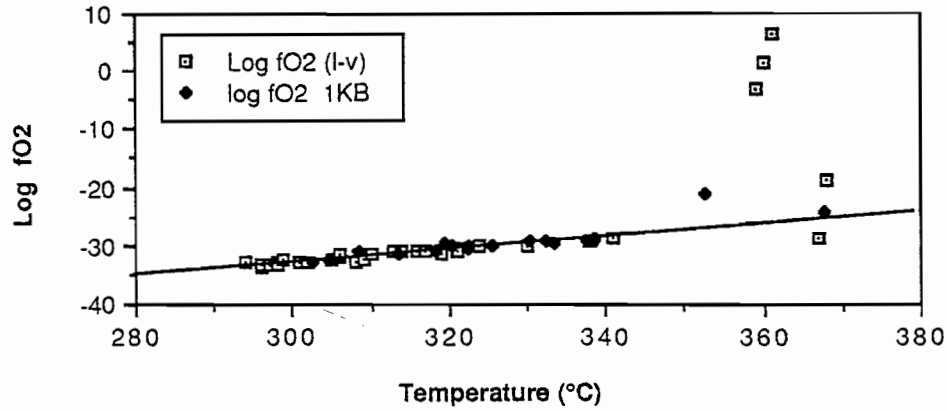

Figure 7.3: Temperature versus Log(fO_2). Conditions were calculated using Walshes' (1986) chlorite solid solution model.

The non-linear results for the chlorites from the sericite altered zone on the plot of log(fO_2) versus temperature may indicate that these chlorites have only been partially re-equilibrized during the metamorphic event.

Section 7.3 Summary

An unusual feature of the Koonya chlorites is their very high manganese content (4.25±0.75). Polya et al. (1986) consider high values of manganese to be consistent with a the element having been leached from a volcanic pile. From the distribution of the MnO content of altered zone chlorites, it was concluded that syn-cleavage chlorite compositions were controlled to some extent by either pre-existing chlorite or the surrounding rock.

One of the most obvious features of the distribution of the various elements within the chlorite, is that chlorites from the quartz-sericite-pyrite altered zone are very different to those from the sericite altered zone. It seems likely that this difference reflects a difference in either the fluid or the physio-chemical conditions associated with the chlorites formation.

The distribution of the element concentration in chlorites from the quartz-sericite-pyrite alteration and the temperatures obtained when using Walshe's (1986) six-component chlorite model suggest that the chlorite has been re-equilibrized by a metamorphic event. This assumption is confirmed by examining the relationship between the calculated temperature and the oxygen fugacity. Assuming a pressure of 1Kb, an average temperature of 328°C was obtained for the metamorphic event.

Chapter 8: GENETIC MODELS

Two models are proposed to explain the geology, mineralization and alteration associated with the main mineralized horizon (comprising both the main lead-zinc zone and the upper zone) at Koonya. The first model is based on an epigenetic vein style origin for the mineralization whereas the second model is based on a syngenetic volcanogenic origin for the mineralization.

Section 8.1: Epigenetic Model

The three stage epigenetic model is illustrated in Figure 8.1.

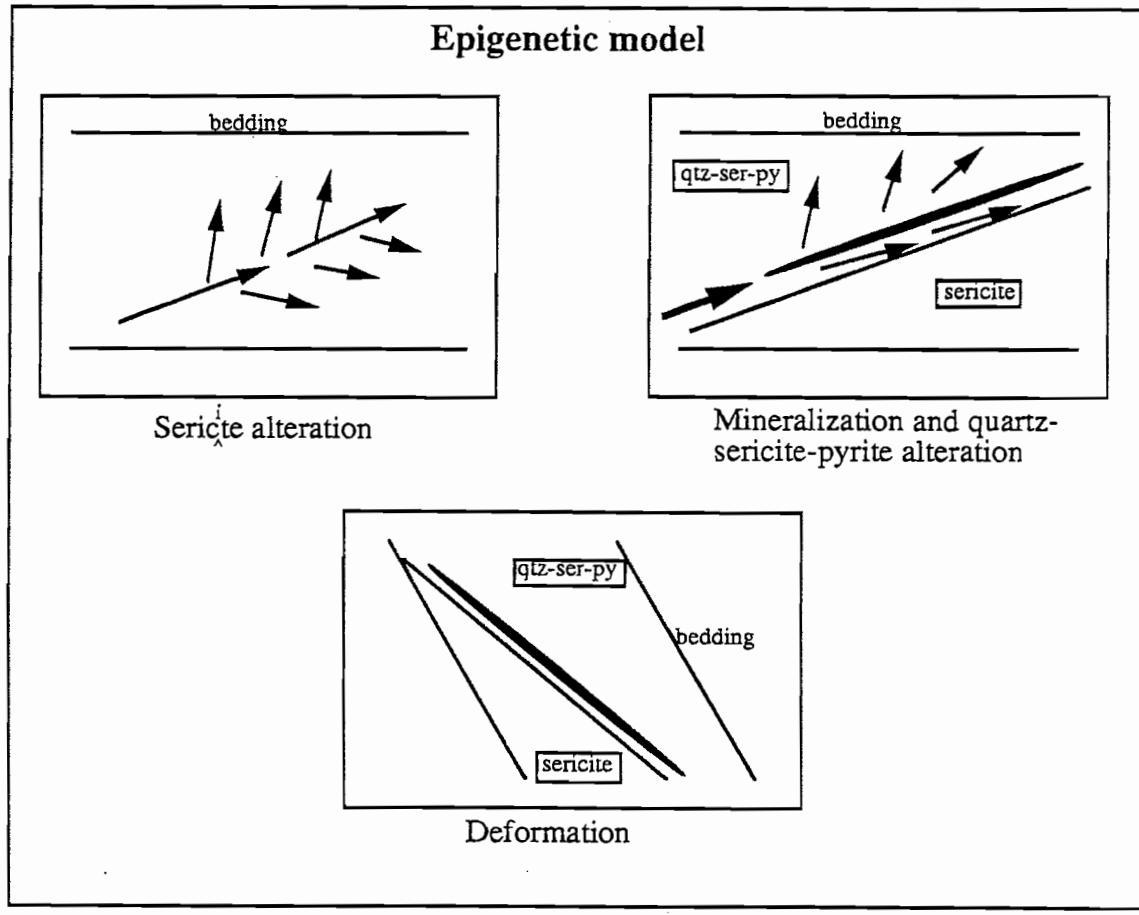

Figure 8.1

Initially convecting Cambrian seawater moves up a structural zone, which crosscuts stratigraphy, within a sequence of uniform rhyolitic volcanics. These fluids cause a strong sericitization of the rocks adjacent to the structural zone.

Secondly, due to a change in the physico-chemical conditions, the fluid deposits the mineralization then spread out into the hanging wall ,and to a lesser extent the footwall, causing quartz-sericite-pyrite±chlorite alteration. The fluids causing the alteration penetrated less than ten metres into the footwall. In the more southern areas of the prospect, fluid were reasonably high temperature (>270°C) and under-saturated with respect to lead. Northern area fluids were cooler (<250°C), varing from being under-saturated in lead, to saturated in both lead and zinc.

Finally, the rock sequence was folded during the Devonian regional deformation, and the mineralization and alteration were reoriented to their present attitude.

Section 8.2: Syngenetic Model

A three stage syngenetic model can also explain features of the main mineralized zone at Koonya (figure 8.2).

In the first stage the massive sulphide is formed from exhalation of hydrothermal fluid, comprising modified convecting seawater, onto the seafloor through a sequence of rhyolitic volcanics. The vein and disseminated style mineralization would represent footwall 'stringer style' mineralization associated with the alteration below the massive sulphide. In the southern areas the fluid temperatures are highest (>270°C), but become progressively cooler to the north. The higher temperature zones are dominated by vein and disseminated 'stringer style' style mineralization.

In the second stage, the massive sulphide horizon is buried by a sequence of rhyolitic volcanics geochemically similar to the footwall rocks, but the hydrothermal system remains active, although the physico-chemical conditions are different to the first stage. The continued fluid activity causes the strong sericitization of the hanging wall.

In order to to arrive at the arrangement of the alteration and mineralization currently seen, the whole mineralized system must have been overturned during the Devonian deformation.

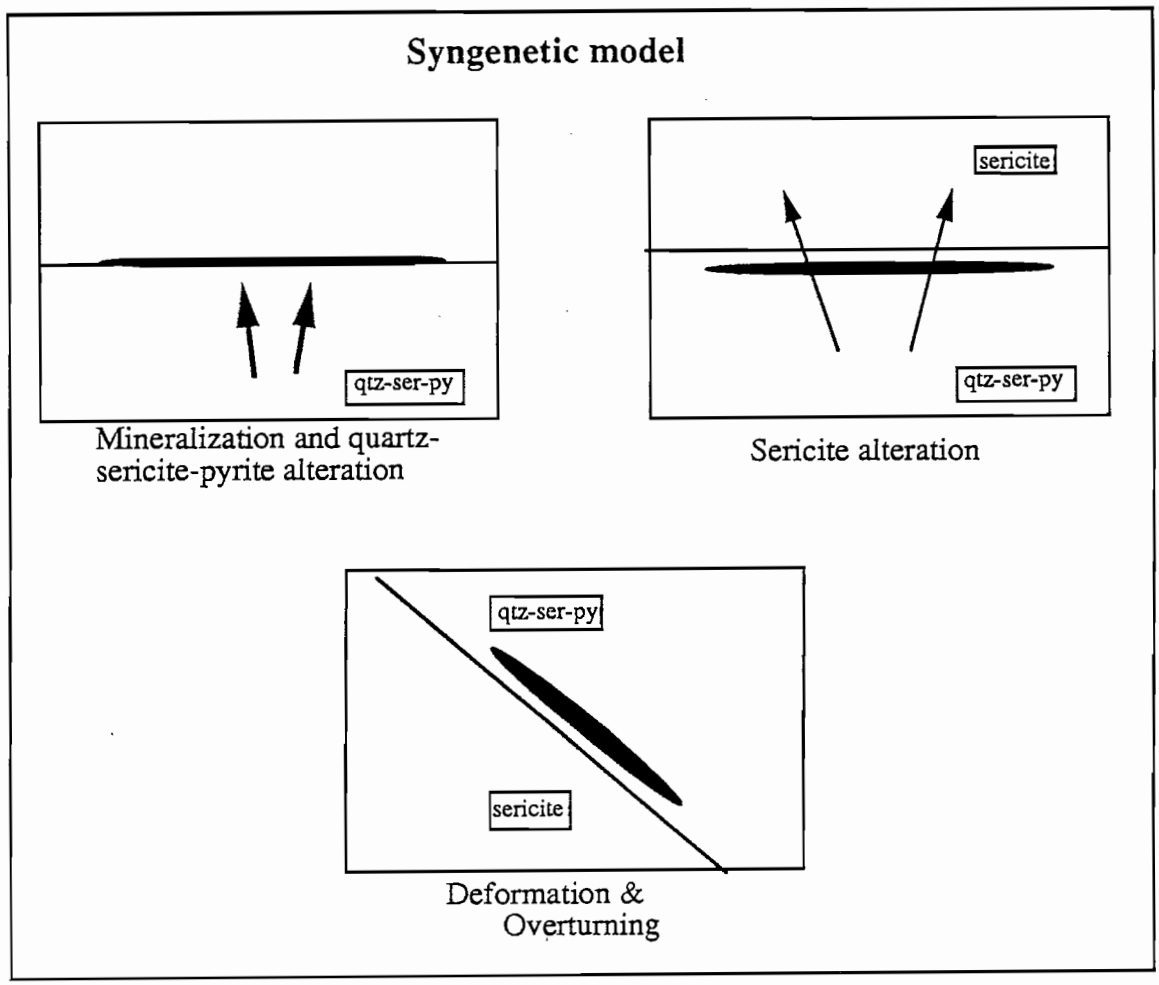

Figure 8.2

Section 8.3: Evidence for/against the Genetic Models

The syngenetic model for the mineralization is supported by the restriction of the mineralization to a very narrow horizon adjacent to the boundary of two different styles of alteration. The massive sulphide is always very close to the boundary between the different types of alteration. Although not typical of volcanogenic massive sulphides, strong alteration of the hanging wall, as seen at Koonya, can occur (Date et al. 1983, Green et al. 1983).

Several problems are envisaged with a syngenetic model. The first is the presence of graded bedding in the Koonya sequence which suggests the sequence is upright and not overturned, although this assumes normal grading which may not be the case. Furthermore, there is no evidence to suggest that the sequence in the surrounding areas has been overturned.

Another problem is that the along-strike continuation of the massive sulphide horizon in the north-south section crosscuts the stratigraphy. The projected down-dip and north-south extensions of the massive sulphide horizon do not show evidence of syngenetic mineralization.

Only one problem is envisaged with the epigenetic model, that is the restriction of the main lead-zinc mineralized zone to a very thin horizon and the limitation of the quartz-sericite alteration to less than 10 metres depth within the footwall.

8.3.1 The Preferred Genetic Model

Of the two models the epigenetic model best explains the observed geology, mineralization and alteration, and is therefore the preferred model to explain the genesis of the Koonya mineralization.

The problem of only having a limited zone of quartz-sericite-pyrite in the footwall could be explained by rising of the hot convecting fluid, particularly if the structural zone is dipping shallowly.

Chapter 9: CONCLUSIONS

Throughout this thesis a number of important conclusions have been made that affect the interpretation of the genesis of the mineralization. These are:

The Koonya mineralization is hosted in a Cambrian sequence dominated by rhyolitic feldspar-phyric units. The origin of these units is uncertain, but they may be unusual pyroclastics. Unfortunately, the bedding attitude at Koonya could not be determined, however, mapping to the west of the prospect by Lees (1987) suggests the sequence is dipping east at approximately 60°. The presence of grading in two units indicates that the sequence is upright (assuming normal grading).

Two major mineralized horizons occur at Koonya, the most important of which contains the main lead-zinc zone and upper zone. The mineralization pre-dates the Devonian regional deformation and thus pre-dates the Devonian granite intrusion in the area. In the north-south section the mineralization crosscuts the stratigraphy.

The major mineralized horizon shows a distinct metal zonation from chalcopyrite-pyrite-arsenopyrite-tetrahedrite-aikinite-native bismuth in the south to a sphalerite-galena-pyrite-chalcopyrite-pyrrhotite assemblage further north. The chalcopyrite-pyrite-arsenopyrite-tetrahedrite-aikinite-bismuth assemblage seen at Koonya is very similar to the assemblage seen in the copper-rich mineralization at Rosebery. This suggests some similarity existed between either the fluids that formed the Rosebery and Koonya mineralization, the source of the metal for the two deposits, or both. The mineralogy of this zone suggests it formed at temperatures in excess of 270°C.

A lens of massive sulphide occurs in the east-west section. This mineralization and its down dip, vein style continuation, form a thin, but laterally extensive horizon termed the main lead-zinc zone. The mineralogy, zinc ratio distribution and high manganese values suggest the main lead-zinc mineralized zone was deposited at temperatures below 250°C. The massive sulphide contains minor colloform textures and may contain some primary banding of sulphides. Zinc ratios indicate that the massive sulphide was precipitated from fluids saturated in lead and zinc. However, the zinc ratio distribution for the other types of the mineralization indicates it was deposited either from lead under-saturated fluids or saturated fluids below 200°C.

Several different isotopic techniques have been applied at Koonya. Lead isotopes indicate that the lead in the mineralization was originally concentrated in the Cambrian. Sulphur

isotopes suggest that the dominant source of sulphur was from reduced seawater sulphate. Oxygen isotope studies also suggest that the fluid responsible for the alteration and mineralization at Koonya was dominated by seawater.

The alteration associated with the main lead-zinc zone shows a very distinctive arrangement relative to the position of the mineralization. Above the mineralization the alteration is dominated by a quartz-sericite-pyrite assemblage which extends upto eight metres below the mineralization. Below this the alteration is dominated by a sericite assemblage. From interpretation of the distribution of elements within chlorites, it appears that the sericite and quartz-sericite-pyrite altered zones were formed under different conditions. Immobile element studies show that the protoliths to the altered rocks above and below the mineralization were geochemically very similar. Both the quartz-sericite-pyrite and sericite alteration are very strong, and have resulted in volume/mass changes exceeding 30% of the rock's original volume/mass.

The manganese content of chlorites is very high(4.25±0.75% MnO), a fact which Polya et al. (1986) considered to be consistent with a leached origin for the metal.

The favoured genetic model for the Koonya mineralization is a three stage epigenetic model. In the first stage heated seawater moving up a structural zone causes sericite alteration of the surrounding sequence of rhyolitic volcanics. After a time the fluid conditions change, possibly increasing in temperature. The fluid moves up the structural zone depositing the mineralization, then spreads out into the hanging wall causing quartz-sericite-pyrite alteration of the rocks. In the final stage the area is deformed and the mineralization re-orientated.

REFERENCES

Allen, R.L., 1988a: False pyroclastic textures in altered silicic lavas, with implications for volcanic-associated mineralization. Econ. Geol., 83, p1424-1446

_____, 1988b: Stratigraphic and volcanic setting of the Rosebery-Hercules ore deposits. Unpub. report to E.Z.

_____, 1988c: Unpublished log of drillhole Kp303

Archer, D., 1989: Devonian Granite Complex. Unpub. B.Sc.(Hons) thesis, Uni. Tasmania, p 139

Beaty, D.W. and Taylor, H.P. Jr., 1982: Some petrological and oxygen isotopic relationships in the Amulet mine, Noranda, Quebec, and their bearing on the origin of Archean massive sulphide deposits. Econ. Geol., 77, p 95-108

Both, R.A., Rafter, T.A., Solomon, M. and Jensen, M.L., 1969: Sulphur isotopes and zoning of the Zeehan mineral field, Tasmania. Econ. Geol., 64, p 618-628

Brathwaite, R.L. 1969: The geology of the Rosebery ore deposit. Unpub. Ph.D. thesis, Uni. Tasmania

Brathwaite, R.L., 1974: The geology and origin of the Rosebery ore deposits, Tasmania. Econ. Geol., 69, p1086-1101

Cas, R.A.J. and Wright, J.V., 1987: Volcanic Successions. Modern and Ancient. Allen and Unwin, London.

Cathelineau, M. and Nieva, D., 1985: A chlorite solid solution geothermometer. The Los Azufres (Mexico) geothermal system. Contrib. Mineral Petrol., 91, p235-244

Clayton, R.N., O'Neil, J.R. and Mayeda, T.K., 1972: Oxygen isotope exchange between quartz and water. J. Geophys. Res., 71, p3869-3882

Clifford, B.A., 1988: Facies analysis in the lower Central Volcanic Sequence, Mount Read Volcanics, Rosebery, Tasmania. Unpub. progress report to E.Z.

Corbett, K.D., 1986: The geological setting of mineralization in the Mount Read Volcanics In Large, R.R. (ed.): The Mount Read Volcanics and associated ore deposits, p1-10

Corbett, K.D., and Lees, T.C., 1987: Stratigraphic and structural relationships and evidence for Cambrian deformation at the western margin of the Mt. Read Volcanics, Tasmania. Aust. Jour. Earth Sci., 34, p45-67

Corbett, K.D. and Solomon, M., 1989: Cambrian Mt. Read Volcanics and associated mineral deposits In Burrett, C.F. and Martin, E.L. (eds.): Geology and mineral resources of Tasmania. Special. Pub. Geol. Soc. Aust., 15, p84-153

Corbett, K.D. and Turner, N.J., 1989: Early Palaeozoic deformation and tectonics In Burrett, C.F. and Martin, E.L. (eds.): Geology and mineral resources of Tasmania. Special. Pub. Geol. Soc. Aust., 15, p154-181

Cox, S.F. and Etheridge, M.A., 1989: Coupled grain scale dilatancy and mass transfer during deformation at high fluid pressures: examples from Mount Lyell, Tasmania. Journ. Struct. Geol., 11, no 1/2, p147-162

Craigh, J.R. and Vaughan, D.J., 1981: Ore microscopy and ore petrography. John Wiley and Sons, New York, pp406

Date, J., Watanabe, Y. and Saeki, Y., 1983: Zonal alteration around the Fukazawa kuroko deposits, Akita Prefecture, northern Japan. Econ. Geol., monograph 5, p365-368

Dean, J.A. and Carr, G.R., 1989: Report to E.Z. on Pb isotopic studies of the Koonya and other prospects in the Rosebery area of Western Tasmania. Unpub. CSIRO isotope report.

Eastoe, C.J., 1973: The Rosebery host rock horizon. Unpub. B.Sc. (Hons) thesis, Uni of Tasmania, pp148

Eastoe, C.J., Solomon, M. and Walshe, J.L., 1987: District scale alteration associated with massive sulfide deposits in the Mount Read Volcanics, Western Tasmania. Econ. Geol., 82, p1239-1258

Finucane, K.J., 1932: The Koonya mine. extract from The geology and ore deposits of the Rosebery district (unpub. report)

Fisher, R.V. and Schmincke, H.V., 1984: Pyroclastic Rocks. Springer-Verlag, Berlin

Gair, J.E. and Slack, J.F., 1984: Deformation, geochemistry and origin of massive sulphide deposits, Gossan lead district, Virginia. Econ. Geol., 79, p 1483-1520

Govett, G.J.S (ed), 1983: Handbook of Exploration Geochemistry: Volume 3: Rock geochemistry in Mineral Exploration. Elsevier, Amsterdam, p461

Grant, J.A., 1986: The Isocon diagram - A simple solution to Gresens' equation for metasomatic alteration. Econ. Geol., 81, p1976-1982

Green, G.R., 1986: Preliminary report on oxygen isotope and petrological investigations in the Rosebery mine lease. Unpub. report to E.Z.

Green,G.R., 1983: The geological setting and formation of the Rosebery volcanic-hosted massive sulphide orebody, Tasmania. Unpub. Ph.D. thesis, Uni. Tasmania

Green, G.R., Ohmoto, H., Date, J. and Takahashi, T., 1983: Whole-rock oxygen isotope distribution in the Fukazawa-Kosaka area, Hokuroku district, Japan, and its potential application to mineral exploration. Econ. Geol., Monograph 5, p395-411

Green, G.R., Solomon, M. and Walshe, J.L., 1981: The formation of the volcanic-hosted massive sulphide ore deposit at Rosebery, Tasmania. Econ. Geol., 76, p304-338

Gregory, R.T. and Criss, R.E., 1986: Isotopic exchange in open and closed systems. In Valley, Taylor, O'Neil (eds.) Reviews in Mineralogy: Volume 16: Stable Isotopes. Mineral. Soc. Am., p91-128

Gulson, G.L. and Porrit, P.M., 1987: Base metal exploration of the Mt. Read Volcanics, Western Tasmania: Pt. II. Lead isotope signatures and genetic implications. Econ. Geol., 82, p291-307

Gulston, G.L. Large, R.R., and Porrit, P.M., 1987: Base metal exploration of the Mt. Read Volcanics, Western Tasmania: Pt. III. Application of lead isotopes at Elliot Bay. Econ. Geol., 82, p308-327

Hashiguchi, H., Yamada, R. and Inoue, T., 1983: Practical application of low Na_2O anomalies in footwall acid lava for delimiting promising areas around the Kosaka and Fulazawa Kuroko deposits, Akita Prefecture, Japan. Econ. Geol., Monograph 5,p387-394

Hunns, S.R., 1988: Koonya. Unpub. Pasminco internal report., pp7

Hunns, S.R., 1987: Mineralisation at the Lake Selina prospect. Unpub. M.Sc.(qualifying) thesis, Uni. of Tasmania, pp46

Huston, D.L., 1988: Aspects of the geology of massive sulphide deposits from the Balcooma district, northern Queensland and Rosebery, Tasmania: Implications for ore genesis. Unpub. Ph.D. thesis, Uni. of Tasmania, pp380

Huston, D.L. and Large, R.R., 1988: Distribution, Mineralogy and Geochemistry of Gold and Silver in the north end orebody, Rosebery, Tasmania. Econ. Geol., 83, p1181-1192

Huston, D.L. and Large, R.R., 1987: Genetic and exploration significance of the zinc ratio (100Zn(Zn+Pb)) in massive sulphide systems. Econ. Geol.,82,p1521-1539

Kyser, T. K., 1987: Equilibrium fractionation factors for stable isotopes. In (Kyser ed.) Short course in Stable Isotope geochemistry of low temperature fluids. Mineralogical Association of America, p1-76

Khin Zaw 1989: Zinc ratio distibution for South Hercules. Unpub. report to E.Z.

Khin Zaw, Huston, D.L. and Large, R.R, 1988: Ore metal distibution, zonation and structural relationships at Rosebery, western Tasmania. Unpub. report to E.Z.

Large, R.R., 1977: Chemical evolution and zonation of massive sulphide deposits in volcanic terrains. Econ. Geol., 72, p549-572

Large, R.R., Crawford, A.J. and Adrichem, S.,1986: Primary and alteration chemistry of the Mount Read Volcanics. AMIRA project 84/P210 report, Nov. 1986

Large, R.R. and Huston, D.L., 1986: The zinc number [100Zn/(Zn + Pb)], a new geochemical discrimination for mineral exploration in the Mount Read Volcanics In Large, R.R.(ed.): The Mount Read Volcanics and associated ore deposits, p57-60

Large, R.R., Huston, D.L., McGoldrick, P.J., Ruxton, P.A. and McArthur, G., 1988: Gold distribution and genesis in Australian volcanogenic massive sulphide deposits, and significance for gold transport models. In press (Econ. Geol., Gold 88 Monograph)

Leaman, D.E. and Richardson, R.G, 1988: The granites of west and north-west Tasmania - a geophysical interpretation. Geol. Surv. Tas. Bull., 66

Lees, T.C., 1987: Geology and mineralization of the Rosebery-Hercules area, Tasmania. Unpub. M.Sc. thesis, Uni. Tasmania, pp164

Loftus Hills., 1915: The lead-zinc sulphide deposits of the Read-Rosebery district. Tas. Dept. of Mines Geol. Survey. Bull., 23

McCarthy, J.H. and Gott, G.B., 1978: Robinson (Ely) mining district near Ely, White Pine County, Nevada. J. Geochem. Explor., 9, p225-232

McGoldrick, P., 1988: Sulphur isotope studies at Que River. Uni. Tas. AMIRA report, Project 84/P210, August 1988

McGoldrick, P.J., Capp, S.C. and Large, R.R., 1987: Progress report on the alteration geochemistry of the Mount Read Volcanics. Uni. Tas. AMIRA progress report, Project 84/P210, November 1987

MacKenzie, W.S., Donaldson, C.H. and Guilford, C., 1982: Atlas of igneous rocks and their textures. Longman Group, Great Britain

McLeod, R.L. and Stanton, R.L., 1984: Phyllosilicates and some associated minerals in some Paleozoic stratiform sulphide deposits of south-eastern Australia. Econ. Geol., 79, p1-22

Michard, A. and Albarede, F., 1986: The REE content of some hydrothermal fluids. Chem. Geol., 55, p 51-60

Mills, J.W., 1976: Metamorphism of the zinc-lead sulphide ores of the Yellowhead horizon, Metaline limestone formation, northeastern Washington. Econ. Geol., 71, p1601-1609

Naschwitz, W., 1985: Geochemistry of the Rosebery ore deposit. Unpub. Ph.D. thesis, Uni. Tasmania

O'Neil, J.R. and Taylor, H.P. Jr., 1967: The oxygen isotope and cation exchange chemistry of feldspars. Am. Mineral., 52, p1414-1437

Ohmoto, H. and Rye, R.O., 1979: Isotopes of sulphur and carbon. In (Barnes, H.L. ed) Geochemistry of hydrothermal ore deposits. Wiley, New York, p509-567

Osterberg, S.A., Morton, R.L. and Franklin, J.M., 1987: Hydrothermal alteration and physical volcanology of Archean rocks in the vicinity of the Headway-Coulee massive sulfide occurrence, Onaman area, northwestern Ontario. Econ. Geol., 82, p1505-1520

Pearce, J.A. and Cann, J.R., 1973: Tectonic setting of basic rocks determined using trace element analyses. Earth Planet. Sci. Letters, 19, p209-300

Polya, D.A., Solomon, M., Eastoe, C.J. and Walshe, J.L., 1986: The Murchison Gorge, Tasmania - A possible cross section through a Cambrian massive sulfide system. Econ. Geol., 81, p1341-1355

Ramamohana Rao, T., 1976: Electron probe microanalysis of chlorites from low grade metamorphic rocks of Tennant Creek area, Central Australia. Journ. Geol. Soc. India, 17, no. 4, p471-483

Rand, S.W., 1988: Geology and Mineralisation at Mt. Charter. Unpub. B.Sc (Hons) thesis, Uni. Tasmania, pp96

Rutherford, N.F., 1986: Preliminary review of exploration in the Mt. Read Volcanics with emphasis on the Rosebery mine lease and nearby areas and proposals for further exploration. Unpub. E.Z. internal report

Solomon, M., Eastoe, C.J., Walshe, J.L. and Green, G.R., 1988: Mineral deposits and sulphur isotope abundances in the Mount Read Volcanics between Que River and Mount Darwin, Tasmania. Econ. Geol., 83, p1307-1328

Solomon, M., Rafter, T.A. and Jensen, M.L., 1969: Isotope studies on the Rosebery, Mount Farrell and Mount Lyell ores, Tasmania. Mineral Deposita, 4, p172-199

Solomon, M., Vokes, F.M. and Walshe, J.L., 1987: Chemical remobilisation of volcanic-hosted sulphide deposits at Rosebery and Mt. Lyell, Tasmania. In B. Marshall and L.B. Gilligan (eds.) Mechanical and chemical (re)mobilisation of metalliferous mineralization. Ore. Geol. Rev., 2, p173-190

Spry, P.G. and Gedlinske, B.L., 1987: Tables for determination of common opaque minerals. Economic Geology Publishing Company, pp 52

Stanton, R.L. and Rafter, T.A., 1966: The isotopic constitution of sulpher in some stratiform lead-zinc sulphide ores. Mineral Deposita, 1, p 16-29

Stefaniski, M.Z., 1951: Koonya (STITT) Silver lead-zinc prospect. E.Z. Internal Report (unpublished)

Taylor, B.E. 1987: Stable isotope geochemistry of ore forming fluids In Kyser (ed.) Short course in stable isotope geochemistry of low temperature fluids. Mineralogical Association of Canada, p 337-445

Taylor, H.P. Jr., 1968: The oxygen isotope geochemistry of igneous rocks. Contr. Min. Pet. 19, p1-71

Taylor, H.P. Jr., 1979: Oxygen and Hydrogen isotope relationships in hydrothermal mineral deposits. In Barnes, H.L. (ed.) Geochemistry of hydrothermal ore deposits. Wiley, New York, p237-277

Vernon, R.H., 1976: Metamorphic processes. George Allen and Unwin, Great Britain, pp243

Vokes, F.M., 1971: Some aspects of regional metamorphic mobilization of pre-existing sulphide deposits. Mineral. Deposita, 6, p 122-129

Walshe, J.L., 1986: A six-component chlorite solid solution model and the conditions of chlorite formation in hydrothermal and geothermal systems. Econ. Geol., 81, p681-703

Walshe, J.L., Hedges, M.M. and Harrold, B.P., 1986: Evaluating the conditions of chlorite formation in hydrothermal and geothermal systems. In Fifth annual symposium on water-rock interaction, extended abstracts Orkustofnun, Reykjavik, p605-607

Walshe, J.L. and Solomon, M., 1981: An investigation into the environment of formation of the volcanic-hosted Mt. Lyell copper deposits using geology, mineralogy, stable isotopes, and a six-component chlorite solid solution model. Econ. Geol., 76, p246-284

Wenner, D.B. and Taylor, H.P. Jr., 1971: Temperatures of serpentinization of ultramafic rocks based on O^{18}/O^{16} fractionation between coexisting serpentine and magnetite. Contr. Min. Pet., 35, p165-185

Whitford, D.J., McPherson, W.P.A. and Wallace, D.B., 1989: Geochemistry of the host rocks of the volcanogenic massive sulphide deposit at Que River, Tasmania. Econ. Geol., 84, p1-21

Williams, E., 1989: Summary and Synthesis. In Geology and mineral resources of Tasmania. Geol. Soc. Aust. spec. pub. 15, pp574

Williams, E., McClenaghan, M.P. and Collins, P.L.F., 1989: Mid-Palaeozoic deformation, granitoids and ore deposits. In Geology and mineral resources of Tasmania. Geol. Soc. Aust. spec. pub. 15, pp574

Williams, W. and McBirney, A.R., 1979: Volcanology. Freeman, Cooper and Company, San Francisco, pp397

Winchester, J.A. and Floyd, P.A., 1977: Geochemical discrimination of different magma series and their differentiation products using immobile elements. Chem. Geology, 20, p325-344

APPENDIX 1 : Rock Catalogue

Sample no	UTGD no	Preparation	NORTHING	EASTING	DESCRIPTION
309 22.9m	72459	R	5370610	378280	disseminated sphalerite and thin veins
309 302.1	72460	R	5370610	378280	disseminated sphalerite
307 29.0	72461	PT,R,C	5370770	378320	quartz-sericite-chlorite-pyrite schist
307 35.6	72462	T,R	5370770	378320	quartz-sericite-pyrite schist
307 zone A	72463	PT,R	5370770	378320	quartz-sericite-pyrite schist
307 48.2	72464	T,R,C	5370770	378320	quartz-sericite-pyrite schist
307 zoneB	72465	PT,R,C	5370770	378320	quartz-sericite-pyrite schist
307 68.5	72466	T,R,C	5370770	378320	quartz-sericite schist
307 70.3	72467	T,R	5370770	378280	quartz-sericite schist
307 86.0	72468	T,R,C	5370770	378320	sericite altered feldspar-phyric unit
307 86.2	72469	PT,R	5370770	378320	sericite altered feldspar-phyric unit
307 120.2	72470	T,R,C	5370770	378320	feldspar-phyric unit
307 120.7	72471	T,R	5370770	378320	feldspar-phyric unit
307 zA1	72472	PT,R	5370770	378320	base metal-quartz-chlorite vein
307 zA2	72473	PT,R	5370770	378320	base metal-quartz-chlorite vein
307 zB1	72474	PT,R	5370770	378320	base metal-quartz-chlorite vein
307 zB2	72475	PT,R	5370770	378320	base metal-quartz-carbonate vein
307 zB2a	72476	PS	5370770	378320	base metal-quartz-carbonate vein
307 zB3	72477	PT,R	5370770	378320	base metal-quartz-chlorite vein
307 zB4	72478	PT,R	5370770	378320	base metal-quartz-chlorite vein
306 66.6	72479	T,R	5370770	378320	quartz-sericite-pyrite schist
305 148.3	72480	PT,R	5370700	378720	base metal-quartz-chlorite vein
305 240.0	72481	PT,R	5370700	378720	late stage altered feldspar-phyric unit
305 315.8	72482	PT,R	5370700	378720	late stage altered feldspar-phyric unit
305 318.7	72483	PT,R	5370700	378720	late stage altered feldspar-phyric unit
304 68.2	72484	R	5370420	378260	post-cleavage vein
304 114.0	72485	T,R	5370420	378260	sericite altered feldspar-phyric unit
304 117.0	72486	T,R	5370420	378260	sericite carb. altered feldspar-phyric unit
304 196.0	72487	T,R	5370420	378260	chlorite ser. altered feldspar-phyric unit
303 255.9	72488	R,C	5370500	378265	sericite altered feldspar-phyric unit
303 283.6	72489	R,C	5370500	378265	quartz-sericite-chlorite pyrite unit
303 296.8	72490	R,C	5370500	378265	quartz-sericite altered unit
303 344.6	72491	R,C	5370500	378265	sericite carb. altered feldspar-phyric unit
303 445.8	72492	R,C	5370500	378265	lower feldspar-phyric unit
303 534.0	72493	R	5370500	378265	slumped epiclatics
303 537.6	72494	R	5370500	378265	slumped epiclastics
303 53.2	72495	R	5370500	378265	chalcopyrite-pyrite vein
303 89.2	72496	R	5370500	378265	chalcopyrite-pyrite vein
303 94.2	72497	R	5370500	378265	pyrite-chalcopyrite vein
303 264.8	72498	R	5370500	378265	sphalerite-sericite-carbonate vein
303 274.3	72499	R	5370500	378265	sphalerite-chlorite vein
Upperadit1	72500	T,R	5370770	378320	massive sulphide
Upperadit2	72501	T,R	5370770	378320	massive sulphide
196 123.4	72502	T,R	5370730	378410	banded sulphide
306 76.3	72503	PT,R	5370770	378320	sphalerite-pyrite-chlorite vein

too fg

" "

all carb too fg.

APPENDIX 2: Assay Data

C	D	E	F	G	H	I	J	K	L	M
DH/Sample Location	Sample Type	From (m)	To (m)	Sample Interval (m)	Pb%	Zn%	Cu ppm	Ag g/t	Au g/t	Fe%
KP303	Core	575.00	576.00	1.00	0.0085	0.0150	10	<0.5	0.02	3.95
KP303	"	574.00	575.00	1.00	0.0105	0.0410	15	<0.5	0.03	5.75
KP303	"	573.00	574.00	1.00	0.0230	0.1700	55	<0.5	<0.008	3.90
KP303	"	572.00	573.00	1.00	0.0385	0.2450	5	0.5	<0.008	3.95
KP303	"	571.00	572.00	1.00	0.0640	0.1500	10	0.5	<0.008	3.10
KP303	"	570.00	571.00	1.00	0.0315	0.1550	30	1	0.01	4.45
KP303	"	569.00	570.00	1.00	0.0330	0.1450	5	0.5	<0.008	3.70
KP303	"	568.00	569.00	1.00	0.0565	0.3500	15	0.5	<0.008	3.45
KP303	"	297.00	298.00	1.00	0.0210	0.0230	15	0.5	<0.008	1.95
KP303	"	296.00	297.00	1.00	0.0415	0.0470	15	<0.5	<0.008	2.00
KP303	"	295.00	296.00	1.00	0.0805	0.0780	15	0.5	<0.008	1.95
KP303	"	294.00	295.00	1.00	0.0345	0.1400	10	2	<0.008	3.20
KP303	"	293.00	294.00	1.00	0.0175	0.5000	10	1.5	<0.008	4.10
KP303	"	292.00	293.00	1.00	0.0050	0.1250	25	<0.5	0.02	5.40
KP303	"	291.00	292.00	1.00	0.0010	0.5750	30	<0.5	0.02	4.40
KP303	"	290.00	291.00	1.00	0.0015	0.7300	30	0.5	0.02	4.15
KP303	"	289.00	290.00	1.00	0.0010	1.1000	40	1	0.02	3.95
KP303	"	288.00	289.00	1.00	0.0015	1.3000	50	1	0.02	4.00
KP303	"	287.00	288.00	1.00	0.0015	1.0000	50	1	0.03	4.30
KP303	"	286.00	287.00	1.00	0.0020	1.2500	50	1	0.02	3.95
KP303	"	285.00	286.00	1.00	0.0015	1.1000	50	1	0.01	4.05
KP303	"	284.00	285.00	1.00	0.0030	1.4500	60	1	0.02	4.10
KP303	"	283.00	284.00	1.00	0.0040	0.8700	85	1	0.02	5.05
KP303	"	282.00	283.00	1.00	0.0025	0.5100	45	<0.5	0.02	5.00
KP303	"	281.00	282.00	1.00	0.0020	0.7350	30	<0.5	0.02	4.20
KP303	"	280.00	281.00	1.00	0.0015	0.9050	35	<0.5	0.02	4.55
KP303	"	279.00	280.00	1.00	0.0020	0.2500	30	<0.5	0.01	4.50
KP303	"	278.00	279.00	1.00	0.0065	0.6850	30	0.5	0.02	4.45
KP303	"	277.00	278.00	1.00	0.0035	0.6000	30	<5	0.03	3.00
KP303	"	276.00	277.00	1.00	0.0025	0.7000	30	<5	0.02	3.05
KP303	"	275.00	276.00	1.00	0.0040	0.9100	45	<5	0.01	2.64
KP303	"	274.00	275.00	1.00	0.0130	0.9100	60	<5	0.03	3.68
KP303	"	273.00	274.00	1.00	0.0770	4.7500	1250	10	0.11	7.24
KP303	"	272.00	273.00	1.00	0.0450	0.7300	300	5	0.11	5.60
KP303	"	271.00	272.00	1.00	0.0430	0.5950	55	<5	0.04	3.28
KP303	"	270.00	271.00	1.00	0.0840	0.7000	100	<5	0.02	2.92
KP303	"	269.00	270.00	1.00	0.1250	2.6300	260	<5	0.10	5.12
KP303	"	268.00	269.00	1.00	0.4100	5.3200	480	10	0.10	6.41
KP303	"	267.00	268.00	1.00	0.5500	1.6300	370	15	0.20	4.54
KP303	"	266.00	267.00	1.00	0.0500	0.6350	30	<5	0.06	2.30
KP303	"	265.00	266.00	1.00	0.0120	0.3700	25	<5	0.03	1.81
KP303	"	264.00	265.00	1.00	0.2000	1.2300	200	10	0.18	2.66
KP303	"	263.00	264.00	1.00	0.1900	0.9350	90	10	0.15	2.38
KP303	"	262.00	263.00	1.00	0.0660	0.7550	65	<5	0.12	3.96
KP303	"	261.00	262.00	1.00	0.0340	0.6200	70	<5	0.08	1.97
KP303	"	260.00	261.00	1.00	0.2400	4.1800	150	15	0.16	5.53
KP303	"	259.00	260.00	1.00	0.0470	1.1500	55	<5	0.03	4.36
KP303	"	258.00	259.00	1.00	0.1050	0.9200	310	5	0.05	1.70
KP303	"	257.00	258.00	1.00	0.0100	0.0110	5	<5	<0.01	1.11

C	D	E	F	G	H	I	J	K	L	M
KP303	"	256.00	257.00	1.00	0.0015	0.0055	<5	<5	<0.01	1.26
KP303	"	255.00	256.00	1.00	0.0190	0.0440	5	<5	<0.01	0.52
KP303	"	95.00	96.00	1.00	0.0020	0.0065	250	<5	<0.01	1.00
KP303	"	94.00	95.00	1.00	0.0065	0.0350	3200	5	0.05	4.60
KP303	"	93.00	94.00	1.00	0.0110	0.0250	1250	5	0.06	5.59
KP303	"	92.00	93.00	1.00	0.0085	0.0230	1150	5	0.02	6.28
KP303	"	91.00	92.00	1.00	0.0110	0.0440	3850	10	0.05	7.68
KP303	"	90.00	91.00	1.00	0.0010	0.0085	120	<5	<0.01	1.54
KP303	"	89.00	90.00	1.00	0.0050	0.0300	3350	5	0.02	3.50
KP303	"	88.00	89.00	1.00	0.0140	0.0110	20	<5	<0.01	3.04
KP303	"	87.00	88.00	1.00	<0.0005	0.0130	10	<5	<0.01	2.24
KP303	"	86.00	87.00	1.00	0.0020	0.0260	85	<5	0.01	9.16
KP303	"	85.00	86.00	1.00	0.0010	0.0190	20	<5	0.02	3.12
KP303	"	84.00	85.00	1.00	0.0010	0.0230	25	<5	0.02	5.04
KP303	"	83.00	84.00	1.00	0.0010	0.0100	25	<5	0.01	1.81
KP303	"	82.00	83.00	1.00	0.0330	0.0130	50	<5	0.02	2.76
KP303	"	81.00	82.00	1.00	0.0010	0.0090	20	<5	<0.01	2.76
KP303	"	80.00	81.00	1.00	0.0020	0.0160	55	<5	0.03	2.66
KP303	"	79.00	80.00	1.00	0.0015	0.0095	20	<5	<0.1	3.24
KP303	"	78.00	79.00	1.00	0.0020	0.0100	40	<5	0.01	3.01
KP303	"	77.00	78.00	1.00	0.0010	0.0100	80	<5	0.03	5.04
KP303	"	76.00	77.00	1.00	0.0030	0.0190	30	<5	0.02	2.26
KP303	"	75.00	76.00	1.00	0.0005	0.0070	30	<5	<0.01	1.25
KP303	"	74.00	75.00	1.00	0.0020	0.0080	85	<5	<0.008	2.81
KP303	"	73.00	74.00	1.00	0.0020	0.0100	220	<5	0.01	1.61
KP303	"	72.00	73.00	1.00	0.0035	0.0270	120	<5	0.08	1.82
KP303	"	71.00	72.00	1.00	0.0105	0.0310	2100	5	0.04	8.24
KP303	"	70.00	71.00	1.00	0.0180	0.0470	5300	5	0.05	3.26
KP303	"	69.00	70.00	1.00	0.0040	0.0110	75	<5	0.01	2.92
KP303	"	68.00	69.00	1.00	0.0055	0.0100	85	<5	0.01	1.26
KP303	"	67.00	68.00	1.00	0.0055	0.0180	280	<5	0.03	5.61
KP303	"	66.00	67.00	1.00	0.0095	0.0350	55	<5	0.01	1.90
KP303	"	65.00	66.00	1.00	0.0060	0.0440	75	<5	<0.01	1.37
KP303	"	63.00	64.00	1.00	0.0140	0.0240	190	<5	0.02	1.03
KP303	"	62.00	63.00	1.00	0.1550	0.1100	12900	<5	0.02	2.82
KP303	"	61.00	62.00	1.00	0.0050	0.0360	20	<5	0.01	1.40
KP303	"	55.00	56.00	1.00	0.0095	0.0400	1350	<5	0.02	1.34
KP303	"	54.00	55.00	1.00	0.0130	0.6900	510	<5	0.10	7.62
KP303	"	53.00	54.00	1.00	0.0230	0.6800	4000	10	0.18	8.08
KP303	"	52.00	53.00	1.00	0.0075	0.0370	2150	<5	0.04	1.91
KP303	"	47.00	48.00	1.00	0.0080	0.0790	55	<5	0.12	6.36
KP303	"	36.00	37.00	1.00	0.0230	0.0450	1900	<5	0.12	5.60
KP303	"	35.00	36.00	1.00	0.0060	0.0360	1850	<5	0.09	4.22
KP303	"	34.00	35.00	1.00	0.0130	0.0330	200	<5	0.06	7.04
KP303	"	33.00	34.00	1.00	0.0170	0.0350	250	<5	0.05	7.20
KP303	"	32.00	33.00	1.00	0.0065	0.0190	840	<5	0.13	3.44
KP303	"	31.00	32.00	1.00	0.0190	0.0370	6050	10	0.10	6.94
KP303	"	30.00	31.00	1.00	0.0130	0.0330	150	<5	0.05	5.55
KP303	"	5.00	6.00	1.00	0.0050	0.0170	540	<5	0.28	7.04
KP303	"	4.00	5.00	1.00	0.0060	0.0140	340	<5	0.05	4.37
KP303	"	3.00	4.00	1.00	0.0070	0.0050	680	<5	0.06	2.01
KP304	**Core**	**73.00**	**74.00**	**1.00**	**0.0055**	**0.0440**	**170**	**1**	**0.05**	**2.55**
KP304	"	74.00	75.00	1.00	0.0022	0.0120	68	<1	<0.01	1.53

C	D	E	F	G	H	I	J	K	L	M
KP304	"	75.00	76.00	1.00	0.0058	0.0700	490	1	0.03	4.95
KP304	"	76.00	77.00	1.00	0.0032	0.0220	165	1	<0.01	2.50
KP304	"	77.00	78.00	1.00	0.0036	0.0125	390	1	0.03	2.25
KP304	"	78.00	79.00	1.00	0.0025	0.0068	135	1	0.01	1.92
KP304	"	79.00	80.00	1.00	0.0052	0.0440	440	<1	0.01	2.55
KP304	"	80.00	81.00	1.00	0.0250	0.2500	1250	2	0.05	2.40
KP304	"	81.00	82.00	1.00	0.0130	0.0500	680	2	0.03	2.40
KP304	"	82.00	83.00	1.00	0.0090	0.0350	230	1	0.02	1.81
KP304	"	83.00	84.00	1.00	0.0900	0.5100	660	11	0.08	3.15
KP304	"	84.00	85.00	1.00	0.0170	0.1440	19	<1	0.01	1.38
KP304	"	85.00	86.00	1.00	0.0175	0.1940	13	1	0.01	1.25
KP304	"	86.00	87.00	1.00	0.0070	0.1850	14	<1	0.01	1.39
KP304	"	87.00	88.00	1.00	0.0150	0.5300	280	2	0.03	2.85
KP304	"	88.00	89.00	1.00	0.0064	0.5700	280	1	0.03	2.35
KP304	"	89.00	90.00	1.00	0.0022	0.0048	165	1	0.01	1.56
KP304	"	90.00	91.00	1.00	0.0105	0.0145	76	1	0.01	1.13
KP304	"	91.00	92.00	1.00	0.0036	0.0195	32	1	0.01	0.99
KP304	"	92.00	93.00	1.00	0.0048	0.0076	26	1	0.01	1.25
KP304	"	93.00	94.00	1.00	0.0046	0.0125	94	1	0.03	1.45
KP304	"	94.00	95.00	1.00	0.0230	0.0024	22	1	<0.01	1.36
KP304	"	47.00	48.00	1.00	0.0120	0.0200	140	2	0.02	1.76
KP304	"	48.00	49.00	1.00	0.0110	0.0390	165	<1	0.01	1.32
KP304	"	54.00	55.00	1.00	0.0034	0.0650	470	1	0.01	1.61
KP304	"	55.00	56.00	1.00	0.0180	0.0210	64	2	0.03	3.40
KP304	"	66.00	67.00	1.00	0.0024	0.0058	65	<1	0.01	1.84
KP304	"	67.00	68.00	1.00	0.0046	0.0078	330	<1	0.04	2.15
KP304	"	68.00	69.00	1.00	0.0020	0.0038	40	<1	0.02	1.11
KP304	"	69.00	70.00	1.00	0.0045	0.0360	62	1	0.02	1.97
KP304	**Core**	**10.00**	**11.00**	**1.00**	**0.0760**	**0.0200**	**125**	**2**	**<0.01**	**1.53**
KP308	"	15.00	16.00	1.00	0.0330	0.0045	26	1	0.06	0.66
KP308	"	18.00	19.00	1.00	0.0710	0.0115	105	20	0.04	1.47
KP308	"	19.00	21.00	2.00	0.0780	0.0400	740	180	0.52	6.25
KP308	"	21.00	22.00	1.00	0.0480	0.0088	105	24	0.02	1.79
KP309	**Core**	**12.00**	**13.00**	**1.00**	**0.1760**	**1.7600**	**200**	**2**	**0.06**	**1.44**
KP309	"	13.00	14.00	1.00	0.3500	1.4300	105	2	0.04	1.29
KP309	"	15.00	16.00	1.00	0.0740	0.0350	240	<1	0.02	2.60
KP309	"	16.00	17.00	1.00	0.0360	0.0125	100	<1	<0.01	2.80
KP309	"	21.00	22.00	1.00	0.1200	0.0260	360	2	0.04	4.95
KP309	"	22.00	23.00	1.00	0.0850	0.6300	105	2	0.02	2.85
KP309	"	35.00	36.00	1.00	0.1120	0.0500	14	1	0.06	1.07
KP309	"	38.00	39.00	1.00	0.1360	0.0740	55	2	0.04	1.65
KP309	"	39.00	40.00	1.00	0.2750	0.3900	240	2	<0.01	1.32
KP309	"	40.00	41.00	1.00	0.8300	0.7600	40	4	0.04	1.63
KP309	"	41.00	42.00	1.00	0.4150	0.3050	120	3	0.08	2.40
KP309	"	42.00	43.00	1.00	0.4150	0.6700	92	2	0.72	1.78
KP309	"	43.00	44.00	1.00	0.5000	0.5500	64	4	0.14	1.71
KP309	"	44.00	45.00	1.00	0.3500	0.3650	36	1	0.08	1.24
KP309	"	45.00	46.00	1.00	0.7100	0.7200	75	3	0.21	1.90
KP309	"	55.00	56.00	1.00	0.2550	0.4150	34	2	0.04	1.85
KP309	"	56.00	57.00	1.00	2.3500	5.0500	420	19	2.00	2.05
KP309	"	61.00	62.00	1.00	0.1200	0.2400	18	2	<0.01	1.41
KP309	"	95.00	96.00	1.00	0.1040	0.0640	12	1	0.04	1.45
KP309	"	284.00	285.00	1.00	0.0230	0.5900	28	<1	<0.01	1.27

C	D	E	F	G	H	I	J	K	L	M
KP309	"	285.00	286.00	1.00	0.0195	0.3800	14	<1	<0.01	1.31
KP309	"	289.00	290.00	1.00	0.5700	1.3900	32	6	0.04	4.70
KP309	"	295.00	296.00	1.00	1.2500	2.8000	130	12	0.16	5.45
KP309	"	296.00	297.00	1.00	0.3050	0.5500	70	2	0.02	3.80
KP309	"	297.00	298.00	1.00	1.4900	2.2000	340	11	0.05	2.50
KP309	"	298.00	299.00	1.00	0.8600	1.1500	82	6	0.10	2.90
KP309	"	299.00	300.00	1.00	0.1440	0.6200	70	2	<0.01	4.00
KP309	"	302.00	303.00	1.00	0.0800	1.8300	86	2	0.03	3.45
KP309	"	303.00	304.00	1.00	0.0360	0.4950	38	<1	0.04	4.60
KP309	"	307.00	308.00	1.00	0.0730	2.9500	690	5	0.16	4.85
KP309	"	308.00	309.00	1.00	0.0155	1.1400	250	1	0.01	3.60
KP309	"	309.00	310.00	1.00	0.0150	1.0300	175	<1	0.02	3.65
KP309	"	310.00	311.00	1.00	0.0490	0.6800	66	4	0.02	4.00
KP309	"	311.00	312.00	1.00	0.0155	0.8300	46	1	0.04	3.30
KP309	"	312.00	313.00	1.00	0.0290	0.7500	64	2	0.02	4.35
KP309	"	313.00	314.00	1.00	0.0490	0.6800	78	3	0.04	6.30
KP309	"	314.00	315.00	1.00	0.0340	0.3300	50	2	0.03	5.40
KP309	"	322.00	323.00	1.00	0.0210	1.2000	76	<1	<0.1	3.30
KP309	"	323.00	324.00	1.00	0.0550	0.7400	115	7	<0.1	2.85
KP309	"	324.00	325.00	1.00	0.4450	0.7100	165	5	0.02	3.30
KP309	"	335.00	336.00	1.00	0.2400	0.6100	310	2	0.02	2.20
KP309	"	336.00	337.00	1.00	0.1260	0.2550	25	1	<0.01	1.69
KP309	"	337.00	338.00	1.00	0.6100	1.1100	420	3	0.01	2.85
KP309	"	359.00	360.00	1.00	0.0750	0.1120	34	<1	<0.01	1.31
KP309	"	360.00	361.00	1.00	0.0370	0.0790	54	<1	<0.01	1.63
KP306	**Core**	**38.15**	**39.55**	**1.40**	**0.0185**	**0.8300**	**600**	**4**	**0.12**	**8.10**
KP306	"	72.70	73.70	1.00	0.1250	0.1180	28	1	0.03	4.90
KP306	"	73.70	74.80	1.10	1.8300	3.7500	420	<1	0.26	6.35
KP306	"	74.80	76.20	1.40	0.0540	1.7800	66	2	0.07	6.55
KP306	"	76.20	77.60	1.40	0.0950	2.5000	110	4	0.05	6.55
KP307	**Core**	**38.50**	**40.00**	**1.50**	0.3250	0.7500	125	3	3.70	3.50
KP307	"	40.00	41.45	1.45	0.8400	0.9400	230	8	0.41	5.15
KP307	"	41.45	42.55	1.10	0.1740	0.3650	70	6	0.05	3.65
KP307	"	44.10	45.10	1.00	0.3200	0.4050	28	4	0.07	3.30
KP307	"	59.00	60.50	1.50	0.3550	0.4350	22	2	0.12	1.53
KP307	"	60.50	62.00	1.50	0.3100	0.4600	42	2	0.12	2.35
KP307	"	62.00	63.50	1.50	0.1440	0.3400	14	1	0.05	2.40
KP307	"	63.50	64.90	1.40	0.2750	0.6600	70	2	0.12	3.35
KP307	"	64.90	66.30	1.40	1.4200	3.5500	160	13	0.17	6.25
KP305	**Core**	**147.00**	**148.00**	**1.00**	**0.1540**	**1.0300**	52	3	**0.03**	**5.75**
KP305	"	148.00	149.50	1.50	0.3900	2.5000	135	4	0.01	5.60
KP305	"	149.50	151.00	1.50	0.8800	3.7500	260	12	0.13	6.35
KP305	"	151.00	152.50	1.50	0.4850	2.6000	280	9	0.04	6.35
KP305	"	152.50	154.00	1.50	0.0550	1.1300	70	2	0.02	5.10
KP305	"	154.00	155.50	1.50	0.0520	1.4400	125	2	0.02	5.80
KP305	"	155.50	157.00	1.50	0.0960	3.0500	470	7	0.05	6.10
KP305	"	194.50	196.00	1.50	0.0105	0.0670	48	1	0.01	5.35
KP305	"	196.00	197.50	1.50	0.0062	0.0105	1340	2	0.06	7.00
KP305	"	197.50	199.00	1.50	0.0060	0.1950	290	1	0.05	5.20
KP305	"	199.00	200.50	1.50	0.0040	0.4500	350	1	0.02	2.45
KP305	"	200.50	202.00	1.50	0.0068	0.5100	220	<1	0.02	2.60
KP305	"	202.00	203.00	1.00	0.0200	0.5300	250	2	0.02	2.50

APPENDIX 3: Oxygen Isotope Derivation

For a closed system the final rock δO^{18} (δRf)is equal to,

$$\delta Rf = \frac{\delta Ri + [\delta Wi + \Delta RW] x W/R}{1+W/R} \quad \text{(Green et al. 1983)}$$

, where δRi is the initial rock δO^{18}, δWi is the initial fluid δO^{18} and W/R is the water to rock ratio. For an open system the term W/R would be replaced with $(e^{W/R})$

For a high water/rock ratio such as 20 this would become

$$\delta Rf = \frac{\delta Ri}{21} + \frac{20x[\delta Wi + \Delta RW]}{21}$$

For this study δRi is assumed to be $\approx$7.5‰ therefore,

$$\delta Rf = 0.38 + 0.95x[\delta Wi + \Delta RW]$$

For the Koonya area the δRf for the early events must have been in the range between 5‰ to 12.2‰. This corresponds to $[\delta Wi + \Delta RW]$ valus of 4.8‰ to 12.5‰, an inaccuracy of $\leq$0.3‰ when compared to the δRf. Therefore,

$$\delta Rf \approx [\delta Wi + \Delta RW]$$

APPENDIX 4: Chlorite Analyses

	Si-iv	Al-vi	Al-iv	Fe3-iv	Fe3-vi	Fe2-vi	Mg+Mn	occupancy	Fe number	Log fO2 (l-v)	Temp(l-v)	Al-vi 1KB	Al-iv 1KB	occupancy 1KB	Fe No 1KB	log fO2 1KB	Temp 1KB
zb1c1	2.5854	1.5825	1.2085	0.2061	0.2539	2.0541	1.9254	9.8132	56.6	-32.99	294	1.6059	1.1773	9.7859	56.6	-30.1	320.5
zb1c2	2.5162	1.53	1.2249	0.2543	0.2629	2.1659	1.8876	9.8499	58.7	-30	324	1.5347	1.2231	9.8444	58.7	-24.02	367.5
zb1c3	2.5587	1.5044	1.1959	0.2454	0.2743	2.2254	1.8419	9.8459	59.8	-32.17	305	1.5185	1.1774	9.8297	59.8	-29.11	337.5
zb1c4	2.6089	1.4458	1.1732	0.2179	0.2617	2.3292	1.8219	9.8639	60.7	-33.6	296	1.4769	1.1326	9.8281	60.7	-31.33	313.5
zb2c1	2.5675	1.4937	1.1887	0.2438	0.2774	2.2505	1.8261	9.8477	60.3	-32.62	302	1.5095	1.1678	9.8293	60.3	-29.39	332.5
zb2c2	2.596	1.4586	1.1732	0.2308	0.2816	2.287	1.8303	9.8575	60.5	-33.4	296	1.4819	1.1428	9.8306	60.5	-29.5	319.5
zb2c3												1.4568	1.1159	9.8298	60.3	-32.23	304.5
zb2c4	2.5242	1.4961	1.2126	0.2632	0.2749	2.3056	1.7819	9.8585	61.5	-30.62	321						
zb3c1	2.5395	1.5288	1.2029	0.2576	0.299	2.6058	1.4036	9.8373	69.3	-32.67	308	1.5553	1.1678	9.8065	69.3	-29.78	333.5
zb3c2	2.4609	1.5561	1.241	0.2981	0.3035	2.5938	1.3892	9.8427	69.7	-29.28	338						
zb3c3	2.4945	1.5698	1.2212	0.2828	0.3024	2.5723	1.3814	9.8259	69.6	-31.28	319						
za1c1	2.4778	1.5379	1.2433	0.2789	0.2828	2.401	1.6313	9.8529	64.5	-29.18	338						
za1c2	2.466	1.5587	1.2518	0.2822	0.2861	2.4419	1.5602	9.8468	65.9	-28.69	341						
za1c3	2.4882	1.5514	1.2366	0.2752	0.2823	2.4014	1.6077	9.4828	64.8	-29.94	330						
za2	2.5447	1.5203	1.2073	0.248	0.2707	2.2094	1.8433	9.8437	59.7	-31.5	310						
za2	2.5744	1.5378	1.1984	0.2271	0.2685	2.1755	1.8487	9.8305	59.1	-32.88	298	1.5588	1.1706	9.8061	59.1	-29.97	325.5
30676c1	2.5901	1.4783	1.1833	0.2266	0.2742	2.3572	1.7431	9.8527	62.1	-33.41	298	1.5074	1.1451	9.8191	62.1	-30.93	318.5
30676c2												1.4822	1.119	9.8186	62	-32.57	302.5
30676c3	2.5205	1.5303	1.2154	0.2641	0.2805	2.3295	1.7026	9.8428	62.8	-31.04	317						
zb0c1	2.5235	1.5777	1.1948	0.2817	0.3559	2.4787	1.3964	9.8088	69.1	-32.9	302	1.587	1.1825	9.798	69.1	-29.2	338.5
zb0c2	2.5254	1.5773	1.193	0.2816	0.3683	2.4584	1.4041	9.8081	68.9	-32.96	301						
zb0c3	2.5345	1.581	1.2214	0.2441	0.2823	2.5645	1.3926	9.8204	68.9	-32.48	309	1.612	1.1801	9.7842	68.9	-29.63	333.5
30666c1	2.5455	1.5163	1.2061	0.2483	0.271	2.2156	1.8422	9.8451	59.8	-31.52	310						
30666c2	2.5726	1.5683	1.2054	0.222	0.2712	2.2187	1.7605	9.8188	60.6	-33.1	297	1.5939	1.1714	9.789	60.6	-30.02	322.5
30666c3	2.5437	1.5319	1.2112	0.2451	0.2678	2.2103	1.8299	9.8399	59.8	-31.52	310						
30666c4	2.554	1.5266	1.2045	0.2415	0.2688	2.2049	1.8389	9.8392	59.6	-32	306	1.5414	1.1848	9.8219	59.6	-28.82	338.5
70.3c1	2.5787	1.5207	1.1969	0.2244	0.2564	2.0432	2.0181	9.8383	55.6	-32.41	299	1.535	1.178	9.8217	55.6	-29.04	330.5
70.3c2	2.5597	1.5343	1.2103	0.23	0.2527	2.043	2.0083	9.8382	55.7	-31.59	306						
70.3c3	2.6423	1.5014	1.3399	0.0178	0.4123	2.0683	1.9374	9.9195	56.3	-28.77	367	1.6325	1.1651	9.7665	56.3	-31.17	308.5
48.2c1	2.527	1.5301	1.2164	0.2566	0.273	2.2368	1.8034	9.8434	60.5	-30.89	316						
48.2c2	2.5644	1.5324	1.1993	0.2363	0.273	2.2413	1.7869	9.8336	60.6	-32.72	301						
48.2c3	2.5923	1.4677	1.1776	0.2301	0.2731	2.2303	1.8841	9.8552	59.2	-33.16	297	1.4886	1.1502	9.831	59.2	-30.33	322.5